

SSD

SCIENCE FOR A SUSTAINABLE DEVELOPMENT



**Integrated Study of Southern Ocean
Biogeochemistry and Climate Interactions
in the Anthropocene
“BELCANTO III”**

F. Dehairs, A.-J. Cavagna, S. Jacquet, P. Mangion, V. Woulé Eboungoué,
J. Navez, C. Lancelot, S. Becquevort, V. Schoemann, J. Naithani, I. Dumont,
F. Masson, L. André, D. Cardinal, F. Fripiat, H. Goosse, A. de Montety,
M. Vancoppenolle, A. Borges, B. Delille



ENERGY 

TRANSPORT AND MOBILITY 

AGRO-FOOD 

HEALTH AND ENVIRONMENT 

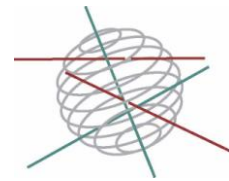
CLIMATE  

BIODIVERSITY   

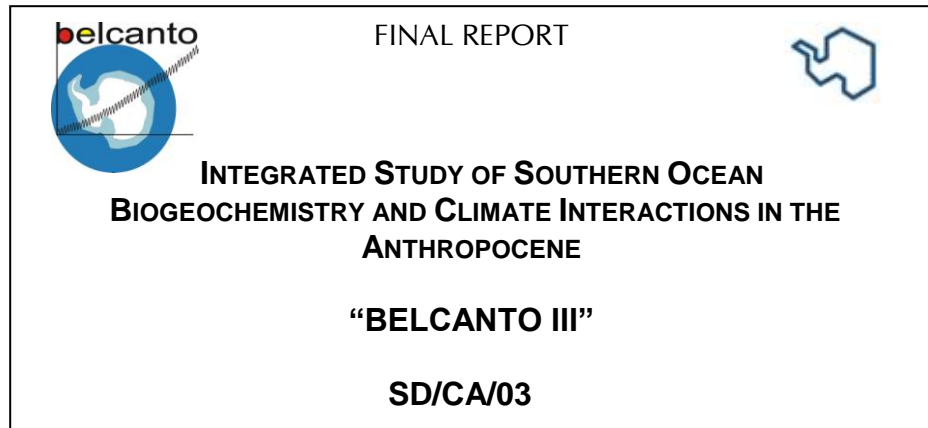
ATMOSPHERE AND TERRESTRIAL AND MARINE ECOSYSTEMS   

TRANSVERSAL ACTIONS 

SCIENCE FOR A SUSTAINABLE DEVELOPMENT
(SSD)



Climate



Promotors

Frank Dehairs

Vrije Universiteit Brussel

Christiane Lancelot

Université Libre de Bruxelles

Luc André

Musée Royal de l’Afrique Centrale/ Koninklijk Museum voor Midden-Afrika

Hugues Goosse

Université Catholique de Louvain

Alberto Borges

Université de Liège

Authors

F. Dehairs, A.-J. Cavagna, S. Jacquet, P. Mangion, V. Woulé Eboungoué, J. Navez
VUB

C. Lancelot, S. Becquevort, V. Schoemann, J. Naithani, I. Dumont, F. Masson
ULB

L. André, D. Cardinal, F. Fripiat
MRAC-KMMA

H. Goosse, A. de Montety, M. Vancoppenolle
UCL

A. Borges, B. Delille
Ulg



Vrije
Universiteit
Brussel





D/2011/1191/37

Published in 2011 by the Belgian Science Policy

Avenue Louise 231

Louizalaan 231

B-1050 Brussels

Belgium

Tel: +32 (0)2 238 34 11 – Fax: +32 (0)2 230 59 12

<http://www.belspo.be>

Contact person: Maaïke Vancauwenberghe

+32 (0)2 238 36 78

Neither the Belgian Science Policy nor any person acting on behalf of the Belgian Science Policy is responsible for the use which might be made of the following information. The authors are responsible for the content.

No part of this publication may be reproduced, stored in a retrieval system, or transmitted in any form or by any means, electronic, mechanical, photocopying, recording, or otherwise, without indicating the reference :

F. Dehairs, A.-J. Cavagna, S. Jacquet, P. Mangion, V. Woulé Eboungoué, J. Navez, C. Lancelot, S. Becquevort, V. Schoemann, J. Naithani, I. Dumont, F. Masson, L. André, D. Cardinal, F. Fripiat, H. Goosse, A. de Montety, M. Vancoppenolle, A. Borges, B. Delille - ***Integrated study of southern ocean biogeochemistry and climate interactions in the anthropocene "BELCANTO III"***. Final Report. Brussels : Belgian Science Policy 2011 – 128 p. (Research Programme Science for a Sustainable Development).

TABLE OF CONTENT

SUMMARY	5
1. INTRODUCTION.....	9
2. METHODOLOGY AND RESULTS.....	15
1. Improved understanding of the iron cycling (WP1)	15
2. Nutrient consumption, CO ₂ uptake and C export (WP2)	26
2.1. Seasonally integrated Si and N utilization	26
2.2. Instantaneous Si, N uptake and dissolution.....	33
2.3. CO ₂ uptake and C export.....	40
3. Characterisation and reactivity of exported biogenic particles (WP3).....	51
3.1. Characterisation of mesopelagic particles.....	51
3.2 Remineralisation	59
3.3. Impact of mesopelagic processes on nutrient profiles.....	68
3.3.1- High resolution dissolved Ba profiles.....	68
3.3.2 Results for silicon stable isotope profiles	71
4. Modelling biogeochemical cycles in the modern Southern Ocean (WP4).....	74
4.1 3D-NEMO-SWAMCO with implicit sea-ice biogeochemistry.....	74
4.1.1. Improvement and tests of NEMO-LIM (Nucleus for European Modelling of the Ocean and Louvain-la-neuve-sea-Ice-Model)	74
4.1.2. 3D NEMO-LIM-SWAMCO simulations of the spatial distribution of the iron supply to phytoplankton in the Southern Ocean.....	77
4.2 Development of an explicit model of sea-ice biogeochemistry	86
4.2.1 Structure of LIM-SIMCO.....	86
4.2.2 LIM-SIMCO implementation and results	87
4.2.3 Collection of validation data set for LIM-SIMCO during the SIMBA cruise.....	89
4.3 3D –NEMO-SWAMCO with explicit sea-ice biogeochemistry	90
4.4 Impact of future climate change (WP5)	94
3. POLICY SUPPORT	95
4. DISSEMINATION AND VALORISATION	97
5. PUBLICATIONS	99
6. ACKNOWLEDGEMENTS.....	115
7. REFERENCES.....	117
Annex 1:	127
Annex 2	127

SUMMARY

A. Context

The Southern Ocean (S.O.) ecosystem plays a crucial role in controlling global biogeochemical cycles (C, N, Si, P, Fe, ...) and regulating climate notably through its capacity to absorb atmospheric CO₂, a major greenhouse gas, and re-distribute unused nutrients to the adjacent ocean basins, sustaining production there. However, current estimates of the contemporary S.O. contribution to the global oceanic CO₂ sink based on global ocean biogeochemical models differ widely and are subject to large uncertainties. Such differences between model results are attributed to the fact that physical and biogeochemical processes are still inadequately resolved at present.

Focus therefore should be on improving our understanding of these complex physical and biogeochemical processes controlling primary production and carbon uptake by the Southern Ocean. The role of Fe, in particular, is still unsatisfactorily known. Fe is commonly accepted to represent a necessary micro-nutrient for phytoplankton growth but also shapes the microbial community structure, thereby impacting on the biological carbon pump. Indeed today we still lack a detailed understanding of the natural complex biogeochemistry of Fe in terms of sources, sinks, bio-availability and the effect of Fe on the efficiency of the biological carbon pump. Such knowledge should stand central in the debate about sense and non-sense of artificial ocean fertilization.

B. Objectives

The overall objective of the BELCANTO III project was to conduct targeted process studies and develop new proxies to construct and validate a realistic 3D ice-ocean biogeochemical model for the area south of latitude 30°S, based on improved understanding of the different factors regulating interactions between the atmosphere, ocean circulation and biogeochemical cycles and on synthesis/collection of existing/new data sets.

The specific objectives were:

- to improve our understanding about the iron cycling, with focus on the significance of iron-organic matter interactions for iron bioavailability and the efficiency of the biological pump (WP1)
- to quantify nutrient consumption, CO₂ uptake and C-export by assessing seasonality and interannuality of nutrient (Si, N) uptake; reconstruct carbon uptake and export from the surface layer via a multi-proxy approach; provide a relevant data set for 3D-NEMO-SWAMCO model validation (WP2)
- to characterise the biogenic particles exported from the surface to the twilight zone and study their fate by quantifying remineralisation rates (WP3)
- to model biogeochemical cycles in the modern Southern Ocean including sea-ice biogeochemistry (WP4)
- to estimate impact of future climate change in the Southern Ocean through process-studies and modelling approaches (WP5).

C. Conclusions

The BELCANTO III project yielded significant insights into the complex chemistry that regulates Fe-availability to phytoplankton and the impact of artificial and natural Fe fertilisation on carbon uptake and sequestration in the deep ocean. In particular, it was shown that saccharides can play a pivotal role in Fe cycling in the Southern Ocean, in that they act as an organic ligand that enhances Fe bioavailability to Southern Ocean phytoplankton.

The network developed a unique trace element and isotope (TEI) toolbox which offers great potential for the study of the processes controlling seasonal utilisation of Si, C and N as well as for paleo-productivity reconstructions. Combined with specific microbiological and biomarker tools, this TEI toolbox has enabled to shed light on the subsurface, mesopelagic processing of organic carbon exported from the surface ocean, a crucial factor which sets the ocean's efficiency for carbon sequestration via the biological pump. It was shown that upper ocean ecosystem functioning, as tuned to a large extent by the climate sensitive actor Fe but also by presence/absence of sea-ice, stratification, grazing, .. controls the potential for carbon export to the deep ocean. More particularly, results obtained with the TEI toolbox highlighted the following points: (i) The difference in terms of carbon export as a function of ecosystem structure and Fe stress. During a diatom bloom induced by artificial Fe fertilization we indeed observed an enhanced deep carbon export (which, however, did not exceed natural export events), though lasting only over a rather limited period of time. However, in the case of a natural Fe fertilization with diatoms not being the dominant phytoplankton group, the carbon export efficiency was reduced; (ii) throughout summer period an upward nutrient (silicate) supply to the mixed layer appears characteristic for several sectors of the Antarctic Circumpolar Current. For a mesoscale structure like an eddy, such supply sustains up to 30% of the nutrients used over the growth season.

Based on a compilation of data from several international groups we highlighted inter-annual variability of CO₂ dynamics and air-sea CO₂ fluxes due to large scale climatic oscillations in the Subtropical and Subantarctic Zones. Such time-series analysis of natural inter-annual variability is crucial for predicting the future changes of marine carbon biogeochemistry under global change. However, for extending such analysis further, to the higher latitude regions of the Southern Ocean, a critical mass of data is needed. Therefore it is crucial to continue field observations as well as the further integration of data at the international level.

A further major achievement concerns the integration of the microbiological and biogeochemical experimental outcomes into the coupled biogeochemical – ocean – sea-ice 3D NEMO-LIM-SWAMCO model, a scientific tool built for testing our understanding of the functioning of the contemporary Southern Ocean ecosystem and predicting the impact of future climate change. Model simulations highlighted for the first time the significance of seasonal sea ice and icebergs as Fe suppliers for phytoplankton growth.

D. Contribution of the project in a context of scientific support to a sustainable development policy

Spatial and temporal variability of carbon fluxes have been documented for different functional entities of the Southern Ocean. Fieldwork, experimental work in controlled laboratory conditions and modelling have provided new insights in the significance of the micro-nutrient iron as a phytoplankton growth limiting factor and in the mesopelagic heterotrophic processing which largely sets the Southern Ocean carbon sequestration capacity. The BELCANTO III project has thereby contributed to an improved appreciation of the effects of natural vs. artificial fertilisation by iron. Overall, the project outcomes improve our understanding about the mechanisms and the significance of carbon uptake and sequestration by the open and sea-ice covered Southern Ocean.

The results obtained by the BELCANTO partners have been included in the main assessment reports devoted to recent and future changes in the Southern Ocean, assessment reports which form the scientific basis for sustainable development policies. In particular, some partners are contributing authors of the 4th assessment report (AR4) of the Intergovernmental Panel on Climate Change and of the Antarctic Climate Change and of the Environment" report published by the Scientific Committee on Antarctic Research.

E. Keywords

Southern Ocean productivity – impact of Fe – carbon sequestration efficiency – impact of climate change

1. INTRODUCTION

The Southern Ocean (SO) ecosystem is crucial in climate regulation and element cycles (C, N, P, Si, Fe). Based on *in situ* partial pressure of CO₂ (pCO₂) and dissolved inorganic carbon DIC measurements (Takahashi et al., 2002; Sabine et al., 2004) and biogeochemical models (Watson and Orr, 2003), the modern SO has been identified as a major player in the uptake of anthropogenic CO₂. However, estimates of the SO contribution to the global oceanic CO₂-sink are subject to large uncertainties and values vary from 20 to 30-50% when based on either pCO₂ data (Takahashi et al., 2002, 2009) or model calculations (Watson and Orr, 2003). Model results differ significantly and this has been attributed to physical and biogeochemical processes being inadequately resolved. These models lack an explicit description of Fe and do not consider links between community structure and biogeochemical cycles. Furthermore, estimates of the SO sink, based on pCO₂ field data, clearly suffer from insufficient geographical and seasonal coverage. Evidence exists that the sink of anthropogenic CO₂ is mainly located in the Subantarctic region, associated with subduction of Antarctic Intermediate Waters and Subantarctic Mode Waters (Sabine et al., 2004), while the role of the deep water formation is still debated (Lo Monaco et al., 2005). Nevertheless, recent time series analyses have provided clear evidence for a decadal increase of CO₂ for the Southern ocean south of 20°S (Metzl, 2009). Moreover, summer and winter observations in the Indian sector indicate that the S.O. is not acting as a year-round CO₂ sink or source (e.g., Metzl et al., 2006). The observed seasonality of air-sea CO₂ fluxes calls for a revision of previous annual carbon budget estimates obtained through indirect methods. In agreement with this, air-sea CO₂ fluxes simulated by the complex biogeochemical SWAMCO-4 model implemented in a vertical 1D frame for the 'KERFIX' time series station located south of Kerguelen (Jeandel et al., 1998) and the Ross Sea show seasonal modulations from source to sink, with biology being responsible of the annual sink of atmospheric CO₂ (Pasquer et al., 2005). These latter authors demonstrate that the magnitude of the sink is linked to the concentration of bioavailable iron and point out ice cover as an important reservoir, releasing iron to the water column after melting.

Increases of temperature, stratification and oceanic acidification are expected as a consequence of raising atmospheric CO₂. These changes will have different impact on planktonic communities and hence on biogeochemical cycles. In regions such as the SO which are presently characterized by deep mixing and light limitation, increased stratification should favor algal growth, but since it reduces supply of nutrients (including iron) to surface waters it could affect the efficiency of the biological carbon pump due to a shift from diatoms towards pico-nanophytoplankton. On the other hand, rising temperatures will increase remineralization efficiency, thereby likely enhancing bioavailability of iron. Increased temperature and light will also affect the biogeography of phytoplanktonic groups, and it is probable for instance, that phytoplanktonic calcifiers, which usually thrive in warmer waters, will spread southwards (Winter et al., 1999; Cubillos et al., 2007; Holligan et al., 2010). The carbonate-forming organisms are important for their role in the downward transport of particulate and inorganic carbon.

However this transport by coccolithophorids, foraminifera and potentially other pelagic organisms such as pteropods, is likely to be affected by increased oceanic acidification (lowered pH subsequent to increase of both atmospheric and oceanic CO₂ concentration) that will decrease production of calcareous phytoplankton by lowering calcification rate (Riebesell et al., 2000; Moy et al., 2009; Fabry et al., 2009), and also affect the plankton community structure (Tortell et al., 2002; 2008). Bottle and mesocosm experiments indicate that main effects of oceanic acidification are: shifts in natural assemblages; increased carbon export associated to coccolithophorids due to increased production of transparent exopolymer particles (TEP) and changes in the inorganic over organic carbon ratio of exported matter (e.g. Delille et al., 2005a). Overall it is expected that carbon export to the deep sea will decrease (Laws et al., 2000; Heinze, 2004).

Iron cycling and control of carbon and nutrient export: adding complexity to an already complex scheme

The pivotal role of iron in regulating rates of primary production and the flux of carbon and nutrients to the deep sea has become increasingly apparent in the past 15 years. Significant improvements in our understanding of the role of iron in regulating ecosystem processes have been made (see de Baar et al., 2005). The addition of Fe stimulates the large class of algae, in particular chain-forming diatoms (de Baar and Boyd, 2000; Boyd et al., 2007). Some species of diatoms and the non-siliceous haptophyte *Phaeocystis* adapt their morphology in function of the available Fe, in order to reduce surface to volume ratio and avoid diffusion-limited supply (Timmermans et al., 2001). The response of heterotrophic bacteria to iron supply has been shown to be indirect due to the supply of larger quantities and/or better quality of organic substrates resulting from iron-enhanced phytoplankton production. (e.g., Church et al., 2000; Becquevort et al., 2007).

It is now known that >99% of the dissolved iron in the upper ocean is strongly complexed by organic molecules (e.g. Wu and Luther, 1995). More evidence is given that not only dissolved inorganic species of Fe are bioavailable but that dissolved as well as colloidal organically-complexed Fe can be available and that the nature of the ligands also plays an important role in controlling Fe bioavailability (e.g. Chen et al., 2003). Phytoplankton and bacteria have a complex array of Fe acquisition systems such as siderophores, membrane reductases, ligand production, and mixotrophy/phagotrophy. Processes such as photochemistry clearly cause redox cycling of iron between different chemical species, thereby increasing bioavailability. Such processes are generally not included yet in biogeochemical models. Further, it is recognized that organisms can increase their iron uptake capacity in response to iron stress, and are capable of luxurious iron uptake. Some phytoplankton species like *Phaeocystis* can accumulate Fe in their mucus, which may constitute storage of Fe in case it becomes limiting (Schoemann et al., 2001, 2005).

Nowadays a better understanding of these processes is needed in order to evaluate their implications in determining the planktonic community composition and the associated biogeochemical cycles. It also is important to understand how climate change will impact the processes acting on the Fe-cycle. Shi et al. (2010), for instance, report a decline in Fe bio-availability to diatoms and coccolithophorids as a result of ocean acidification.

Of further particular interest is the verification of the silica leakage hypothesis (Matsumoto et al., 2002; Sarmiento et al., 2004) based on the demonstrated ability of diatoms to silicify less in Fe-replete conditions (Takeda et al., 1998; Hutchins and Bruland, 1998), resulting in an increase of the silicate:nitrate ratio of subducting AAIW and SAMW carrying their unused nutrient load (N, P) into the other major oceanic basins. This process makes the modern S.O. an important nutrient provider sustaining production at lower latitudes (Toggweiler et al., 1991; Sarmiento et al., 2004), therefore impacting at a distance on the global ocean carbon storage capacity.

Fate of exported carbon: the neglected twilight zone

Both dissolved (DOC) and particulate organic carbon (POC) exported from the mixed layer to the deep ocean via the biological pump will be sequestered over time scales of decades or centuries depending on mineralization processes during transfer from surface ocean to the seafloor. Studies of carbon export generally focus on the upper mixed layer (e.g., ^{234}Th -deficit; New Production) or on the deep ocean (fluxes from sediment traps, sediment core tops), while processes in the intermediate waters (Twilight Zone) have been much less investigated, mainly because of technical limitations. Today there is a lack of information on the fate of organic carbon in intermediate waters, and biogeochemical models seeking to develop a predictive representation of the fluxes and material transformations in the mesopelagic layer need to include information about the depth dependence of nutrient mineralisation and the factors that control it (see IMBER Science plan). Improving the characterisation of these processes should lead to a better estimation of the responses of export production and deep ocean remineralisation to climate change. Armstrong et al. (2002) proposed a model indicating that bio-minerals (opal, carbonate) act as ballast of sinking particles and control mineralization length-scales in the water column. François et al. (2002) and Klaas and Archer (2002) point out carbonates as main controllers of deep ocean carbon export, while ballasting of sinking aggregates by diatoms would lead to shallow mineralization. Deep POC fluxes from the S.O. (WOCE SR3 line; Australian sector) corroborate this picture. Deep fluxes were larger in the Subantarctic Zone (no diatom dominance) relative to the Polar Front Zone (diatom dominance) (Trull et al., 2001) whereas export from the surface exhibited the inverse pattern (Elskens et al., 2002; Savoye et al., 2004). Particulate mesopelagic excess-Ba (meso-Ba_{xs}), a proxy for mesopelagic mineralization (Dehairs et al., 1997), showed that POC mineralisation is up to 4 times higher in the PFZ where diatoms dominate, as compared to the SAZ, where other phytoplankton, including coccolithophorids and dinoflagellates, were dominant (Cardinal et al., 2005a). However, it is unclear to what extent conclusions drawn from a single transect can simply be extrapolated to the whole S.O. . A multi-proxy approach integrating physical and biogeochemical processes from surface to deep ocean is therefore necessary to assess export and fate of carbon.

Physical and biological resolution of existing ice-ocean biogeochemical models: success and caveats

To our knowledge none of the published models satisfactorily describes the cycling of carbon and biogeochemical elements at the seasonal and circumpolar scale.

A comparative review of zonally-integrated air-sea fluxes of anthropogenic CO₂ obtained by 12 Global Ocean Biogeochemical Models (Watson and Orr, 2003) reveals large uncertainties in the magnitude of the S.O. CO₂ sink. These uncertainties are partly due to insufficient description of some physical processes (e.g. surface layer definition, tide effects, bottom topography...) but mostly to low trophic resolution of biogeochemical models and insufficient description of the processes involved in iron cycling.

Ice-ocean models are now able to simulate reasonably well the large-scale characteristics of the SO. For instance, using the coupled ice-ocean model ORCALIM which results from the coupling of the Louvain-la-Neuve sea ice model (LIM) (Fichefet and Morales Maqueda, 1997) with the hydrostatic, primitive equation ocean model OPA (Océan PARallélisé; Madec et al., 1999) driven by NCEP/NCAR reanalysis, we obtained a reasonable climatology of ice cover and surface oceanic circulation. Interannual variability of ice cover is also in good agreement with observations and the ice-ocean processes responsible for this variability appear realistic (Timmermann et al., 2004; 2005; Lefebvre et al., 2004). Nevertheless, ice-ocean models still have trouble to correctly represent ventilation processes, such as formation of dense water over the continental shelf and its export to the deep ocean, or the amplitude of the seasonal cycle of the mixed layer depth, with a potential impact on the simulation of physical and biological mechanisms driving the ocean carbon cycle. Current atmosphere-sea-ice-ocean general circulation models (AOGCM's) appear to have more trouble to simulate Southern Ocean ice cover and large differences are obtained when analyzing the results of different models (e.g. Arzel et al., 2006). This is related to the fact that, in contrast to ice-ocean models driven by reanalysis, the full atmosphere-ocean-ice system is now free to evolve and any inaccuracies in the representation of the state of one of those three media has an impact on the other ones and would trigger feedbacks that may lead to large discrepancies between model and observations.

Biogeochemical models of higher complexity and including explicit or implicit iron parameterizations have been developed specifically for the S.O. over the last decade. These have been applied either locally in a 1D vertical frame (Polar Front: e.g. Fennel et al., 2003; Permanently Open Ocean Zone: e.g. Moore et al., 2002; Marginal Ice Zone: e.g. Lancelot et al., 1991, Hecq et al., 2000) or regionally (Ross Sea: 3D CIAO model of Arrigo et al., 2003). These models are all bottom-up based, closed at the level of mesozooplankton and consider light and iron co-limitation. However, they are non-generic and differ in the number of biological variables, biogenic elements and related parameterizations. Among those, only the SWAMCO-4 model (Pasquer et al., 2005) which considers 4 phytoplankton functional groups (diatoms, non-siliceous pico & nanophytoplankton, calcifying coccolithophorids, *Phaeocystis* colonies) and describes the C, N, P, Si and Fe cycling between aggregated biological and chemical compartments of the planktonic food web, will be able to tackle expected shifts in species dominances and related biogeochemical fluxes in response to a changing climate. However, iron parameterisation in the SWAMCO model is rather crude and does not consider interactions between iron and organic matter which are important for determining iron bio-availability. As a result, the 1D application of this model in ice-free and ice-covered latitude reveals a high sensitivity to iron concentration and parameterisation (Pasquer, 2005).

There is need to better parameterize these processes as in the CIAO model (e.g., Tagliabue et al., 2005). Preliminary implementation of SWAMCO-4 in the ice-Ocean model ORCA-LIM (Timmermann et al., 2005) for the area south of 30°S (Pasquer, 2005) also shows that without an additional source of iron (either from above or from below) no bloom can be simulated in regional seas and bays close to the continent. This result highlights the importance of iron storage in the sea-ice resulting from the sea-ice formation process itself and accumulation of atmospheric dust, during the period the ice-cover lasted. With the onset of ice melting Fe is released in the water column, boosting phytoplankton blooms at the ice edge.

Clearly, while over the past few years our general understanding of the processes involved with ocean-atmosphere carbon redistribution in the Southern Ocean has significantly increased, there are still major knowledge gaps left. This situation impedes the proper understanding, not only of crucial modern Southern Ocean biogeochemical and physical processes which impact on climate, but also of mutual feed-backs between them.

The BELCANTO network (**BEL**gian research on **C**arbon uptake in the **ANT**arctic **O**cean) set out at improving the understanding of the S.O.'s role in regulating the climate system. Therefore we applied an integrated methodology that combined process-level studies under laboratory-controlled conditions, field work in key S.O. areas involving direct measurements of core biogeochemical parameters along with an original use of multi-proxies and rate measurements and numerical development and experimentation.

2. METHODOLOGY AND RESULTS

List of the different expeditions involving BELCANTO partners:

EIFEX: The European Iron Fertilization Experiment (EIFEX) took place in late austral summer (Jan.-Mar. 2004 - cruise ANT XXI/3 on board R/V Polarstern) to test the iron hypothesis at the Antarctic Polar Front (APF).

KEOPS: The KEOPS cruise was conducted in the Kerguelen Plateau area (19 Jan.-13 Feb. 2005, aboard R.V. Marion Dufresne II) to investigate the biological pump under natural iron fertilization by the plateau using a multiproxy approach

ISPOL: The ISPOL (Ice Station POLarstern) cruise onboard the RV Polarstern took place in the Western Weddell Sea (68°S, 55°W) near the Antarctic Peninsula in November - December 2004 (spring-summer). During the ISPOL cruise, the RV Polarstern was anchored to a large pack ice floe (few km in size) in order to follow the temporal variations of the physical and biological atmospheric-ice-ocean processes at a drifting station during the transition from austral spring to summer.

SIMBA: The SIMBA (Sea Ice Mass Balance in Antarctica) drifting station experiment was carried out onboard the RV N.B. Palmer between the 1st and 23rd October 2007 in the Bellingshausen Sea (69-71°S, 90-95°E).

ANT XXII/3: The FS Polarstern cruise ANT XXII/3 departed from Cape Town, South Africa, 22 January and ended in Punta Arenas, Chile, 6 April 2005.

SAZ-Sense: The Sub-Antarctic Zone Sensitivity to Environmental Change (SAZ-Sense) cruise (AAV0307 of R/V *Aurora Australis*; Jan. 17 to Feb. 20, 2007; mid-austral summer) was carried out in the Australian sector of the Southern Ocean (43-54°S; 140-155°E) in order to investigate the zonal variability of the productivity and the carbon sequestration potential of the Subantarctic Zone (139-155°E and the Polar Front (54°S).

BONUS-GoodHope: The MD166 BONUS-GoodHope cruise was conducted on board R/V Marion-Dufresne II from Febr. 8, to Mar. 17, 2008 in the Atlantic sector of the S.O. (33.58°S 17.14 °E - 57.33°S 00.02°W).

1. Improved understanding of the iron cycling (WP1)

The synthesis of mesoscale iron-enrichment experiments from 1993-2005 highlights the crucial role of iron due to its control on the dynamics of plankton blooms that subsequently impacts on the biogeochemical cycles of carbon, nitrogen, silicon and sulphur and ultimately influence the earth climate system (Becquevort et al., 2007; Boyd et al., 2007).

The episodic release of bio-available iron from melting sea ice seems an important factor regulating phytoplankton production, particularly ice-edge blooms, in seasonally ice-covered Antarctic waters (Pasquer et al., 2005).

In the East Antarctic, pack ice (September-October 2003) reveals high Fe contents in the sea ice up to two orders of magnitude higher than those in the under-ice seawater (Lannuzel et al., 2007, 2008). During the melting period, Fe inputs to surface waters from sea ice may represent a significant daily total flux into surface seawater. The combined analysis of the organic pools and iron in the sea ice environments give close relationships between iron and organic carbon, showing that most of the Fe in the sea ice is likely bound to organic matter (Schoemann et al., 2008). In oceanic surface waters, more than 99% of dissolved Fe is strongly bound to organic ligands (FeBLs). These FeBLs may increase Fe solubility, retain Fe in the upper ocean, and influence Fe bioavailability. Only certain phytoplankton and bacteria species can develop efficient organic Fe acquisition systems like siderophores, membrane reductases, ligand production and mixotrophy/phagotrophy. This will consequently confer a competitive advantage to those species, having an impact on the microbial community. In turn, the microbial community will determine Fe distribution, speciation and bioavailability. An international workshop addressing the biogeochemistry of iron in the context of global change across marine ecosystems was held in Gothenburg, Sweden (14–16 May, 2008) conclude that future research directions should encompass further in depth characterizations of the different phases (particulate, colloidal, soluble), which may lead to a redefinition of the term dissolved iron. This will also lead to a better structural definition of bioavailable iron (Breitbarth et al., 2010).

The general objective of this workpackage was to acquire a better knowledge of the biogeochemical cycle of Fe and its controlling factors. Specific objectives were to study the availability of different forms of Fe to the micro-organisms and its impact on the microbial community structure and consequently on the biological carbon pump. This was investigated through the set-up of methodology, field observations and shipboard experiments on natural sympagic and planktonic communities.

Methodological developments

Measurement of dissolved iron

In collaboration with J. de Jong (IPE, ULB) a robust and simple method to determine seawater dissolved iron (DFe) concentrations down to <0.1 nM was developed. The method is based on isotope dilution multiple collector inductively coupled plasma mass spectrometry (ID-MC-ICP-MS) using a ^{54}Fe spike and measuring the $^{57}\text{Fe}/^{54}\text{Fe}$ ratio (de Jong et al., 2008). The protocol includes a pre-concentration step (100:1) using micro-columns filled with NTA resin Superflow, which are loaded with 50 mL seawater samples acidified to pH 1.9. NTA Superflow is demonstrated to quantitatively extract Fe from acidified seawater samples at this pH. Blanks are kept low (grand mean 0.045 ± 0.020 nM, $n = 21$, $3 \times \text{S.D.}$ limit of detection per session 0.020–0.069 nM range), as no buffer is required to adjust the sample pH for optimal extraction, and no other reagents are needed than ultrapure nitric acid, 12mM H_2O_2 , and acidified (pH 1.9) ultra-high purity (UHP) water. We measured SAFe (sampling and analysis of Fe) reference seawater samples Surface- 1 (0.097 ± 0.043 nM) and Deep-2 (0.91 ± 0.17 nM) and obtained results that were in excellent agreement with their DFe consensus values: 0.118 ± 0.028 nM ($n = 7$) for Surface-1 and 0.932 ± 0.059 nM ($n = 9$) for Deep-2.

We also present a vertical DFe profile from the western Weddell Sea collected during the Ice Station Polarstern (ISPOL) ice drift experiment (ANT XXII-2, RV Polarstern) in November 2004–January 2005. The profile shows near-surface DFe concentrations of ≈ 0.6 nM and bottom water enrichment up to 23 nM DFe (**Figure 1.1**).

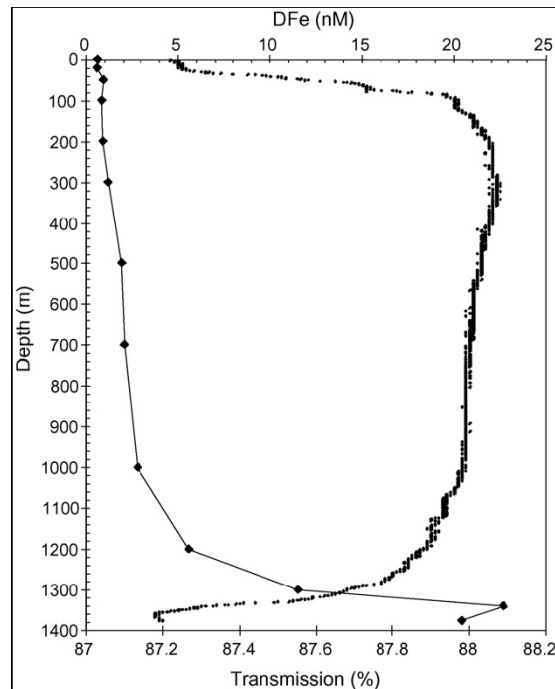


Figure 1.1: Vertical profiles of total dissolved Fe (nM, black diamonds) measured by ID-MC-ICP-MS and transmission (black dots) in the western Weddell Sea at Ice Station Polarstern (ISPOL, ANT XXII/2, station PS67/06-142; Jan. 1st, 2005; 67°22'S, 55°25'W).

Discriminating between intra- and extracellular metals using chemical extractions: an update on the case of iron (Hassler and Schoemann, 2009)

Iron influences the climate system by limiting primary productivity. It is therefore essential to accurately measure the iron fraction associated with phytoplankton in aquatic systems. A washing procedure using EDTA, being efficient for numerous trace metals, is not strong enough to remove iron adsorbed to the surface of microorganisms. Stronger washing solutions are used for iron, but these have only been assessed for a marine diatom. This study assesses the applicability of the oxalate washing procedure for both fresh- and seawater aquatic systems. We assessed iron solubilization as a result of oxalate washing in both synthetic and natural freshwater and seawater, and we tested it on several model phytoplankton and natural assemblages from Lake Champlain, the Southern Ocean, and the Derwent River estuary. We report the effects of the oxalate solution contact time, concentration, and amendment. Our study shows that 20-min washing provides an efficient measurement of the intracellular phytoplanktonic pool of iron in both freshwater and seawater. The direct amendment of oxalate in the experimental solution presents many advantages that are critical for the measurement of size-fractionated particulate iron. These include fine control of bioaccumulation termination, a significant gain in time, and homogeneity of the washing treatment.

Fe bioavailability and solubility

The impact of Fe bioavailability and solubility on the microbial community structure and consequently on the biological carbon pump was investigated through field observations and shipboard experiments on natural sympagic and planktonic communities. The sampling was conducted in an open ocean area, in the Sub-Antarctic and Polar Front zones, which are not directly influenced by sea ice (SAZ-Sense cruise on board the R.V. *Aurora Australis*, 17 Jan-20 Feb 2007) and in the pack ice zone (SIMBA cruise on board R.V. *Nathaniel B. Palmer* in the Bellingshausen sea, Sept.-Oct. 2007). Additional laboratory controlled experiments were carried out with monospecific cultures of Antarctic algae (diatoms and Haptophyceae).

Field observations

During the SAZ-Sense cruise, 3 process stations were studied (P1, in the SAZ west of Tasmania; SAZ-West; P2 in the Polar Front Zone and P3 in the SAZ east of Tasmania; SAZ-East) characterized by contrasting Fe concentrations and phytoplankton communities. Chl-a concentrations ranged from 0.09 to 0.77 $\mu\text{g L}^{-1}$ in surface waters. Maximum surface Chl-a values were observed at P3, SAZ-East. At P2, a Chl-a maximum (0.23 $\mu\text{g L}^{-1}$) was recorded below the surface, around 75 m. Iron concentrations were higher in the SAZ-East than in the SAZ-West (Lannuzel et al., 2011).

During the SIMBA cruise we sampled two ice stations, 'Bruxelles' (70.24°S, 94.07°W) and 'Liège' (70.05°S, 94.34°W) at 5 day intervals (Tison et al., 2008). Chl a concentration ranged between 1.1 and 25.7 $\mu\text{g L}^{-1}$. Large (>10 μm) algae dominated in sea-ice whereas small algae (0.8 – 10 μm) contributed most to Chl a in surface waters. Total Fe ranged between 2.54-54.74 nM, 0.77-18.65 nM and 0.43-2.20 nM, in sea-ice, brines and water column, respectively. Dissolved Fe ranged between 0.82-30.22 nM, 0.41-12.06 nM and 0.18-0.63 nM in sea-ice, brines and water column respectively. Particulate Fe ranged between 1.49-45.43 nM, 0.31-6.59 nM and 0.17-1.57 nM in sea ice, brines and water column respectively.

Shipboard and laboratory experiments (see publications Hassler & Schoemann 2009, Schoemann et al. in prep.)

To study the impact of Fe bioavailability on plankton community structure and identify functional groups of micro-organisms capable (or not) of utilizing the different forms of Fe, we conducted, we conducted both, shipboard and laboratory experiments. These experiments tested the availability of Fe bound to different types of organic ligands to natural pelagic and sympagic communities and to characteristic Southern Ocean phytoplankton. In parallel, the effect of organic ligands on iron solubility was investigated. Radiotracer experiments using ^{55}Fe (uptake of Fe) and ^{14}C (algal production) and ^3H (bacterial production) combined with model ligands were carried out. During the SAZ-Sense cruise we studied contrasted natural assemblages from the Chl-a maximum depth at the 3 process sites. , During the SIMBA cruise (Bruxelles station) we studied phytoplankton assemblages from the interface between surface water and sea-ice, and from the bottom of the pack ice during 3 successive days (Julian Day 284, 289, 294).

For the latter study a 10 cm slice of bottom ice was cut and melted in 15L of 0.2 μm filtered seawater (*Sartorius* membrane filter cartridge Sartobran 300) in order to avoid an osmotic chock. Laboratory experiments were conducted on four characteristic Southern Ocean phytoplankton species (*Phaeocystis* sp., *Chaetoceros* sp., *Fragilariopsis kerguelensis* and *Thalassiosira antarctica* Comber).

Ethylenediamine tetraacetic acid (EDTA; not tested during SIMBA), desferrioxamine B (DFB), protoporphyrin IX (PIX), glucuronic acid (GLU) and alginic acid (ALG; not tested during SAZ-Sense) were selected as model ligands for shipboard experiments. In the laboratory experiments the organic ligands (L) were selected to represent the groups of hydroxamate (desferrioxamine B, DFB) and catecholate (Galocatechin, CAT) siderophores, porphyrins (protoporphyrin IX, PIX), organic amine (N,N'-Di(2-hydroxybenzyl)ethylenediamine-N,N'-diacetic acid monohydrochloride hydrate, HBED) and saccharides (mono-saccharides: D-Galacturonic acid (GAL), D-Glucuronic acid (GLU), Alginic acid from brown algae (ALG); polysaccharides: Alginic acid from brown algae (ALG), dextran from *Leuconostoc* ssp. (DEX). EDTA is a synthetic well characterized FeBL; DFB and CAT are models for siderophores; PIX for ligands released following lysis and zooplankton grazing; GLU, GAL, DEX and ALG are models for acid mono- and poly-saccharides excreted by micro-organisms or released during lysis or grazing processes.

In order to reveal a potential limitation of iron on planktonic and sympagic microorganisms, the intracellular uptake rates of Fe were compared for each size class for the control and for samples with an Fe enrichment of 1 nM.

During SAZ-Sense the Fe intracellular uptake rates at all 3 process sites (after addition of 1 nM Fe) were higher as compared to the controls (no Fe added) for large and small phytoplankton and bacteria. These results reveal Fe limitation for the whole plankton community, especially at site P1 in the SAZ-west (**Figure 1.2**).

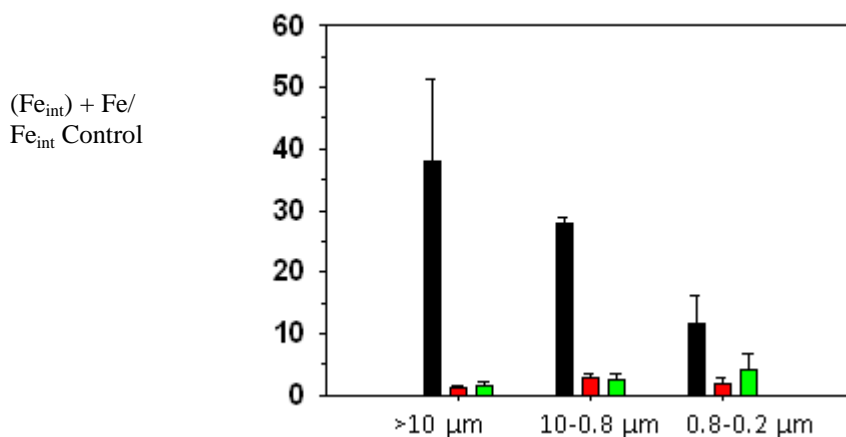


Figure 1.2: SAZ-Sense cruise. Intracellular Fe uptake rates after addition of 1 nM Fe at the 3 process sites, relative to controls (no Fe added) for large (> 10 μm) and small phytoplankton (10-0.8 μm) and procaryotes (0.8-0.2 μm).

Contrasting with these findings, algae and bacteria in the pack ice zone did not appear Fe limited at all times. For the large and small pelagic phytoplankton and bacteria no significant difference in intracellular Fe uptake rate was noticed after addition of 1 nM and sometimes uptake rates were even lower than controls, except on JD 284 when a clear increase of uptake rate was observed for the large phytoplankton (**Figure 1.3a**). On the other hand, for the sea-ice community similar Fe uptake rates were observed for large, Fe supplied, cells compared to controls, whereas for small algal cells and bacteria, Fe uptake rates increased when Fe was added (**Figure 1.3b**).

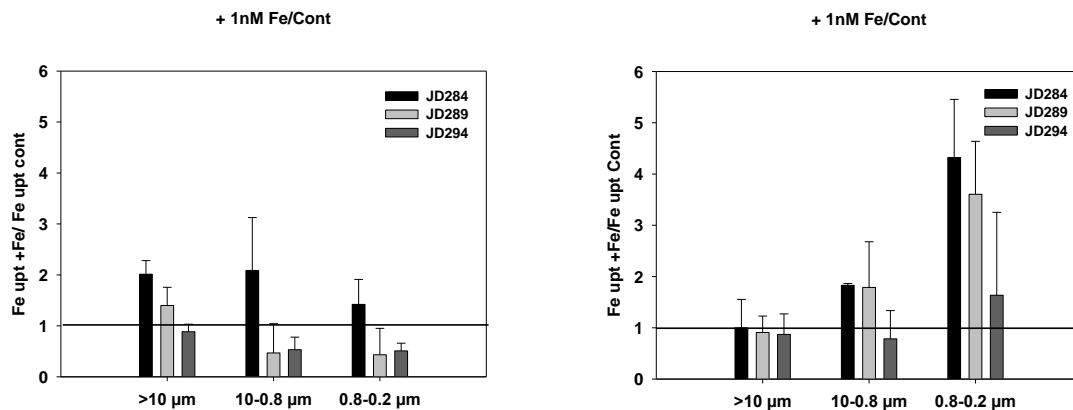


Figure 1.3: SIMBA cruise. Intracellular Fe uptake rates after the addition of 1 nM Fe at 3 Julian days (Bruxelles station) relative to controls (no Fe added) for large (> 10 µm) and small phytoplankton (10-0.8 µm) and prokaryotes (0.8 – 2 µm). (A) Planktonic organisms. (B) Sympagic organisms in filtered seawater.

In the growth experiments conducted on the four phytoplankton species (*Phaeocystis* sp., *Chaetoceros* sp., *Fragilariopsis kerguelensis* and *Thalassiosira antarctica* Comber), the bioavailability of organic forms of Fe appeared related to intracellular Fe uptake rates. The addition of Fe (1 nM) resulted in increased bioavailability as attested by higher intracellular and extracellular Fe for all strains. The intracellular Fe uptake rates (0.4 to 3.3×10^{-18} mol cell⁻¹ h⁻¹) and the corresponding Fe_{ext}: Fe_{int} ratio (1.2 – 1.8) in S.O. seawater (control treatment) were similar to those reported by others (e.g., Hudson and Morel, 1989; Hutchins et al., 1999). The increase in cellular iron pools for a 1 nM Fe addition, also suggested that both transport and non-specific cellular Fe sites were not saturated in the control treatment for all the studied strains (e.g., Wilkinson and Buffle, 2004) (**Figure 1.4**).

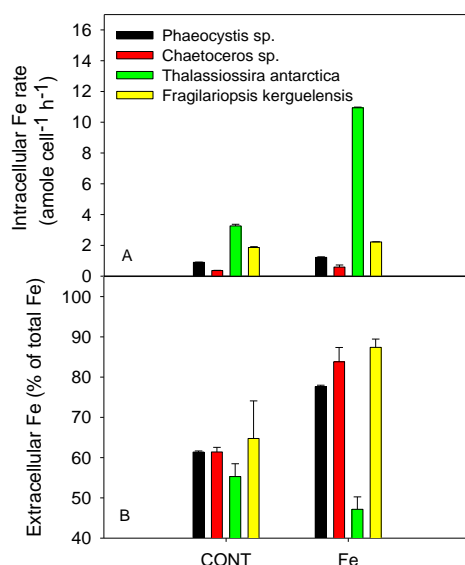


Figure 1.4: ISPOL cruise. Intracellular Fe uptake rates (A) and % of extracellular Fe (B) for *Phaeocystis sp.*, *Chaetoceros sp.*, *Thalassiosira antarctica* and *Fragilariopsis kerguelensis* in filtered water (CONTROL treatment) and with 1 nM Fe enriched seawater (Fe treatment). Both intracellular and extra-cellular Fe is expressed on a cellular basis. Error bars represent half of data interval (n=2).

The addition of various Fe - organic ligands had a different effect on the intracellular Fe uptake rates compared to the enrichment experiment without organic ligands (Figures 1.5, 1.6, 1.7 & 1.8). All natural microbial communities revealed that some model Fe ligands resulted in decreased Fe bioavailability (i.e. EDTA, DFB), whereas other ligands (PIX, GLU, ALG) favoured Fe bioavailability (Figures 1.5, 1.6 and 1.7). However, the stimulation and/or inhibition by different ligands was not constant over time, implying complex interactions between Fe, organic compounds and micro-organisms. In general, the highest stimulation of Fe uptake after addition of Fe bound to saccharides and protoporphyrin are observed for large (> 10 μm) cells.

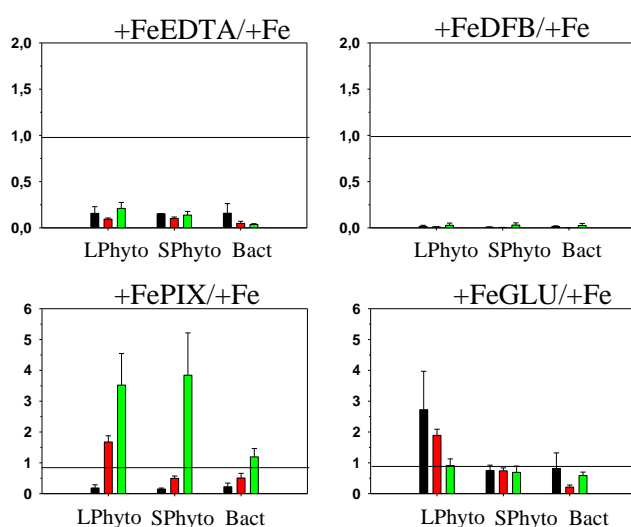


Figure 1.5: SAZ-Sense cruise. Fe uptake rates of planktonic organisms after addition of Fe bound to model ligands relative to control (addition of 1 nM of inorganic Fe) for large (> 10 μm) and small (10-0.8 μm) algae and bacteria (0.38-0.2 μm). Black = P1, SAZ-West; red = P2, PFZ; green = P3, SAZ-East.

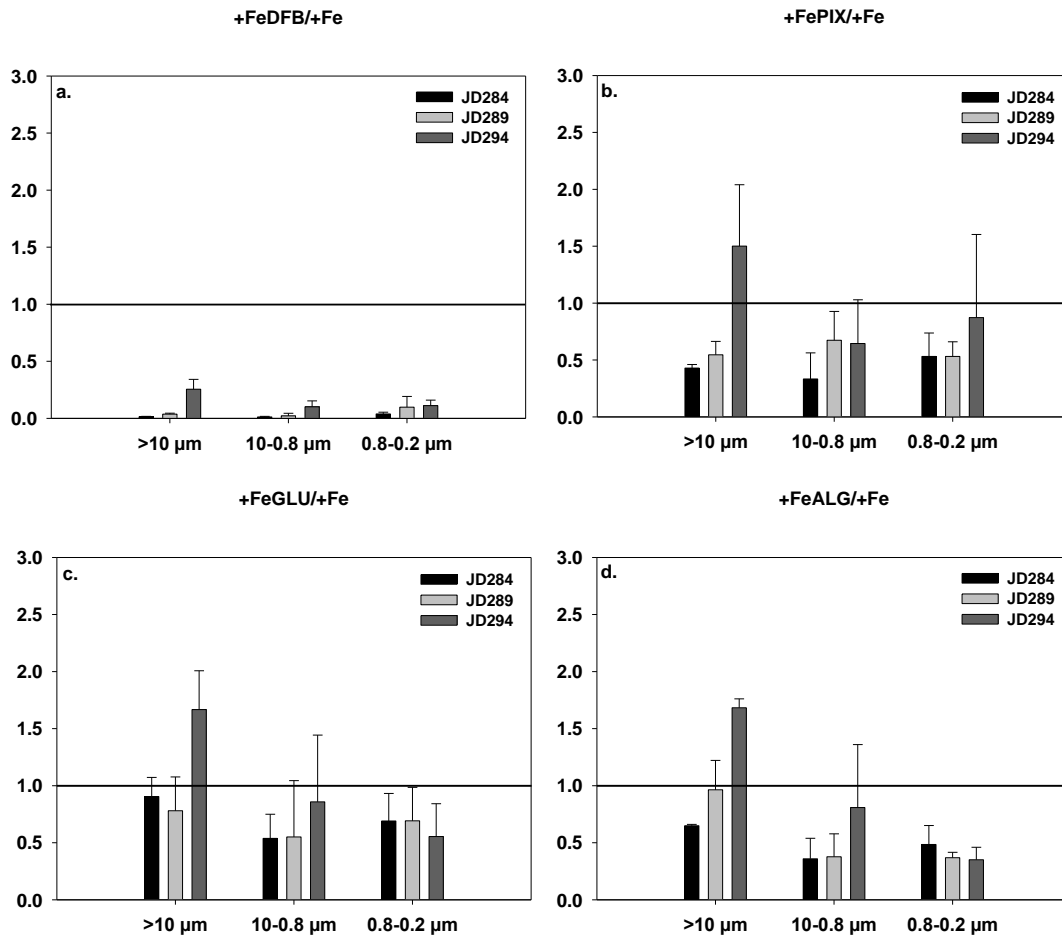


Figure 1.6: SIMBA cruise. Fe uptake rates of microbial copumunities after addition of Fe bound to model ligands relative to the control (the latter with addition of 1 nM inorganic Fe without organic ligands) for large (> 10 μm) and small (10-0.8 μm) cells and bacteria (0.8-0.2 μm).

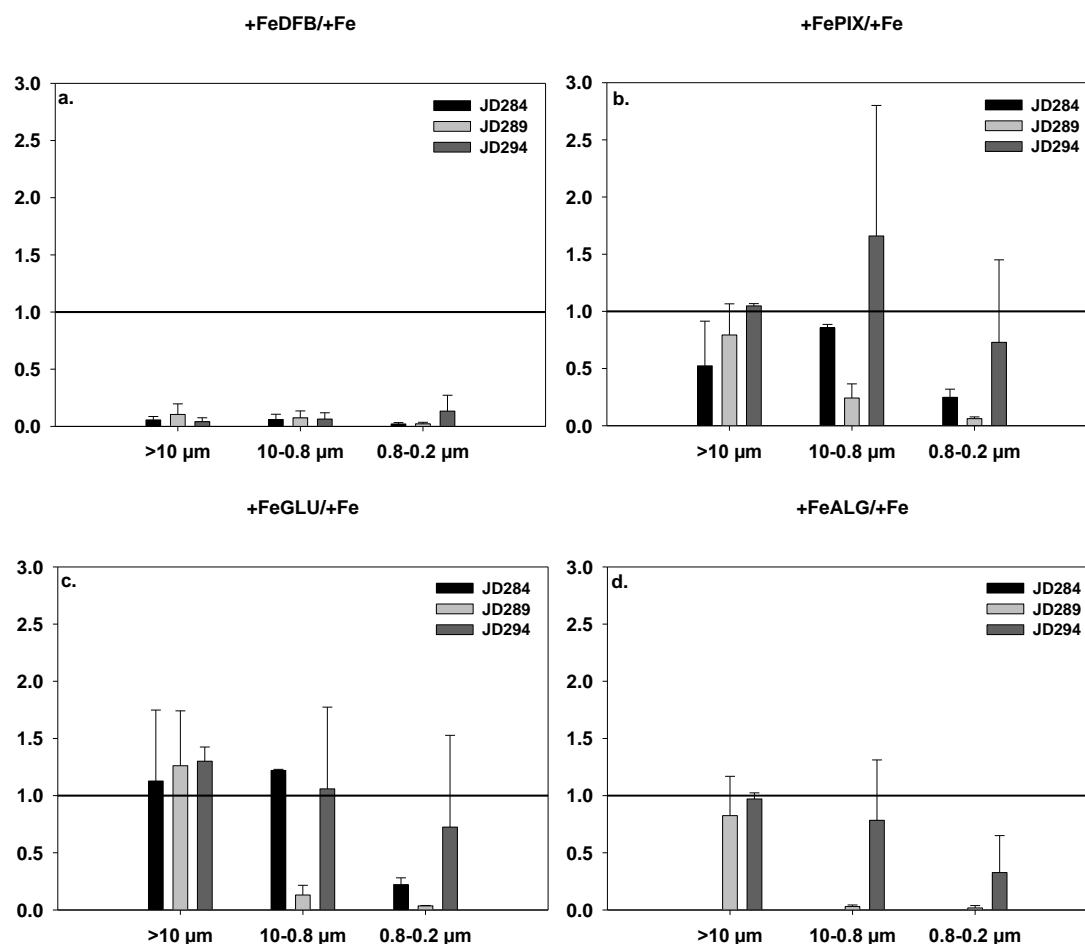


Figure 1.7: SIMBA cruise. Fe uptake rates of sympagic organisms after addition of Fe bound to model ligands relative to the Control (the latter with addition of 1 nM inorganic Fe without organic ligands) for large (> 10 μm) and small (10-0.8 μm) cells and bacteria (0.8-0.2 μm).

Results of laboratory experiments show that for all strains studied Fe bioavailability can be enhanced in the presence of porphyrin, catecholate and saccharides whereas it is decreased in the presence of hydroxamate (HBDE) and organic amine(DFB) (Figure 1.8).

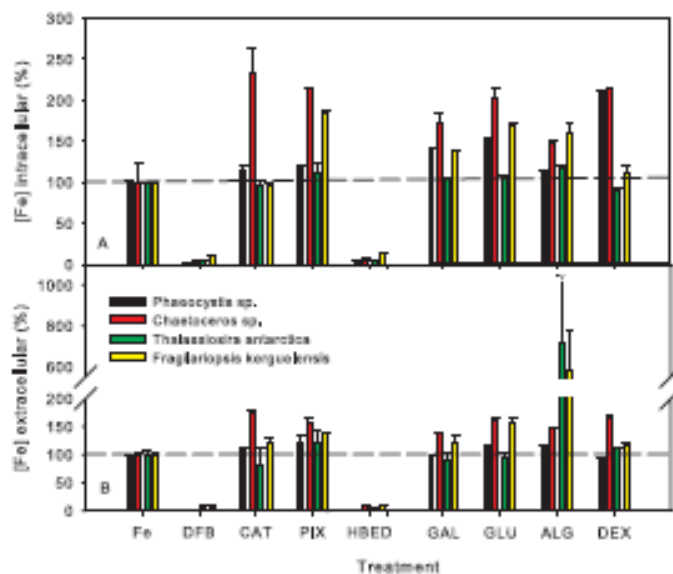


Figure 1.8: Intracellular Fe uptake rates (A) and extracellular Fe (B) for *Phaeocystis* sp., *Chaetoceros* sp., *Thalassiosira antarctica* and *Fragilariopsis kerguelensis* in filtered seawater enriched with 1 nM Fe (Fe treatment) and 15 nM organic ligands (desferrioxamine B = DFB; Gallic catechin = CAT; protoporphyrin IX = PIX; N,N’Di(2hydroxybenzyl)ethylenediamine-N,N’-diacetic acid monohydrochloride hydrate = HBED; D-Galacturonic acid = GAL; D-Glucuronic acid = GLU; Alginic acid from brown algae = ALG; dextran from *Leuconostoc* ssp. = DEX). Both intracellular and extracellular Fe was expressed in % of the Fe-only treatment (i.e., without organic ligand addition) on a cellular basis. The dashed line represents results for the Fe-only treatment (100%). Error bars represent half of data interval (n=2).

The addition of ligands will affect Fe bioavailability, but also its overall solubility. In this study, Fe solubility was assessed by discriminating between particulate (>0.2 μm) (not measured in field environments), colloidal Fe (0.02–0.2 μm) and soluble Fe (<0.02 μm) following sequential filtration of the seawater (Figures 1.9 & 1.10) in the absence of microorganisms.

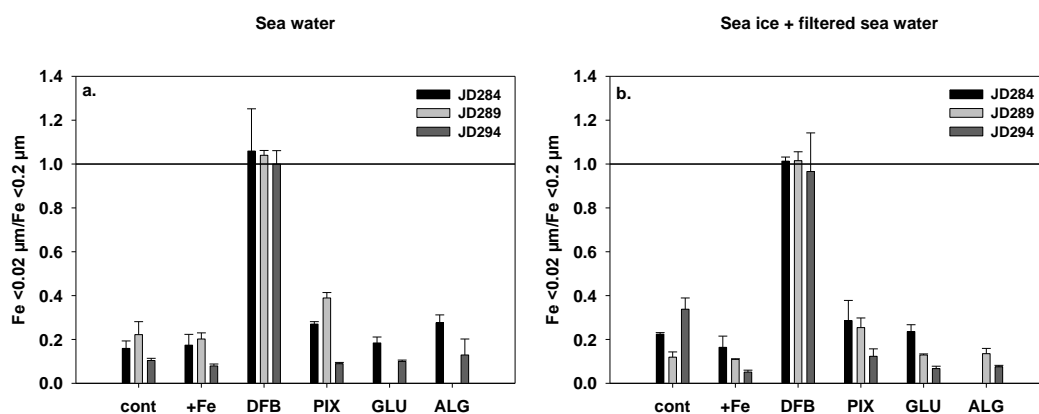


Figure 1.9: SIMBA cruise. Ratio of soluble Fe (Fe < 0.02 μm) to total dissolved Fe (Fe < 0.2 μm) after addition of iron and ligands.

Figure 1.9 shows the ratio of soluble Fe (Fe <0.02 μm) to total Fe dissolved pool (Fe < 0.2 μm) for each addition of ligands in natural environments (SIMBA cruise). In the control treatment, most of the Fe is in the colloidal phase (0.2-0.02 μm).

In both environments (i.e., seawater and sea ice melted in filtered seawater) addition of 1 nM Fe slightly decreased Fe solubility as compared to the control.

In general, the presence of the different ligands (except DFB) resulted in Fe being mostly in the colloidal fraction.

In the laboratory experiments the addition of the different ligands to ISPOL seawater (without any micro-organisms) also controlled iron solubility (**Figure 1.10**). In the Fe treatment, both soluble and colloidal Fe decreased as compared to the control. The addition of 1 nM Fe increased the concentration of particulate Fe. For an addition of 1 nM Fe together with organic ligands, particulate Fe remains lower than in the Fe treatment, except in the presence of ALG. In the presence of DFB and HEBD Fe is fully relocated within the soluble phase. For the other ligands (except ALG) the soluble and colloidal Fe fraction is increased as compared to the Fe treatment, to a level close to what is observed in natural water (control).

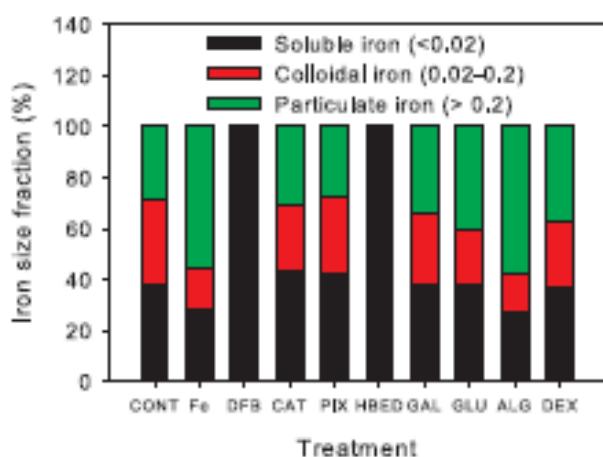


Figure 1.10: Average Fe size distribution following successive filtration on 0.2 and 0.02 μm of the seawater in absence of micro-organisms. Colloidal Fe is defined as <0.2–0.02 μm and soluble Fe as <0.02 μm . Experimental treatments are filtered Antarctic seawater without (CONT) and with an Fe enrichment (1 nM Fe); an Fe enrichment together with 15 nM organic ligands: desferrioxamine B (DFB), Gallocatechin (CAT), protoporphyrin IX (PIX), N,N'-Di(2-hydroxy benzyl) ethylene diamine-N,N'-diacetic acid monohydrochloride hydrate (HRED), Dgalacturonic acid (GAL), D-Glucuronic acid (GLU), Alginic acid (ALG) and dextran (DEX).

In conclusion, given the ubiquitous presence of saccharides in the ocean, these compounds might represent an important factor controlling the basal level of soluble and bioavailable Fe. Thus, the importance of saccharides on iron bioavailability in the ocean needs to be investigated further, especially with natural plankton communities. In addition, further studies are required to understand the mechanism by which saccharides can promote iron bioavailability to phytoplankton. Results presented here demonstrate that the use of model phytoplankton is promising for improving our mechanistic understanding of Fe bioavailability (in presence of natural or model organic ligands) and of primary productivity in HNLC regions of the ocean. This study also formulates considerations about the controls that Fe might have on the species distribution observed in the S.O. The differential effect organic ligands have on the solubility and the bioavailability of Fe shows that no direct link exists between soluble and bioavailable Fe. In fact, colloidal Fe seems to be an important pool to sustain Fe bioavailability.

2. Nutrient consumption, CO₂ uptake and C export (WP2)

2.1. Seasonally integrated Si and N utilization

Methods

Some major methodological contributions have been carried out to improve the measure of the isotopic signatures of Si ($\delta^{30}\text{Si}$) and N ($\delta^{15}\text{N}_{\text{NO}_3}$ and $\delta^{18}\text{O}_{\text{NO}_3}$) which were needed before we can apply these tools to quantify Si and N utilizations:

1/ For Si isotopes, an upgrade of the mass spectrometer and a new methodology allows now measurement of the three Si isotopes (instead of 2 for the original method; Cardinal et al., 2003). This method, published in Abraham et al. (2008) improves the sensitivity and the direct comparison of our results with other teams. This new method has been used for EIFEX (Cavagna et al., 2011), KEOPS (Fripiat et al., 2011) and BONUS-GoodHope samples. We also contributed significantly to the set-up and follow-up of the first inter-comparison of $\delta^{30}\text{Si}$ measurements in which eight institutions worldwide participated. The results have show that all groups are able to determine $\delta^{30}\text{Si}$ accurately at ± 0.2 ‰ (Reynolds et al., 2007). This new method has been applied for EIFEX (Cavagna et al., 2011), KEOPS (Fripiat et al., 2011) and BONUS-GoodHope samples. We also contributed to a GEOTRACES intercalibration exercise.

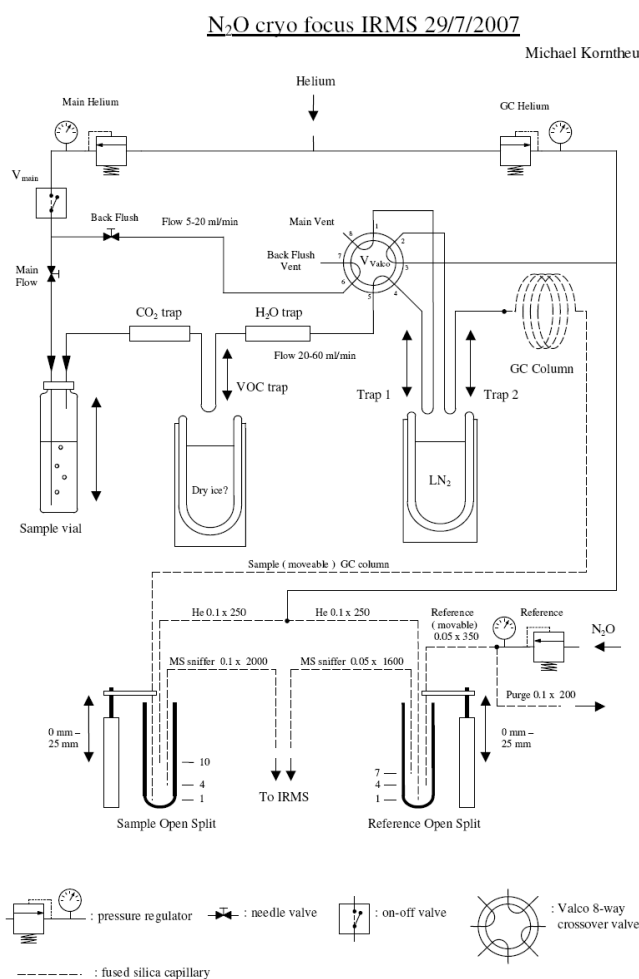


Figure 2.1.1: Schematic of the cryo-focusing system which was build for the analysis of $\delta^{15}\text{N}_{\text{NO}_3}$, $\delta^{18}\text{O}_{\text{NO}_3}$

2/ We implemented the denitrifier method for N and O isotopic composition of nitrate; a method originally elaborated by Casciotti et al. (2002) and Sigman et al. (2001). PhD student P. Mangion was trained in the laboratory of K. Casciotti at WHOI, and subsequently M. Korntheuer, IRMS technician at VUB, built the necessary hardware, consisting of an automatic sampler, the cryo-focusing system and the open-split interface connecting the sampling line to the IRMS (see **Figure 2.1.1**). Method validation was then completed on our analytical set up. Reproducibility (1σ) was always below 0.3‰ for $\delta^{15}\text{N}$ ($n=20$) and below 0.4 ‰ for $\delta^{18}\text{O}$ ($n=5$), which is consistent with standard deviations reported by others using this same technique. Accuracy obtained on the analyses of IAEA N3 reference material was ~ 0.1 ‰ ($n=20$).

Proxy calibration

The extent of Si isotopic fractionation during silicon uptake by diatoms is represented by the fractionation factor, $^{30}\epsilon$. From *in vitro* incubations of tropical diatoms De la Rocha et al., (1997) estimated $^{30}\epsilon$ as 1.1 ± 0.4 ‰. To improve this estimate (which has a quite large uncertainty) and to check its validity for the Antarctic Circumpolar Current we used data from our three in situ studies (Cardinal et al., 2005; Fripiat et al., 2011, Cavagna et al., 2011) and the work of Varela et al. (2004). The average $^{30}\epsilon$ value we obtained for the ACC is 1.2 ± 0.2 ‰. Since the data base used to deduce the latter $^{30}\epsilon$ value includes also data from the artificial Fe-fertilisation EIFEX experiment (Cavagna et al., 2011) we can conclude that the fractionation factor is unaffected by iron availability. Moreover, our results for the CLIVAR-SR3 cruise (SR-3 transect between Tasmania and Antarctica; spring 2001) show there is no significant systematic variation of diatom $\delta^{30}\text{Si}$ signature with size (Cardinal et al., 2007), nor probably with species.

Low temperature (1, 3, and 7°C) growth experiments under different conditions of $\text{Si}(\text{OH})_4$ availability (40 and 70 μM) were carried out using three different Antarctic diatom species (*Chaetoceros brevis*, *Chaetoceros dichaeta*, *Thalassiosira antarctica*). The average $^{30}\epsilon$ obtained was 1.6 ± 0.4 ‰, similar to the value reported by Milligan et al. (2004). Though our value is larger, it is not significantly different from the one of De La Rocha et al. (1997). Both in vitro $^{30}\epsilon$ averages have larger standard deviations than the one based on in-situ studies. The in-vitro results indicate there are no significant effects of temperature, species or Si contents, so far (a remaining 6 of the 17 incubations have yet to be analyzed, along with some replicates). Once all the $\delta^{30}\text{Si}$ data will have been acquired we will discuss our results with regard to the Si cell cycle (Martin-Jézéquel et al., 2000), influx vs. efflux, and dissolution which are the potential key factors controlling Si isotopic fractionation (Milligan et al., 2004; Cardinal et al., 2007; Demarest et al., 2009).

Identification of Si sources and quantification of Si fluxes

As a result of sustained efforts to improve calibration of the Si-proxy and further develop analytical know-how we were able to achieve one of our main goals: the use of modern ocean natural stable Si isotopic signatures for reconstructing seasonally integrated Si utilization. We applied it in two case-studies in the High Nutrient Low Chlorophyll (HNLC) waters of the Southern Ocean (Antarctic Zone):

- Indian Sector: HNLC area off Kerguelen Islands (KEOPS cruise, summer 2005, $\sim 50^\circ\text{S} - 75^\circ\text{E}$) (Blain et al., 2007)
- Atlantic Sector: in an eddy detached from the Polar Front with water masses characteristic from the northern part of the AZ (EIFEX cruise, summer 2004 $\sim 50^\circ\text{S} - 2^\circ\text{E}$) (Hoffmann et al., 2006; Cisewski et al., 2008)

Si isotopic signatures of the HNLC stations from these two studies show that:

- The ultimate source of Si to the Mixed Layer is the Upper Circumpolar Deep Water (UCDW), supplying Si to the Antarctic Surface Water (AASW) mainly via winter mixing (**Figure 2.1.2**). During spring this layer subdivides through stratification into the (summer) Mixed Layer and the Winter Water below.
- Summer ML, WW and UCDW fit perfectly the mixing line for each cruise (**Figure 2.1.2**) what is evidence for a WW supply of Si to the mixed layer.
- From **Figure 2.1.2** the relative mass contribution of the UCDW to the AASW can be estimated at 78 ± 12 % of the Si(OH)_4 standing stock for KEOPS and 79 ± 16 % for EIFEX.

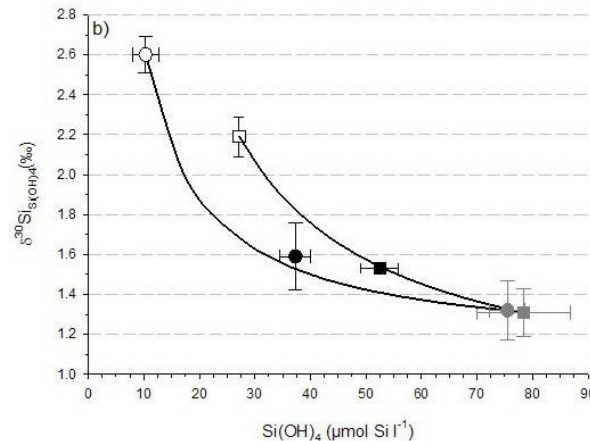


Figure 2.1.2: $\delta^{30}\text{Si}_{\text{Si(OH)}_4}$ vs. $[\text{Si(OH)}_4]$ for the different Si-pools in the HNLC area ($\pm 1\text{sd}$) during KEOPS (Fripiat et al., 2011) and EIFEX for waters inside the eddy but outside the fertilized patch (Cavagna et al., 2011). Mixing curves are drawn between HNLC ML and UCDW. Squares = KEOPS; Circles = EIFEX; White = ML; Black = WW; Grey = UCDW.

- For the HNLC waters of the Indian sector around Kerguelen (KEOPS) the UCDW supply to the mixed layer via the AASW, is estimated to reach 4.0 ± 0.7 mol Si $\text{m}^{-2} \text{yr}^{-1}$. Assuming steady state on an annual time scale this net annual Si-supply should be equivalent to the net annual bSiO_2 production. This value is higher than the seasonal depletion estimated from a simple mass balance calculation for the mixed layer (2.5 ± 0.2 mol Si $\text{m}^{-2} \text{yr}^{-1}$). The difference between the two fluxes provides an estimate of the Si-supply (1.5 ± 0.7 mol Si $\text{m}^{-2} \text{yr}^{-1}$) which likely occurs during the stratification period.
- For the eddy isolated from the Polar Front in the Atlantic sector (EIFEX) the UCDW Si-supply to the ML is estimated at 2.9 ± 0.6 mol Si $\text{m}^{-2} \text{yr}^{-1}$, what is significantly lower than observed during KEOPS. The seasonal Si-depletion is estimated at 2.7 ± 0.4 mol Si $\text{m}^{-2} \text{yr}^{-1}$, what is not significantly different from the annual UCDW Si-supply. So in the latter case seasonal Si-depletion seems to agree well with net bSiO_2 production (equated to the UCDW supply of Si), suggesting there was no significant Si-supply from upwelling or advection during the stratification period.

- Nevertheless, based on the temporal $\delta^{30}\text{Si}$ variations of $\text{Si}(\text{OH})_4$ and bSiO_2 during EIFEX (the experiment lasted 38 days) we calculate a small Si supply from Winter Water to the ML. We used the steady-state model (Sigman et al. 1999) and took initial conditions for WW which was considered the Si source (**Figure 2.1.3**). From this temporal approach a supply of $6.5 \pm 1.1 \text{ mmol Si m}^{-2} \text{ d}^{-1}$ was estimated. However, such a small flux is not detectable using the annual balance approach described above.

Biogeochemical cycle of Si in Fe-enriched Southern Ocean waters

Above we presented the main results for those EIFEX and KEOPS sites which are characteristic for the HNLC Southern Ocean (i.e., where Fe is depleted). However, EIFEX and KEOPS were actually designed to study the impact of Fe fertilization (natural Fe supply for KEOPS, artificial Fe supply for EIFEX) on the carbon and silicon cycles (Mosseri et al., 2008; Hoffmann et al., 2006). Below we present the main features for the stations that were located within the bloom areas.

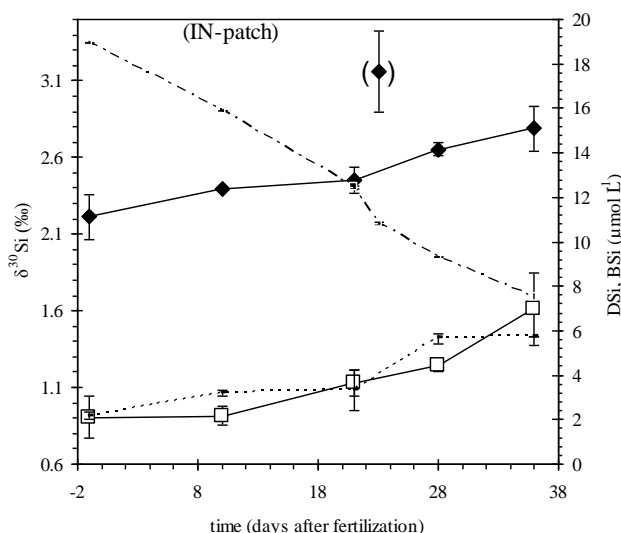


Figure 2.1.3: EIFEX cruise. Temporal variation of $\delta^{30}\text{Si}_{\text{DSi}}$, $\delta^{30}\text{Si}_{\text{BSi}}$, [BSi] and [DSi] in the surface layer (0–50 m) IN-patch. Filled diamonds = $\delta^{30}\text{Si}_{\text{DSi}}$ (‰); Empty squares = $\delta^{30}\text{Si}_{\text{BSi}}$ (‰); dashed line = [BSi] (μM) and solid line = [DSi] (μM). The bracketed data point (= station 544/63) was not considered as part of the temporal trend. (Cavagna, 2010; Cavagna et al., 2011).

- For both the KEOPS and EIFEX diatom blooms our results indicate that the pattern of Si isotopic fractionation is consistent with an open system mode of operation regarding Si supply and can not be reconciled with the one of a closed system (Rayleigh fractionation). This is a firm evidence of continuous Si supply to the ML during the growth season. It is also supported by physics showing that the Kerguelen plateau is a highly dynamic system (Park et al., 2008) and by the fact that vertical diffusivity is significant in a cyclonic eddy as studied during EIFEX (Cisewski et al. 2008). From $\delta^{30}\text{Si}$, it appears clearly that HNLC WW represents the most likely Si source and the initial conditions before the bloom started (not shown). Such type of continuous nutrient supply during the stratification season is however often overlooked or not quantified.

- The Si sources could be identified based on the $\delta^{30}\text{Si}$ signatures. For KEOPS, the ultimate Si source for AASW both on and off plateau is UCDW. Noteworthy, for KEOPS the AASW above the Kerguelen Plateau is ventilated at the seasonal time scale by AASW from the HNLC area. Therefore the AASW Si-composition prevailing at the onset of the growth period must have been similar to the one in the HNLC area, in agreement with the timescale of the prevailing hydrodynamic processes (Venchiarutti et al., 2008; Park et al., 2008).
- Above the Kerguelen Plateau (KEOPS), we estimate a net integrated bSiO_2 production of $10.5 \pm 1.4 \text{ mol Si m}^{-2} \text{ yr}^{-1}$ in the AASW with a significant contribution (max. 38%) of diatoms silicifying in the deep bSiO_2 maximum. Along with silicate pump and iron-light co-limitation, and in agreement with recurrent observations of deep bSiO_2 maximum, such deep silicification where no or less photosynthesis occurs, might contribute to the enhanced depletion of Si(OH)_4 compared to NO_3 , a characteristic feature in the Antarctic Zone. Moreover, the decoupling between $\delta^{30}\text{Si}_{\text{bSiO}_2}$ and $\delta^{30}\text{Si}_{\text{Si(OH)}_4}$ (not shown) suggests that a significant part of the senescent bSiO_2 pool in the Mixed Layer had already dissolved.
- Compared to previous estimates for the Antarctic Zone the Kerguelen Plateau sustained an extremely high integrated net bSiO_2 production (Mosseri et al., 2008) in the higher range of opal export estimates for the Southern Ocean reported by Jin et al. (2006). Natural iron fertilization clearly boosts diatoms productivity as is observed for artificial iron fertilization (see e.g., de Baar et al., 2005).
- For EIFEX, the $\delta^{30}\text{Si}$ values of bSiO_2 and Si(OH)_4 increase during the 37-day monitoring along with a decrease of Si(OH)_4 concentration and an increase of bSiO_2 concentration, reflecting Si uptake by diatoms (Figure 2.1.3). Applying the open-system rationale, we estimate vertical Si-supply ($6.7 \pm 1.2 \text{ mmol Si m}^{-2} \text{ d}^{-1}$) represents $30 \pm 5\%$ of the total amount of consumed dissolved Si. Overall, three processes were acting to control dissolved silicon isotopic signature: biological uptake, Si-supply from a deeper layer, and export of biogenic silica. We estimate the relative utilisation of Si(OH)_4 by the natural bloom prior to the start of the fertilisation at $49 \pm 4\%$ of the initial, early spring silicate stock. As a result of the Fe enrichment a further $31 \pm 4\%$ of the Si(OH)_4 reservoir was consumed. We further estimate a bSiO_2 export of $644 \pm 61 \text{ mmol Si m}^{-2}$ what is in accordance with C-export calculated independently from the ^{234}Th deficit (Jacquet et al., 2008). Such export of Si and C is actually in the average of natural S.O. conditions (cf. § 2.3 and 3.2).

The sea-ice case study

We produced the very first results for Si isotopic composition in Antarctic Sea Ice. The data indicate that diatom activity and the Si dynamics in sea ice vary significantly between different brine structures. The brine channels, their feeder branches, and the intracrystalline brine layers in the skeletal layer represent semi-closed systems where diatoms consume a significant part of the Si(OH)_4 pool (i.e., brine) which is only partially replenished by convection or diffusion with the underlying seawater. The brine pockets and the intracrystalline brine layers trapped in the ice structure behave as closed systems, where a more significant part of the small Si(OH)_4 pool is consumed. In snow ice, the diatoms can be cut off from the nutrient supply initially provided by seawater infiltration and will therefore use a large part of their available dissolved silicon pool.

The silicon-isotopic composition (+1.22 ‰, Fripiat et al., 2007) of the sea-ice diatoms is much heavier than the one of biogenic silica in the seasonal ice zone mixed layer (+0.2 ‰; Cardinal et al., 2007). This pioneer work suggests that sea-ice diatoms either contribute for only an insignificant part of the diatom biomass in the upper water layer, or that they are directly exported below the mixed layer. We propose that the contrasted Si-isotopic signature between sea-ice diatoms and surface seawater diatoms might be used to determine the relative contributions of sea-ice diatoms and pelagic diatoms that bloomed after the sea ice melting to the biogenic silica flux to the deep sea.

Conclusions and perspectives

More information regarding $\delta^{30}\text{Si}$ results can be found in the following papers:

- Cardinal et al. 2005, 2007 (Global Biogeochemical Cycles and Deep-Sea Research) for CLIVAR-SR3;
- Fripiat et al., 2007 for the study on sea-ice;
- Fripiat et al. , 2011 for KEOPS (published in Marine Chemistry) ;
- Cavagna et al. 2011 for EIFEX (published in Limnology & Oceanography).

Overall, these results support the view that the Southern Ocean is a highly dynamic system which strongly influences the Si biogeochemical cycle. Our results call for the preferential use of open-system rather than closed-system approaches for quantitative paleo-reconstructions based on $\delta^{30}\text{Si}$. Our results confirm that Si isotopic signatures provide a powerful constraint for understanding the Si biogeochemical cycle and are useful for the identification of sources and for quantifying fluxes. They largely contribute to Deliverable # 2 (*Sources and isotopic signatures of N and Si in surface waters*) and # 3 (*Time-dependent dynamics of nutrients in surface waters*) of BELCANTO III.

$\delta^{15}\text{N}_{\text{NO}_3}$, $\delta^{18}\text{O}_{\text{NO}_3}$

We implemented the WHOI method for nitrogen and oxygen stable isotope analysis of nitrate (actually nitrate + nitrite). This method is based on the denitrifier approach (Sigman et al., 2001; Casciotti et al., 2002). The method utilises specific strains of denitrifying bacteria that lack nitrous oxide reductase activity and can convert nitrate (and nitrite) into N_2O . The produced N_2O is subsequently analysed via isotope ratio mass spectrometry. We used the *Pseudomonas aureofaciens* strain and prepared working cultures following Casciotti et al. (2002). Analysis vials consisted of 20 mL headspace vials to which 3 mL aliquots of the working culture were added. These vials were then flushed for 3h with N_2 . Samples and/or standards were subsequently injected in the vials and left incubating overnight. Volumes added were adjusted according to the original nitrate concentration so that analysis of samples and standards was done on a similar amount of nitrate. Final nitrate contents targeted were 20 nmoles. This was achieved by adding variable sample volume to the headspace vials. Several international references were prepared and analyzed within the sample run. Reference materials were: IAEA N3, USGS 32, USGS 34 and USGS 35. Bacteria blanks consisting of 3 mL bacteria culture without sample.

N_2O analyses were carried out on an automated N_2O purification and cryo-focusing system connected to a Delta V IRMS (ThermoScientific) and operated under a continuous flow of helium through an open split interface.

A second open split is used for injecting pulses of reference N₂O from a gas cylinder before each analysis. Our home-built analytical set up is similar to the one described by Casciotti et al. (2002). Standard series were analysed at the beginning of the run and after every 10 samples. Blanks were rather small and constant: 0.04 ± 0.01 V (1σ). They represented $\sim 0.5\%$ of the signals for the 20 nmol samples. Averages and reproducibility of the IAEA-N3 reference are 4.68 ± 0.04 ‰ and 25.31 ± 0.10 ‰ for $\delta^{15}\text{N}$ and $\delta^{18}\text{O}$, respectively. Such values reflect the usual reproducibility and accuracy of our routine measurements.

We participated in a GEOTRACES inter-calibration exercise and the outcome presented by K. Casciotti at a GEOTRACES workshop (Old Dominion University, Norfolk, Virginia; 8-10 March 2010) revealed we scored very well. A publication about this intercalibration is in preparation by K. Casciotti.

First results for a few profiles for the BONUS GoodHope expedition (2008) are shown in **Figure 2.1.4**.

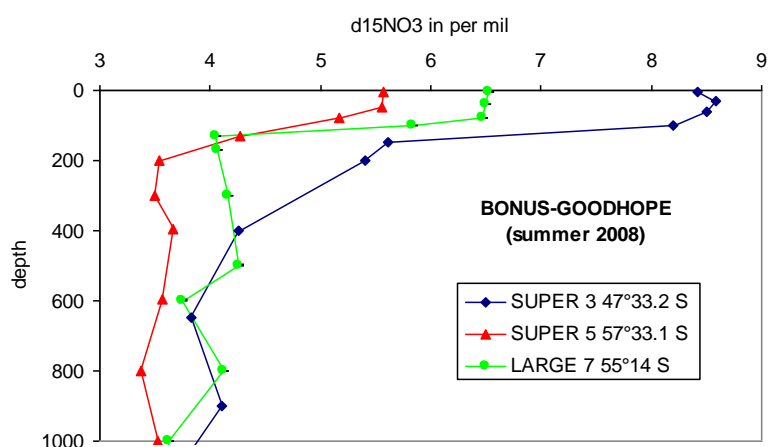


Figure 2.1.4: BONUS-GoodHope. First results of the $\delta^{15}\text{N}_{\text{NO}_3}$ analysis via the denitrifier method. Shown are 3 profiles for stations 'SUPER 3' ($47^\circ 33.2\text{S}$, between SAF and PF); 'LARGE 7' ($55^\circ 14\text{S}$, between the Southern ACC front); 'SUPER 5' ($57^\circ 33.1\text{S}$, northern Weddell Gyre).

Profiles clearly show ^{15}N -enrichment in surface ocean nitrate while isotopic signatures in deep water tend to more constant and lower values. This surface ocean enrichment is due to nitrate consumption as indicated also by the inverse correlation between $\delta^{15}\text{N}_{\text{NO}_3}$ and nitrate concentration (**Figure 2.1.5**). A clear gradient is apparent in surface waters, with ^{15}N enrichment of nitrate increasing northward.

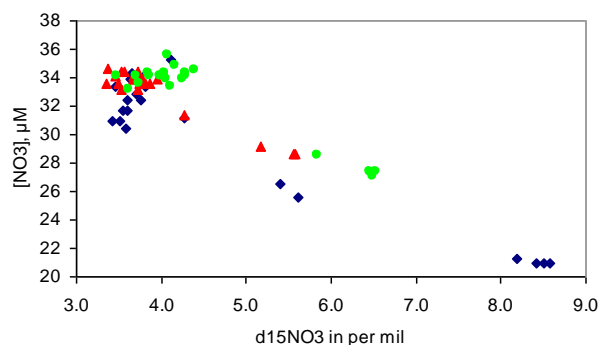


Figure 2.1.5: BONUS-GoodHope: correlation between $\delta^{15}\text{N}_{\text{NO}_3}$ and nitrate concentration

We only show values for $\delta^{15}\text{N}_{\text{NO}_3}$ since seawater samples were acidified to pH 1-2 using HCl. There is discussion as to the impact this acidification has on the $\delta^{18}\text{O}_{\text{NO}_3}$ values. Till 2008 literature results for $\delta^{15}\text{N}_{\text{NO}_3}$ and $\delta^{18}\text{O}_{\text{NO}_3}$ were presented based on acidified seawater samples (see e.g. Sigman et al., 2005; DiFiore et al., 2006), while more recent literature mentions seawater samples are not acidified but preserved deep frozen (e.g., Trull et al., 2008; Sigman et al., 2009). So at present we are unsure whether or not the $\delta^{18}\text{O}_{\text{NO}_3}$ values are valid. We do observe, however, a linear correlation between N and O isotopic composition as expected in case uptake and denitrification are the main processes acting on the nitrate pool (the other important one being nitrification, which breaks down this linear correlation).

As for Si isotopic composition, such results will help in assessing nitrate uptake over seasonal time scales (work in progress).

2.2. Instantaneous Si, N uptake and dissolution

Methods

Regional and seasonal variability of the Si dissolution / production ratios in the surface ocean are but poorly documented (to date only 56 integrated values in ocean are available), mainly because of analytical constraints. Till recently the only way to assess bSiO₂ dissolution in the open ocean was via the ³⁰Si-isotopic dilution technique developed by Nelson and Goering (1977a, b) using TIMS or IRMS. Briefly, the ³⁰Si enrichment of the biogenic silica from a ³⁰Si-spiked, and incubated seawater sample is used to estimate the production rate. The bSiO₂ dissolution rate is deduced from the dissolved phase increase in ²⁸Si resulting from the dissolution of initial biogenic silica (still having the natural isotopic composition). We have developed a new analytical method (Fripiat et al., 2009) for determining these rates with a high-resolution sector field inductively coupled plasma mass spectrometer (HR-SF-ICP-MS; Element 2). Relative analytical precision of the isotopic measurement is better than 1% (**Table 2.2.1**), similar to the one obtained by thermal-ionization-quadrupole mass spectrometry (TIMS).

Table 2.2.1: Triplicates (analysed during the same run) of the same batch of a solution spiked with increasing ^{30}Si amounts. The relative difference between two consecutive solutions prepared is 0.5% and the abundances measured follow this trend as expected. The measurements are significantly different for a difference of 1%, e.g., between solutions 1 and 3, 2 and 4, etc.. (data from Fripiat et al., 2009)

Atom % ^{30}Si	Atom % ^{28}Si
8.04 ± 0.03	87.52 ± 0.04
8.07 ± 0.05	87.50 ± 0.05
8.11 ± 0.03	87.44 ± 0.01
8.16 ± 0.03	87.40 ± 0.03
8.21 ± 0.03	87.36 ± 0.02
8.29 ± 0.06	87.27 ± 0.07

Accuracy and reproducibility of the isotopic measurements have been checked on artificial and natural solutions by inter-comparison between two HR-SF-ICP-MS instruments (IUEM, Brest and RMCA, Tervuren) and one TIMS (IUEM). Measurements of real Si production and dissolution rates were processed for two contrasted situations with an average relative precision of 10%, including one from waters with low Si content (2 μM), which required an additional purification step by cation exchange chromatography. During the SAZ-Sense cruise a complete set of incubations ($n = 36$) was combined with radiotracer ^{32}Si incubations (Tréguer et al., 1991; Brzezinski and Phillips, 1997) to determine the bSiO_2 production rates (collaboration with K. Leblanc and B. Quéguiner, COM, Marseille). The two methods agree ver well and results are not significantly different from the 1:1 slope ($R^2 = 0.9$) (**Figure 2.2.1**).

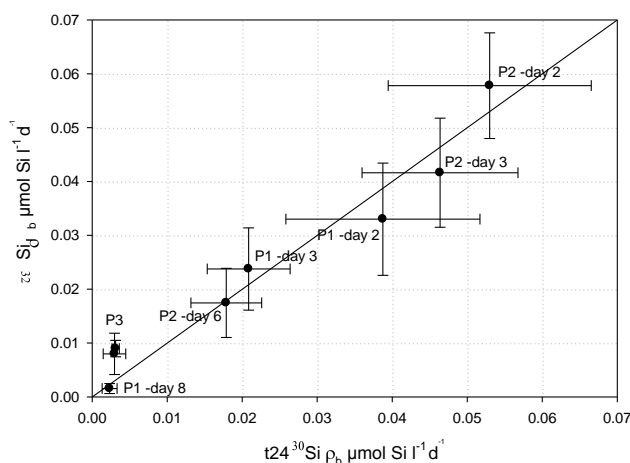


Figure 2.2.1: bSiO_2 production rates determined from ^{30}Si and ^{32}Si incubation; shown are station averages. Line = 1:1 slope.

Our new method is 2-4 times faster and is also simpler than TIMS or isotope ratio mass spectrometry (IRMS). It's sensitivity is more than one order of magnitude better than TIMS, and it can cover the whole range of Si concentrations encountered in the ocean. This new method constitutes Deliverable 3a of the project: *Method for assessing 30-Si uptake via HR-ICP-MS*.

It has been successfully developed at RMCA through a collaboration between three BELCANTO partners (MRAC, ULB, VUB; making use of the incubation expertise of the ULB group and the modeling expertise of the VUB group; Elskens et al. 2007) and two foreign laboratories (IUEM, Brest and COM, Marseille).

Coupled nutrient uptake (C, N, Si) in contrasting biogeochemical environments (SAZ-Sense)

Combined ^{15}N , ^{13}C (ammonium, nitrate, bicarbonate), ^{30}Si (see above) uptake experiments (using on-deck flow through incubators) were conducted during the SAZ-Sense expedition (SAZ and PFZ south of Tasmania; Jan.-Feb. 2007, R/V *Aurora Australis*) to assess spatial and temporal variability of primary production, new production and diatom production.

SeaWiFS 8-day composite, 1 km resolution, pictures for the area south of Tasmania reveal differences in the spatial distribution of chlorophyll-a distribution with evidence for higher phytoplankton biomasses in the eastern part of the SAZ relative to the western part (**Figure 2.2.2**; Bowie et al., in review). Reasons for this could include changing patterns of the East Australian Current (EAC) advecting warmer and saltier stratified waters, (possibly enriched with Fe) to the south, changing patterns of aeolian transport of Fe from the Australian continent (Mackie *et al.*, 2008), and/or advection of Fe from the Tasman Plateau. The main objectives of the SAZ-Sense expedition were to identify these possible causes and to assess their impact on the zonal variability of the carbon sequestration potential.

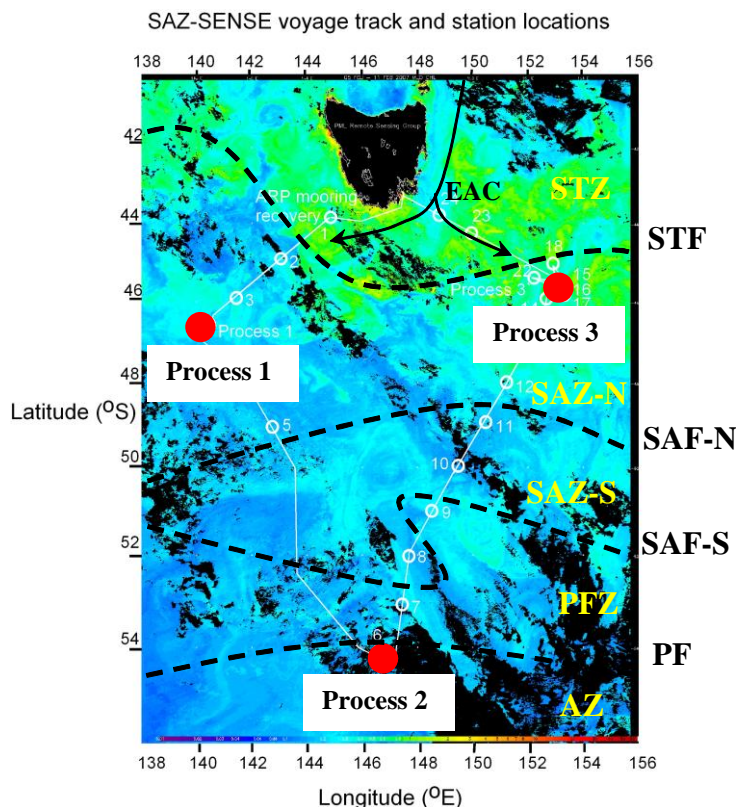


Figure 2.2.2: SAZ-Sense cruise track and station locations. The background shows chlorophyll (mg m^{-3}) from MODIS (courtesy of the Remote Sensing Group at the Plymouth Marine Laboratory) and is a composite for the period 5 to 11 February 2007. A chlorophyll scale is given at the bottom of the image. The north-south and east-west gradients in phytoplankton chlorophyll biomass are typical of the region in summer. EAC = East Australian Current, STF = Sub-Tropical Front, SAF-N = Sub-Antarctic Front North, SAF-S = Sub-Antarctic Front South, PF = Polar Front; STZ = Sub-Tropical Zone, SAZ-N = Sub-Antarctic Zone North, SAZ-S = Sub-Antarctic Zone South, PFZ = Polar Front Zone, AZ = Antarctic Zone.

Three "Process" stations were selected on the basis of their physico-chemical and ecosystem characteristics under different nutrient regimes. Process 1 site in the Western SAZ was low in Fe, typical for the HNLC Sub-Antarctic Zone. In contrast, Process 3 site in the eastern SAZ appeared to be Fe replete, probably as a result of Fe supply via the East Australia Current and atmospheric deposition (Bowie et al., 2009; Lannuzel et al., 2011). Process 2 site in the Polar Front Zone also had low Fe content and a deep bSiO₂-Chl-a maximum characteristic for this HNLC area. At all 3 stations Si(OH)₄ concentration was low (<2 µM), nitrate was low in the SAZ (mostly < 5 µM; but up to 25 µM in the PFZ) while ammonium was substantial (up to 1.4 µM in subsurface maxima) at each process station ¹³C, ¹⁵N-nitrate, ¹⁵N-ammonium and ³⁰Si uptake experiments were processed simultaneously using seawater from the same CTD casts at four PAR depths (100, 50, 25 and 1%).

At the 3 Process stations we conducted short term incubations (6h) in parallel with ³⁰Si uptake incubations for assessment of diatom importance in the N, C uptake experiments. C and N-translocation rates were calculated using the compartmental model developed by Elskens et al. (2002, 2005). Primary production values were equivalent to gross primary production (GPP). New production was calculated from GPP and *f*-ratios (i.e., the ratio of nitrate uptake over the sum of nitrate and ammonium uptake).

Table 2.2.2 compares the euphotic layer integrated gross primary production and new production between the 3 areas investigated during SAZ-Sense and **Figure 2.2.3** shows the depth profiles of the *f*-ratios at the 3 sites. Gross Primary Production estimates from ¹³C-uptake are in agreement with GPP estimates based on the ¹⁴C method (the latter data from Westwood et al., 2011).

Table 2.2.2: SAZ-Sense. Daily gross primary production (¹³C-GPP); new production NP; export production from upper 100 m (Jacquet et al. accepted-b) and mesopelagic remineralization in the 100-600 m mesopelagic layer (Jacquet et al. accepted-a).

Site	date UTC	# casts ¹³ C-GPP ¹⁵ N-upt.	Mixed layer depth (m) (III)	Euphotic layer depth (m)	¹³ C-GPP (mmol C m ⁻² d ⁻¹)	New production ¹³ C-uptake x <i>f</i> -ratio (mmol C m ⁻² d ⁻¹)	Export production at 100 m (I) (mmol C m ⁻² d ⁻¹)	export ratio EP/ ¹³ C-GPP (%)	Meso-remin. (100-600 m) (II) (mmol C m ⁻² d ⁻¹)	remin. ratio MR/EP (%)
Process 1	21-01-07	9	20	50	147.8	74.6		13%		
	23-01-07	17	43	50	70.8	15.2	10.2 ± 1.3	7 to 75%	2.1 ± 0.4	21%
	28-01-07	34	73	50	13.6	1.9		(highly variable)		
Process 2	01-02-07	42	57	80	36.8	7.2				
	02-02-07	47	47	80	33.9	10.3	7.8 ± 1.5	22%	5.0 ± 1.6	64%
	05-02-07	58	62	80	35.9	8.5				
Process 3	11-02-07	81	13 80	30	52.9	10.7				
	12-02-07	85	15 80	30	51.2	13.4	4.1 ± 0.8	7%	3.7 ± 0.4	90%
	15-02-07	96	14 75	30	65.9	11.9				

(I) Jacquet *et al.* -a

(II) Jacquet *et al.* -b

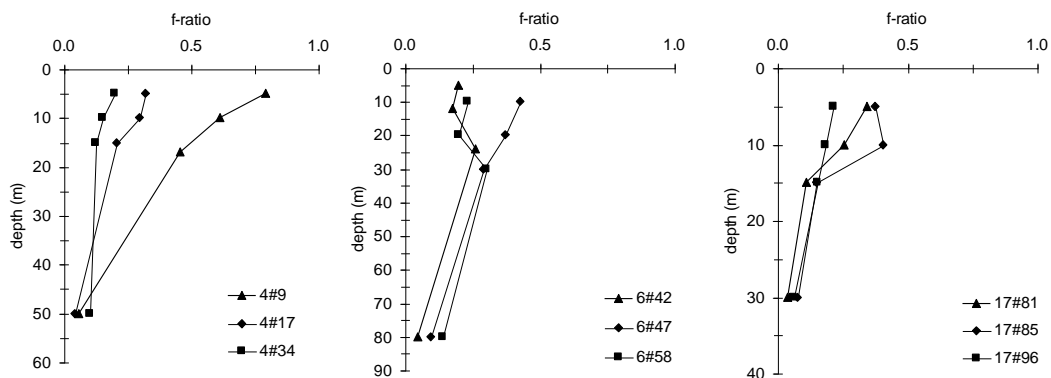


Figure 2.2.3: SAZ-Sense. Depth profiles of f -ratios observed in SAZ-West (Left: site P1, casts #9, #17, and #34), PFZ (Middle: site P2, casts #42, #47, and #58), and SAZ-East (Right: P3, casts #81, #85, and #96).

f -ratios are mostly <0.3 and overall, recycled production, based on ammonium uptake, appears to predominate in the investigated PFZ and SAZ areas.

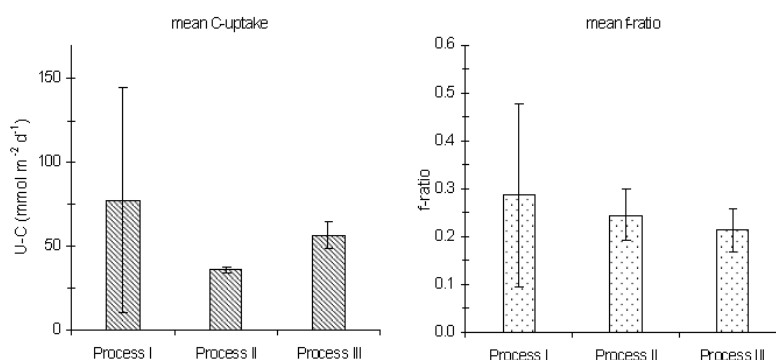


Figure 2.2.4: SAZ-Sense. Mean euphotic layer integrated gross primary production ($\text{mmol C m}^{-2} \text{d}^{-1}$) and f -ratio for SAZ-West (Process I), PFZ (Process II) and SAZ-East (Process III) (Cavagna et al., 2011).

As appears from **Figure 2.2.4** and as previously observed in this area, integrated GPP in the SAZ area exceeded GPP in the PFZ. Mean integrated New Production estimated from f -ratios was quite uniform across the study area and indicated that primary production was mainly driven by regenerated production. This is in agreement with Pearce et al. (2011) who report that a large fraction of the primary production is reprocessed within the microbial loop (microzooplankton and heterotrophic nanoflagellates). Interestingly, New Production, which is a proxy of potentially exportable production, was closer to C export at 100m (as estimated from ²³⁴Th deficit; see below) when the euphotic layer depth approached 100m (Jacquet et al., 2011).

Contrary to expectation, the Fe replete eastern SAZ and its higher phytoplankton biomass did not sustain a significantly higher productivity compared to the western SAZ. Furthermore, potential for carbon sequestration there was low, as confirmed by low C-export fluxes (see below) and high mesopelagic remineralisation efficiency.

From the specific Si(OH)_4 uptake rates (**Figure 2.2.5**), a gradient in diatom affinity for Si(OH)_4 appears, reflecting the high Fe-Si co-limitation in the PFZ and the Si-limitation in the eastern SAZ. The western SAZ also appears to experience Fe-Si co-limitation but to a lesser extent than the PFZ.

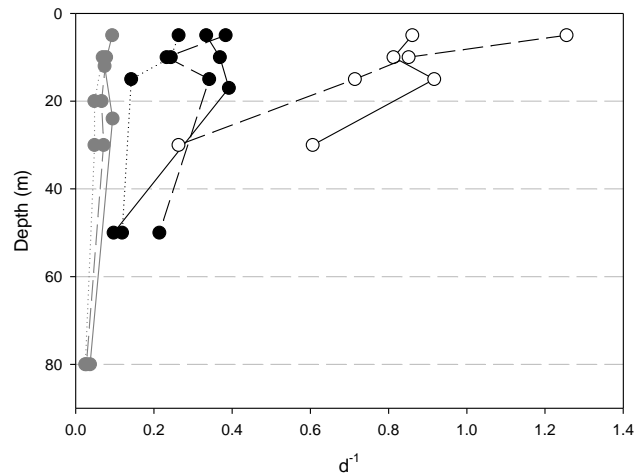


Figure 2.2.5: SAZ-Sense. Specific Si(OH)_4 uptake rates (d^{-1}) in PFZ (grey dots), western SAZ (black dots), and eastern SAZ (white dots) (data from Fripiat et al. in review)

This Si(OH)_4 affinity gradient could result from a gradient in Fe-Si colimitation exerting significant control on the Si(OH)_4 kinetic parameters (Leynaert et al., 2004). In contrast, bSiO_2 production (**Figure 2.2.6**) and content (not shown) increased towards PFZ as previously observed in this area.

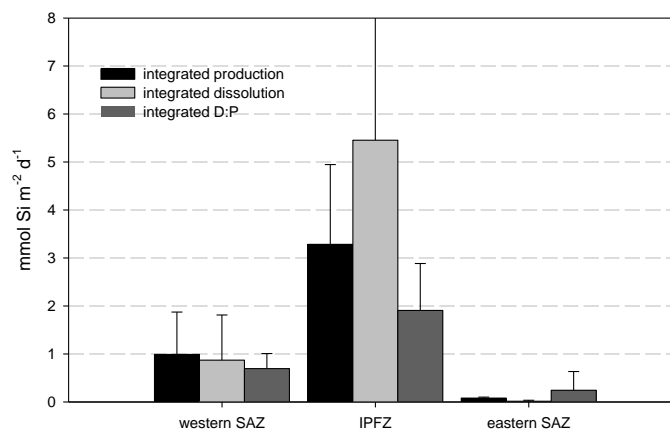


Figure 2.2.6: SAZ-Sense. Mean integrated bSiO_2 production, dissolution, and ratio between dissolution and production rates for the SAZ-West, PFZ and ZAS-East.

Such a decoupling between growth rate and stocks could come from specific differences in kinetics parameters and mortality pressures. As stated by Smetacek et al. (2004) in iron-limited HNLC systems, GPP is mainly driven by regenerated picoplankton under heavy grazing pressure but large or chain forming slowly growing diatoms could escape grazing pressure and accumulate in the system (e.g. like in western SAZ and PFZ). In contrast, in Fe-replete areas, large diatoms may grow rapidly and drive large blooms with high carbon export efficiency. Hutchins et al. (2001) and Sedwick et al. (2002) show that low Si contents exert a control on microbial community structure. This was probably the case for the eastern SAZ where Fe availability and Si depletion favored small diatoms with high specific Si uptake rates, preventing growth of large diatoms. These small species are more prone to be grazed preventing diatom accumulation in the euphotic layer, consistent with low bSiO₂ content. This is in agreement with a low contribution of diatoms to GPP and with Pearce et al. (2011) who observed a high grazing pressure in the eastern SAZ.

As shown in **Figure 2.2.6**, bSiO₂ dissolution can sustain most of the Si(OH)₄ uptake, indicating an intense silicon loop in mid-summer PFZ and SAZ. bSiO₂ dissolution rates in the euphotic layer are higher when bSiO₂ content is high ($R^2 = 0.61$). This is likely to result from an accumulation of inactive/death diatoms at the end of the productive period. Notwithstanding this, some difference in the efficiency of bSiO₂ dissolution environment between PFZ and SAZ is observed. There is a coarse correlation between specific dissolution rates and temperature ($R^2 = 0.43$). bSiO₂ dissolution is strongly facilitated when bacteria degrade the protective organic matrix coating around the frustule. During SAZ-Sense a significant correlation between hydrolytic ecto-enzymatic activity and temperature was observed ($R^2 = 0.74$). This complex interplay between bacteria and temperature, which would also be influenced by the type of substrate and species, could explain the relatively coarse correlation between specific bSiO₂ dissolution and temperature. Indeed, C and Si regeneration rates show significant variability (up to fourfold) among different bacterial assemblages and isolates (Bidle and Azam, 1999; 2001) implicating species composition, colonization dynamics, metabolic state and ecto-enzyme profiles as important variables.

Conclusions and perspectives

More information regarding these data can be found in the following papers:

- Fripiat et al. (2009), for ³⁰Si methodology
- Cavagna et al. (2011) for GPP and NP
- Fripiat et al. (in review) for uptake ratios and Si-biogeochemical cycle

Instantaneous uptake rates provide important information about the functioning of the ecosystems (new and regenerated production), and the degree of coupling of the major nutrients (N, Si, C). Knowing how much of the N, Si, C gross uptake was sustained by new and regenerated processes has important implications on the ecosystem's capacity to drive biogeochemical properties of the surface ocean and on its ability to export organic or biogenic matter to the deep sea. Moreover, biogeochemical processes occurring in the surface water of the Southern Ocean have significant impact on the availability of nutrients in the surface water of the three-quarters of the global ocean (Sarmiento et al., 2004). The data from SAZ-Sense have only been recently completed for Si uptake – dissolution and in the near future these will be fully integrated with the other SAZ-Sense data. In addition, data from the BONUS-GoodHope 2008 expedition are currently being processed.

This work is a contribution to Deliverable # 3b- Time-dependent dynamics of nutrients in surface waters (uptake vs. dissolution; inter vs. intra seasonal variation).

2.3. CO₂ uptake and C export

Air-Sea CO₂ exchange

CO₂ dynamics along the 0° meridian

During the BONUS-GoodHope cruise, pCO₂ ranged from 325 to 415 ppmV, and exhibited significant changes across fronts and eddies whose position can be tracked from step changes in SST (**Figures 2.3.1 & 2.3.2**). The subtropical area appeared to be undersaturated in CO₂ while the Subantarctic and Polar Front Zones were below or near saturation and the polar open oceanic zone was oversaturated. The maximum pCO₂ was observed at the Southern Circumpolar Antarctic Front (SACCF). Comparison with pCO₂ measurements carried out during the ISPOL cruise in spring 2004 and early summer 2004-2005 (data not shown) suggest that pCO₂ was significantly higher during the Bonus-Goodhope cruise south of the subtropical front (STF). At first sight this indicates that we encountered a late summer regime with conjugated warming of surface water and remineralisation of organic matter that increased pCO₂ in the subantarctic zone. South of the Polar Front (PF), upwelling of CO₂ rich subsurface waters (**Figure 2.3.2**) may contribute to the increase of CO₂ and lead to the CO₂ oversaturation.

Significant increase of DIC over the upper 1000 m is related to mesopelagic remineralisation (**Figure 2.3.3**). Below 1000 m, the imprints of main water masses of the subtropical area and circumpolar current (e.g. North Atlantic Deep Water, Circumpolar Deep Water, Antarctic Intermediate Water, among others) can be discerned in the vertical DIC distribution. For instance, in the subtropical area a tongue of Antarctic Intermediate Water with DIC ranging between 2210 and 2235 $\mu\text{mol kg}^{-1}$ water is transported northward between 1000 and 1500 m. We observed an overall DIC increase southwards. Between the STF and the Southern Boundary (SBy) DIC increases with depth while south of the SBy the DIC increase with depth correlated with an increase of dissolved oxygen (data not shown). The maximum of DIC was observed south of the SBy in the upper 1000 m

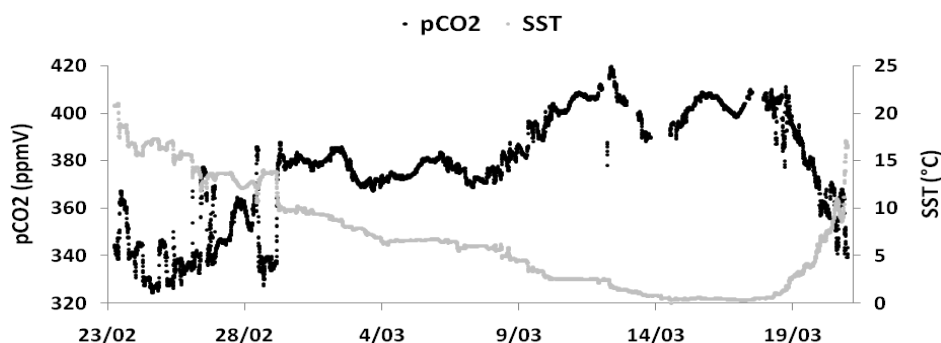


Figure 2.3.1: BONUS-GoodHope. Sea surface temperature (SST) and pCO₂ along the cruise track.

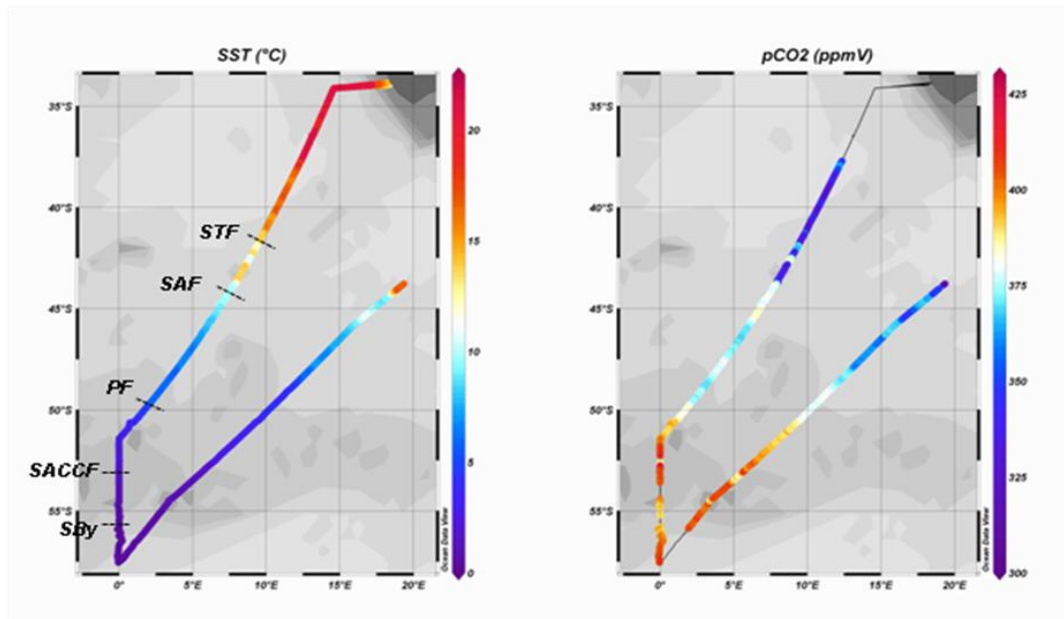


Figure 2.3.2: BONUS-GoodHope: Distribution of sea surface temperature (SST) and $p\text{CO}_2$ along the cruise track. Approximate positions of the subtropical (STF), subantarctic (SAF), polar (PF), southern antarctic circumpolar (SACCF) fronts and southern boundary (SBy) are indicated by the black dotted lines.

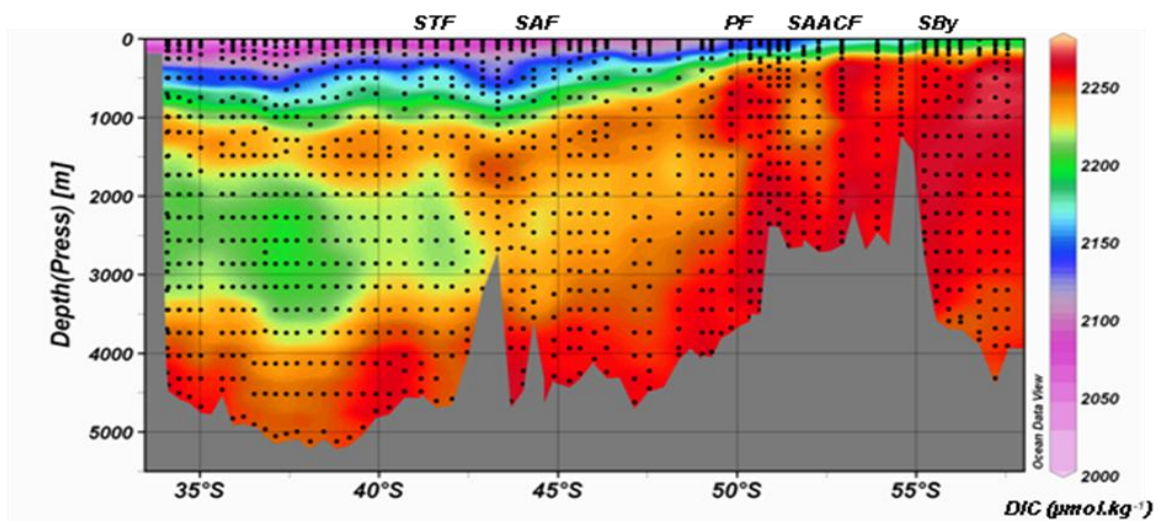


Figure 2.3.3: BONUS-GoodHope. Vertical distribution of dissolved inorganic carbon (DIC) along the section. Approximate position of the subtropical (STF), subantarctic (SAF), polar (PF), southern antarctic circumpolar (SACCF) fronts and southern boundary (SBy) are indicated.

Assessment of the overall sink of CO₂ of the Southern Ocean

One of the best approaches to budget air-sea CO₂ fluxes over the Southern Ocean was to gather data collected in the frame of the project together with the large data set of pCO₂ compiled by T. Takahashi. Underway pCO₂ measurement carried out during this project and during previous BELCANTO I and II projects (6 cruises) were added to 3.0 million measurements of surface water pCO₂ compiled at the Lamont-Doherty Earth Observatory to provide a climatological mean distribution for the surface the surface water pCO₂. BELCANTO results contributed to a doubling of number of Southern Ocean data since the last climatology (Takahashi et al., 2002). The Southern Ocean is a potentially significant contributor to the global air-sea CO₂ fluxes, yet has been poorly sampled. A significant increase of data coverage was a prerequisite to better constrain overall oceanic CO₂ fluxes.

The new climatology (Takahashi et al., 2009) shows large seasonal changes in the seasonal ice zone. Phytoplankton blooms promote large decrease of pCO₂ in summer, while vertical mixing of deep waters lead to significant winter increases of pCO₂. The subpolar Southern Ocean between 50° and 62°S (Fig.16D) has a net sea-to-air CO₂ flux in winter and a net air-to sea flux in summer. In this zone, ΔpCO₂ is small in magnitude ranging between +12 μatm in winter (enhanced vertical mixing) and -12 μatm in summer (biological drawdown). Although this region is mostly within the high wind speed zone (40-60°S), the flux is moderate ranging between +1 (winter) and -1 ton C month⁻¹ km⁻² (summer) because of the small ΔpCO₂ values. The seasonal ice covered zone (south of 62°S) acts as a moderate source of CO₂ to the atmosphere as a result of the summer sink flux canceling with the winter source flux. The sea-to-air CO₂ flux is very high per unit area of exposed water, but is small for the ice covered area as a whole. As ice fields retreat in springtime, surface waters become a strong sink due to locally intense phytoplankton blooms.

On the whole, the air-sea CO₂ fluxes over the Southern Ocean were estimated to reach -0.06 Pg C y⁻¹ for the 50 - 62°S latitudinal band and +0.01 Pg C y⁻¹ south of 62°S. The overall flux for the Southern Ocean (area south of 50° S) is -0.05 Pg C y⁻¹, what is rather small, mainly because of the large seasonal ice cover reducing gas exchange.

pCO₂ in the Southern Ocean appears to increase at a rate of 2.13 μatm y⁻¹ exceeding the rate of change for atmospheric pCO₂. This supports the idea that the CO₂ sink south of 45°S is decreasing (Le Quéré et al., 2007)

Decadal changes

We compiled a large pCO₂ data-set for surface waters over the continental shelf (CS) and the adjacent open ocean, south of Tasmania (22 cruises spanning the period 1991 to 2003).

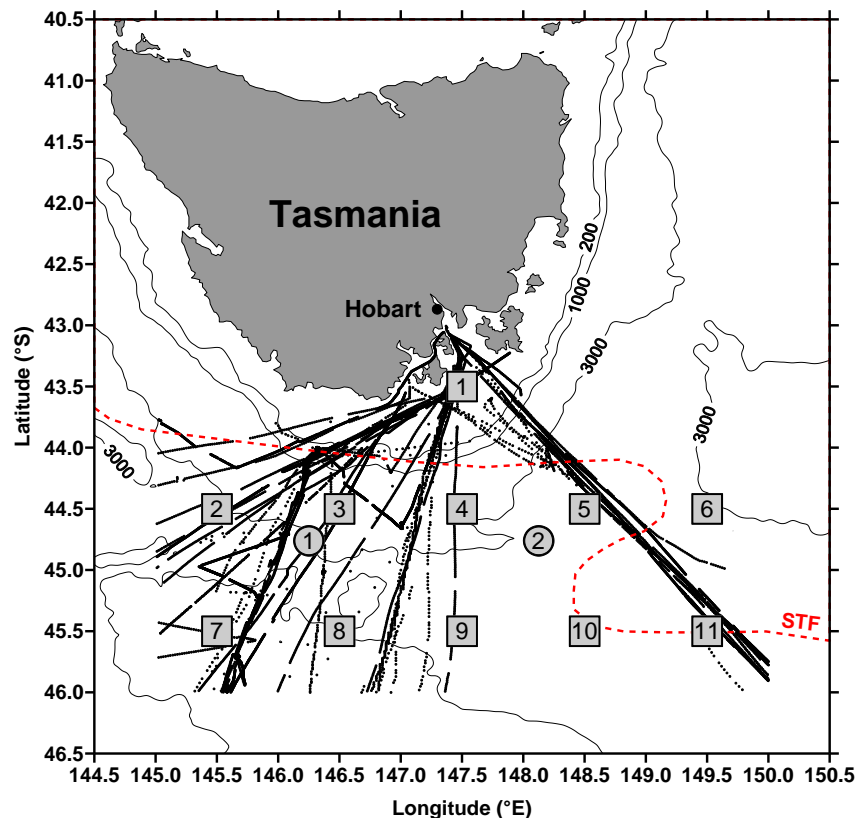


Figure 2.3.4. Map showing ship tracks, bathymetry based on the Smith and Sandwell (1997) global seafloor topography, the climatological position of sub-tropical front (STF) based on Belkin and Gordon (1996) and Hamilton (2006), grid nodes from the Reynolds et al. (2002) sea surface temperature monthly climatology (squares), and the grid nodes of the Kalnay et al. (1996) National Centers for Environmental Prediction daily wind speeds (circles).

Climatological seasonal cycles of $p\text{CO}_2$ in the CS, the subtropical zone (STZ) and the subAntarctic zone (SAZ) were described and used to determine monthly $p\text{CO}_2$ anomalies. These are used in combination with monthly anomalies of sea surface temperature (SST) to investigate inter-annual variations of SST and $p\text{CO}_2$. Sea surface temperature (SST) anomalies (as intense as 2°C) are apparent in the subtropical zone (STZ) and subantarctic zone (SAZ). These SST anomalies also propagate on the CS, and seem to be related to the Antarctic Circumpolar Wave (ACW). The consistency in timing and amplitude of SST anomalies in the STZ and SAZ can only be attributed to a large scale coupled atmosphere-ocean oscillation. Overall, anomalies of 14°C normalized $p\text{CO}_2$ ($p\text{CO}_2@14^\circ\text{C}$) are negatively related to SST anomalies in the CS, STZ and SAZ (**Fig 2.3.5**). This seems to be related to a depressed winter-time vertical input of dissolved inorganic carbon during the ACW phases of positive SST anomalies, in relation to a poleward shift of westerly winds, and concomitant local decrease in wind stress.

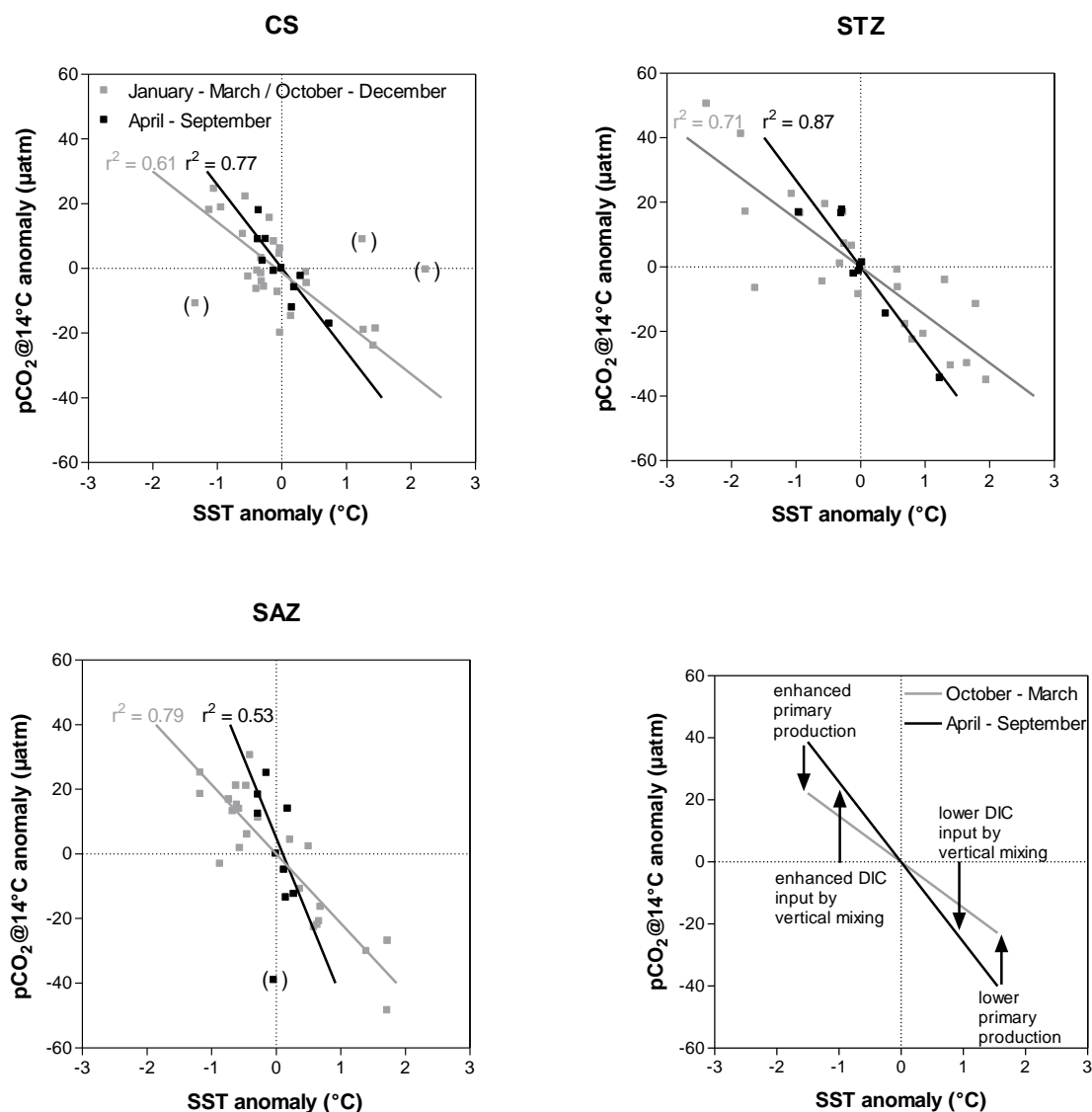


Figure 2.3.5. Monthly anomalies of the partial pressure of CO₂ (pCO₂) normalized to a temperature of 14°C (pCO₂@14°C) plotted against the monthly anomalies of sea surface temperature (SST) over the continental shelf (CS), in the subtropical zone (STZ) and the SubAntarctic zone (SAZ), south of Tasmania, and conceptual frame for the spring-summer period (grey squares) and the fall-winter period (black squares). Solid lines correspond to linear regression functions and r^2 to the corresponding coefficient of determination (winter-fall in black, spring-summer in grey). Symbols in brackets were excluded from the linear regressions.

In order to examine the relationship of SST anomalies to inter-annual variations of air-sea CO₂ fluxes, we extended the oceanic pCO₂ time series to include the years 1982 to 2005 using SST time-series and our previously established relationships between observed SST and pCO₂@14°C for the period 1991-2003. The general pattern is an increase in the sink for atmospheric CO₂ associated with positive SST anomalies, mainly during the fall-winter period. However, this general pattern is strongly modulated by inter-annual variations of wind speed that affects the gas transfer velocity and the intensity of the air-sea CO₂ flux.

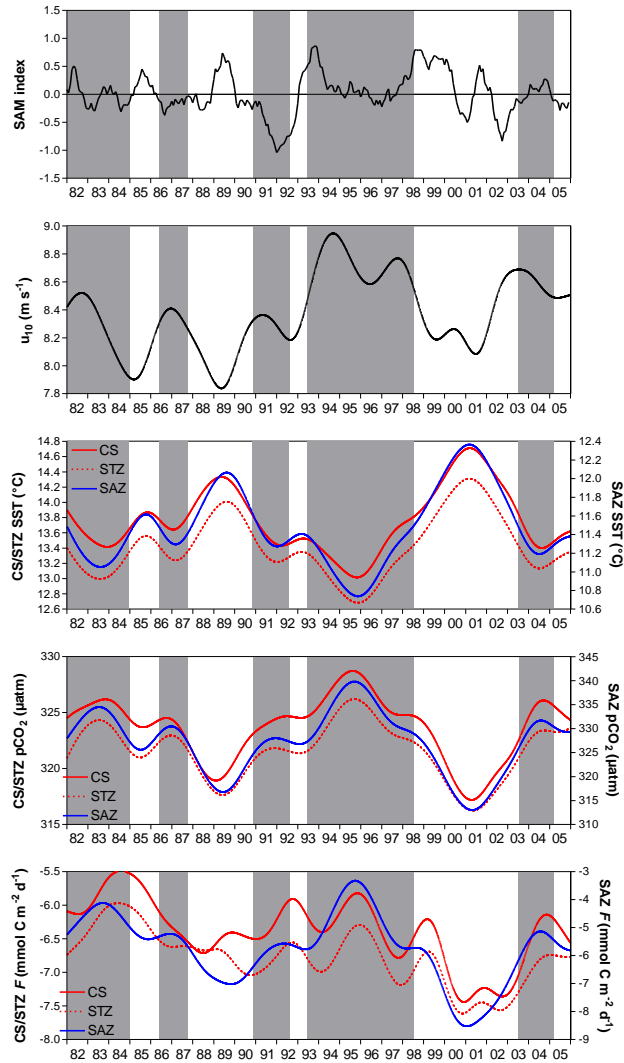


Figure 2.3.6. Time-series from 1982 to 2005 of southern annular mode (SAM) index and of de-seasonalized wind speed (u_{10}), sea surface temperature (SST), partial pressure of CO_2 ($p\text{CO}_2$) and air-sea CO_2 fluxes (F) in the continental shelf (CS), the subtropical zone (STZ) and subAntarctic zone (SAZ) south of Tasmania. Grey areas correspond to periods of sustained negative SST anomalies. Signals were deseasonalized using a Gaussian one year low pass filter. SAM index was obtained from the National Oceanic and Atmospheric Administration Climate Prediction Centre (<http://www.cpc.ncep.noaa.gov/>) and smoothed with a one year running mean.

Assuming that phases of positive SST anomalies are indicative of the future evolution of ocean biogeochemistry under global warming, we show that based on a spatially restricted observational data-set, some provinces of the Southern Ocean could provide a potential negative feedback on increasing atmospheric CO_2 and associated climate change. The observations from our region are in agreement with recent modelling studies that show a decrease of the CO_2 sink in high latitude areas of the Southern Ocean during positive phases of SAM, due to enhanced upwelling and an increase of the CO_2 sink in the low latitude areas of the Southern Ocean (Le Quéré et al., 2007; Lenton and Matear, 2007; Lovenduski et al., 2007).

It is clear that larger scale investigations in the Southern Ocean are required to quantify more rigorously potential feedbacks on the increase atmospheric CO₂ due to SST changes in surface waters (Borges et al., 2008).

Carbon export

Method

We applied the small-volume (4L) technique for total (dissolved + particulate) ²³⁴Th measurements (Buesseler et al., 2001, Benitez-Nelson et al., 2001) based on the 20-L method developed by Rutgers van der Loeff and Moore (1999). Seawater was processed for total ²³⁴Th following the double-spike method of Pike et al. (2005). Briefly, seawater was acidified to pH 2 using concentrated HNO₃ and spiked with ²³⁰Th yield monitor to estimate ²³⁴Th recovery by Mn precipitation. After 12h equilibration, pH was increased to 8.5 using concentrated NH₄OH. KMnO₄ and MnCl₂ were added to form a precipitate and the samples were allowed to stand for 12h followed by filtration on quartz fiber QMA filters (nominal porosity =1 μm; 25 mm diameter). Filtered precipitates were dried at 50°C overnight and then counted on board using low level beta counters (Risø, Denmark) until counting uncertainty was below 2%. We also measured ²³⁴Th activity on size-fractionated particles (>1-53μm; >53 μm) sampled with via large volume in-situ filtration. ²³⁴Th fluxes were subsequently transformed into POC fluxes using suspended matter ²³⁴Th/POC ratios. All filters were re-counted for beta background determination in the home base laboratory after a delay of six ²³⁴Th half-lives (144 days) of decay. Total ²³⁴Th samples were then processed for ²³⁰Th measurement following Pike et al. (2005) and using ²²⁹Th as a second spike to correct for losses of ²³⁰Th during sample digestion and ion-exchange chemistry. ²³⁰Th and ²²⁹Th were measured using a Sector Field (High Resolution) ICP-MS (Element 2, Thermo Finnigan) in low resolution mode.

C-export results for EIFEX, KEOPS, SAZ-Sense and BONUS-GoodHope

Carbon export during EIFEX was clearly boosted due to the iron infusion as indicated by a major export pulse occurring about one month after the Fe release and lasting a few days (carbon export reached up to 144 and 128 mmol C m⁻² d⁻¹ at 100 and 150m, respectively, at day 33), which to our knowledge is the highest POC export flux ever recorded in the Southern Ocean (**Figure 2.3.4**).

A further striking result from EIFEX is the coincidence of the demise of the high-export period with the one of the bloom. However, it should be noted that the huge export occurred during a very short period. The excess in export flux due to iron addition is estimated at 12.8 mmol C m⁻² d⁻¹ at 100m. This value is similar to what Buesseler et al. (2005) report for the SOFeX Fe fertilisation experiment. It also is similar to what we estimated for the KEOPS study (natural Fe fertilization study): excess export flux between 12 and 15 mmol C m⁻² d⁻¹ (see **Figure 2.3.5**; and Blain et al., 2007).

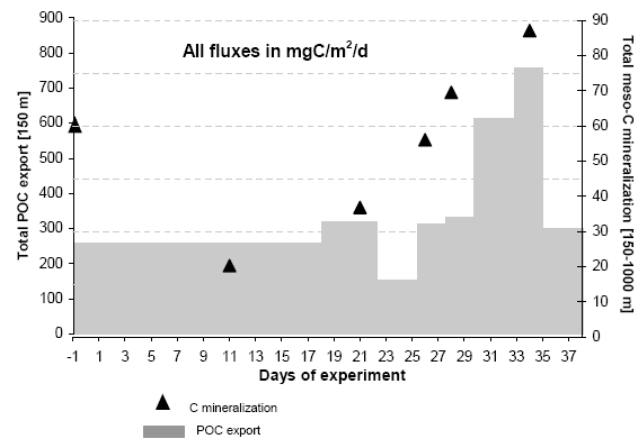


Figure 2.3.4: EIFEX, 2004. Particulate organic carbon export (0-150m) and POC remineralization (150-1000 m) over a 37-day observation period during the EIFEX Fe-fertilization experiment in a mesoscale eddy of the Polar Front (Atlantic sector; summer 2005). All fluxes in $\text{mg C m}^{-2} \text{d}^{-1}$. From Jacquet et al. (2008).

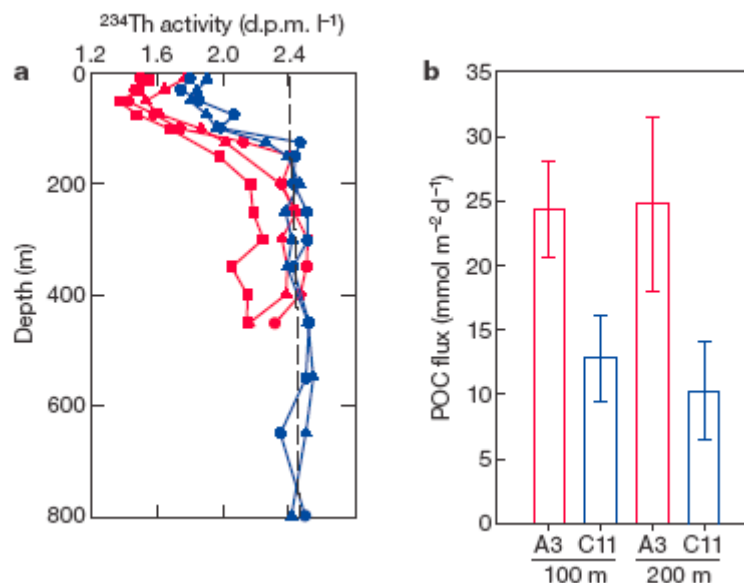


Figure 2.3.5: KEOPS cruise. Carbon export at sites A3 (above the Fe fertilised plateau) and C11 (open ocean, HNLC area); (a) Profiles of ^{234}Th activity at A3 (red lines) and C11 (blue lines); (b) POC fluxes at A3 and C11. POC fluxes were derived from ^{234}Th fluxes using a non-steady-state model and from POC/ ^{234}Th ratios. POC fluxes were substantially higher inside the bloom above the plateau compared to the open ocean HNLC site. Excess export is given by the difference in POC export flux between plateau and HNLC station; from Blain et al. (2007).

POC export via the ^{234}Th flux method has also been assessed during the SAZ-Sense cruise (2007); Jacquet et al. (2011b). **Figure 2.3.6** shows the spatial variability of POC export (EP) in SAZ and PFZ. POC export flux appears higher in the PFZ and the SAZ-West compared to the SAZ-East, though the latter region has higher surface water phytoplankton biomass (from Chl-a and POC contents; see Modis picture in **Figure 2.2.2**). The SAZ-West also has higher export ratios (i.e., EP / GPP), and thus appears as the area with highest potential for C sequestration.

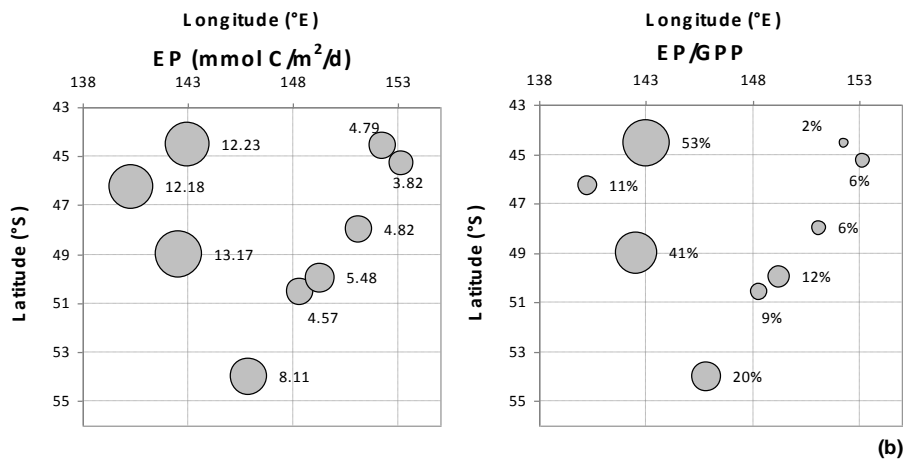


Figure 2.3.6: SAZ-Sense. Bubble plot showing the Export Production (EP) flux at the export depth (100m) (a) and EP vs. gross primary production (GPP) (b). The size of the bubble is proportional to the flux and ratio magnitude.

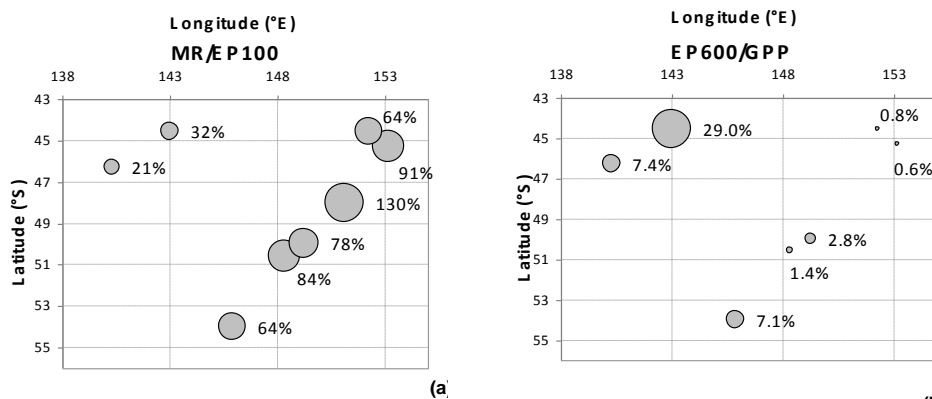


Figure 2.3.7: SAZ-Sense. Bubble plot showing mesopelagic remineralisation between 100 and 600m (MR) vs. export production (EP) at 100 m (a) and ratio of export from 600m / export from 100m (EP600 / GPP) (b). The size of the bubble is proportional to the ratio.

During the BONUS-GoodHope (BGH) cruise (Jan.-Mar. 2008) along the Greenwich Meridian, we assessed POC export (from total ^{234}Th flux) along a transect from the subtropics (40°S) till the eastern extension of the Weddell Gyre (58°S), crossing the Subtropical Front, the Subantarctic Front, the Polar Front, the Southern ACC Front and the Southern ACC Boundary.

At present we still need to correct these numbers for recovery of the ^{234}Th activity during sample handling on board, so total ^{234}Th values are still preliminary. The >1-53 μm particle fraction had 10x higher ^{234}Th activity than the >53 μm fraction, with activities of both size fractions strongly decreasing with depth. Strongest ^{234}Th -deficits occurred in Cape Basin subsurface waters (80 to 100m) north of the Subtropical Front (**Figure 2.3.8**). Between the SAF and the Southern Boundary significant ^{234}Th -depletion was observed in the upper mixed layer. The density gradient marking the bottom of the mixed layer also marks the transition to less ^{234}Th -depleted waters. Sites with enhanced surface waters fluorescence (PFZ; Weddell Gyre) were slightly less depleted suggesting local phytoplankton blooms keep the ^{234}Th activity within the surface.

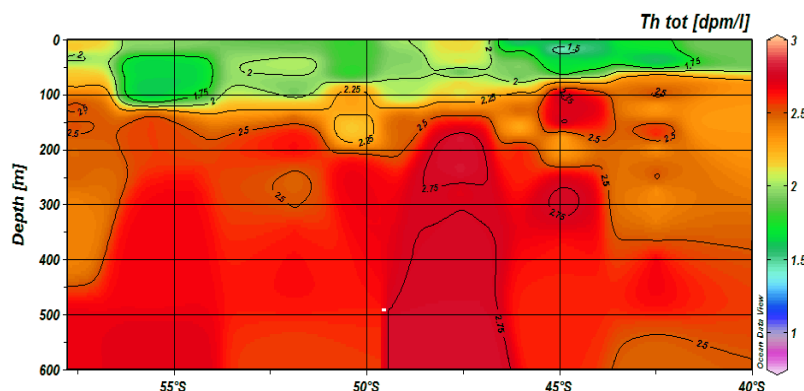


Figure 2.3.8: BONUS-GoodHope. Total ^{234}Th activity (dpm l^{-1}) distribution as a function of depth and latitude for 10 stations along the cruise section. The lowest β activity is encountered in the mixed layer (ML) with values $< 2.5 \text{ dpm l}^{-1}$ (secular equilibrium with ^{238}U) reflecting Th export via scavenging on sinking particles. Below the ML, Th excess ($> 2.5 \text{ dpm l}^{-1}$) is observed indicating a variable input of Th to the dissolved phase due to remineralisation of sinking particles, (Planchon et al., in prep.)

Figure 2.3.9 shows ^{234}Th fluxes from the upper mixed layer (blue bars). These represent subtraction of Th from the surface via sinking particles, estimated by applying the steady state approach. Between the ML and 600m, Th is released ($^{234}\text{Th}/^{238}\text{U}$ ratios > 1) and results in a negative flux (red bars).

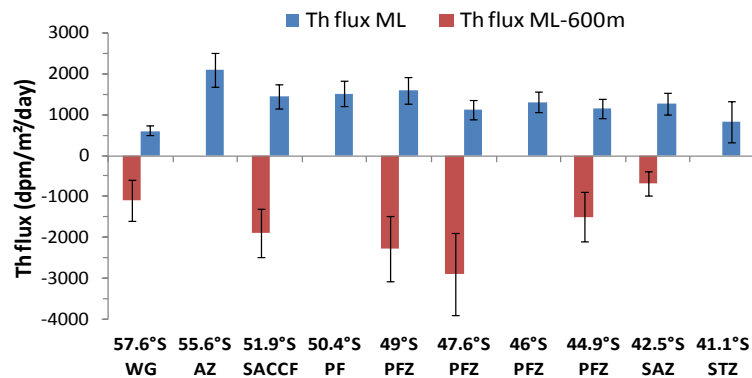


Figure 2.3.9: BONUS-GoodHope. ^{234}Th fluxes ($\text{dpm m}^{-2} \text{d}^{-1}$) estimated from a steady state one box model for the mixed layer (ML) and sub-surface waters (bottom of ML bottom to 600m). STZ: Sub-Tropical zone; SAZ: Sub-Antarctic zone; PFZ: Polar Frontal zone; PF: Polar Front; SACCF: South Antarctic Circumpolar Current Front; AZ: Antarctic Zone; WG: Weddell Gyre; (Planchon et al., in prep).

Table 2.3.1 provides first estimates for C-export during BONUS-GoodHope. Highest fluxes ($6.3 \text{ mmol m}^{-2} \text{d}^{-1}$) are observed for the SACCF at 52°S and lowest ($1.8 \text{ mmol/m}^2/\text{d}$) in the vicinity of the subantarctic front (42.5°S). Values are similar in magnitude with those observed for the section between PFZ and SAZ-East during SAZ-Sense (compare with **Figure 2.3.6**).

Table 2.3.1: Estimates of ^{234}Th and POC export fluxes in the Mixed Layer and the twilight zone along the BONUS-GoodHope section using POC/Th (C/Th) and N/Th ratios of sinking particles ($>53\mu\text{m}$, between 0 to 200m depth) and comparison with literature data for the Southern Ocean. SAF= Subantarctic Front; PFZ=Polar front Zone; SACCF= Southern Antarctic Circumpolar Front; WG=Weddell Gyre.

Zone	Lat	Th flux		POC/Th		PON/Th		C flux				N flux				Ref
		Surf - ML	ML - 600m	below ML	below ML	Surf - ML	ML - 600m	Surf - ML	ML - 600m	Surf - ML	ML - 600m	Surf - ML	ML - 600m			
		dpm/m²/d	err	dpm/m²/day	err	$\mu\text{mol/dpm}$	$\mu\text{mol/dpm}$	mmol/m²/d	err	mmol/m²/d	err	mmol/m²/d	err	mmol/m²/d	err	
SAF	42.5°S	1200	260	-690	300	1.5	0.25	1.8	0.4	-1.0	0.4	0.30	0.07	-0.2	0.1	This study
PFZ	47.6°S	1100	220	-2900	1000	2.4	0.29	2.6	0.5	-6.9	2.4	0.32	0.06	-0.9	0.3	This study
SACCF	51.9°S	1400	280	-1890	600	4.5	0.72	6.3	1.3	-8.6	2.7	1.01	0.20	-1.4	0.4	This study
WG	57.6°S	600	120	-1100	500	3.7	0.51	2.2	0.4	-4.1	1.9	0.30	0.06	-0.6	0.3	This study
		At 100m				At 100m										
PF to Weddell Sea	-100/1700					6 - 12		0 - 39								Rutgers Van der Loeff et al. (1997)
Ross Sea	-300/2600					8 - 17		-2 - 91								Cochran et al. (2000)
PF	865					9 - 11		8.8								Rutgers Van der Loeff et al. (2002)
SAZ to PFZ	100/1800					1.4		0.1 - 2.5								Coppola et al. (2005)
SAZ to Southern	260/3000															Savoye et al. (2004)
		At 200m														
SAZ to Weddell Gyre	-400/2600															Usbeck et al. (2002)

3. Characterisation and reactivity of exported biogenic particles (WP3)

3.1. Characterisation of mesopelagic particles

How does the elemental composition and specific compound composition of exported biogenic matter change over time (and depth), once exported from the surface mixed layer? What is the fate of this exported material: remineralisation vs. preservation.

This part represents the contribution to Deliverable # 8b- Geochemical, biochemical, microbiological characterisation of mesopelagic particles

Do acantharia influence the mesopelagic Ba cycle?

The excess-Ba (Ba_{xs}) barite proxy for mesopelagic remineralisation rests on the documented knowledge that Ba_{xs} is carried essentially by barite ($BaSO_4$ microcrystals) formed within degrading micro-environments composed of biogenic detritus. However, formation of barite from Sr-Ba substitution in $SrSO_4$ skeletons of Acantharia has been described in literature (Bernstein et al., 1998). In order to validate the Ba_{xs} proxy it is of importance that such contributions to the Ba_{xs} pool be assessed. Therefore, particulate biogenic Ba, Sr and Ca and barite crystal contents from suspended matter were compared with acantharian water column distributions and individual Ba/Sr acantharian skeletal ratios during the European Iron Fertilization Experiment (EIFEX) in the Southern Ocean (Jacquet et al., 2007). We calculated the contribution of acantharian associated Ba in the upper 150 m to the mesopelagic Ba_{xs} signal (150 – 1000 m), which was shown to be accounted for mainly by barite particles. We assume that the entire Ba contents carried by acantharians in the surface layer are translocated into barite at mesopelagic depths, yielding a maximalized estimate of the contribution of acantharians to barite production. Considering our measured average acantharian Ba content (5 pmol/acantharian) and the upper 150 m acantharian abundance ($73,700\text{ m}^{-3}$) we calculate that the acantharian-associated Ba, if entirely translocated into barite and re-distributed into the 150–1000 m layer, could account for 18% of the mesopelagic Ba_{xs} contents. In a further calculation we also estimated the maximum contribution of acantharians in the upper mesopelagic waters (i.e. between 150 and 350 or 500 m) to the Ba_{xs} content of the corresponding depth layer. We note that the regression between acantharian abundance and Ba_{xs} at these depths is poor ($R^2 = 0.13$, not shown), indicating mesopelagic acantharians are not in control of mesopelagic Ba_{xs} . For the calculation we assume the average Ba content in mesopelagic acantharians is the same as for surface ocean specimens (i.e., 5 pmol/acantharian). It appears that mesopelagic acantharians can at most explain 10% of Ba_{xs} in the upper part of the mesopelagic zone. Finally, the combined acantharian Ba from the upper 150 m and the upper mesopelagic layer (150 to 350 or 500 m) are calculated to account at most for 20% of the Ba_{xs} concentrations in the 150 to 1000 m layer, with a predominant contribution of the upper ocean acantharians. Unless the turn-over rate of Ba_{xs} -barite formation in the upper 150 m is faster than the one in the mesopelagic layer, thereby inducing an accumulation effect of Ba_{xs} in the latter, it seems unlikely that acantharians thriving in surface water are the major source of barite in the mesopelagic layers.

Overall, results indicate that while acantharian associated Ba can potentially explain the entire Ba_{xs} signal in surface water, acantharian contribution to the Ba_{xs} content at

mesopelagic depths, although significant, remains minor, indicating acantharians are not the main source of barite in mesopelagic waters. This conclusion is strengthened further when considering the fact that acantharian abundances in the upper 150 m observed here exceed published abundances (e.g. Bernstein and Byrnes, 2004) by up to a factor 5, while Ba_{XS} values are similar to, or even smaller than, values reported elsewhere. It thus appears that the acantharian contribution to barite formation estimated here represents an upper limit, emphasizing that acantharians are not the main factor controlling barite formation in the water column. Further information and details of the results can be found in Jacquet et al. (2007b).

The role of diatoms in the subsurface Si cycle

We reported the first sub-surface $\delta^{30}\text{Si}$ isotopic signatures of diatoms in Cardinal et al. (2007) on the CLIVAR-SR3 transect from Polar Front Zone to Seasonal Ice Zone in late spring. Comparison of $\delta^{30}\text{Si}_{\text{bSiO}_2}$ in the mixed layer with $\delta^{30}\text{Si}_{\text{bSiO}_2}$ just below the mixed layer supports the view of dynamic changes in the Southern Ocean during spring, involving spatial differentiation due to progressive (latitudinal) delay of the season's onset as controlled by light, temperature and stratification: although sampled in early October, the PFZ had already exported diatoms which were isotopically lighter than the ones found in the mixed layer while farther south (AZ and SIZ) no depth-related isotopic change was observed in agreement with an ongoing recently started bloom. Furthermore, from our study on sea-ice (Fripiat et al., 2007; see also § Task 2.1 above) our data suggest that sea-ice diatoms are rapidly exported to the deep ocean.

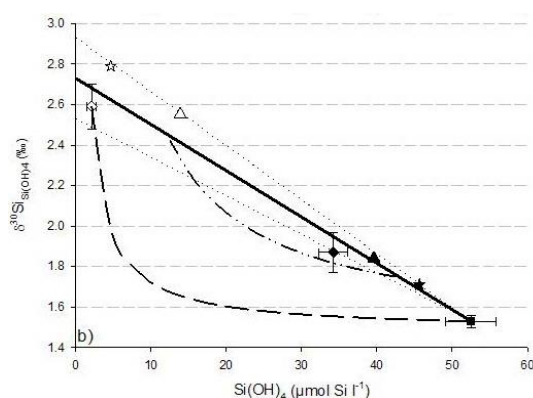


Figure 3.1.1: KEOPS. $\delta^{30}\text{Si}_{\text{Si(OH)}_4}$ vs. $[\text{Si(OH)}_4]$ for the different Si-pools in the HNLc area and in the fertilized (plateau) bloom area; error bars = $\pm 1\text{sd}$. Plain line: fractionation trends following the steady state model with HNLc WW as Si-source and the average ACC fractionation factor ($^{30}\epsilon = -1.2 \pm 0.2\text{‰}$). Mixing lines with HNLc WW and fertilized ML (dashed line). Example of mixing line between hypothetical fertilized ML and a WW having undergone Si uptake (dashed-dotted line); empty symbols = ML; filled symbols = WW. The squares, diamonds, triangles, and stars represent HNLc, plateau, B5, and A11 stations, respectively (see Fripiat et al., 2011 for more details).

A deep bSiO_2 maximum was observed during KEOPS, associated with chlorophyll-a maximum (Mosseri et al., 2008; Uitz et al., 2009). This is a recurrent feature in the S.O. (e.g. Parslow et al., 2001; Holm-Hansen and Hewes, 2004). Brzezinski and Nelson (1989) report that diatoms can produce substantial amounts of bSiO_2 at depths where little or no photosynthesis is taking place.

It is in agreement with numerous studies (cf. review by *Martin-Jézéquel et al.*, 2000; see also § 2.2) showing that energy implicated in the silicifying process is mainly of respiratory origin and so decoupled from photosynthesis. It is thus possible that the deep bSiO₂ maximum observed in the winter water below the ML consists also of silicifying diatoms which settled out of the surface waters and accumulated because of density gradients. We used our $\delta^{30}\text{Si}_{\text{Si(OH)}_4}$ data to test this hypothesis. **Figure 3.1.1** shows that plateau Winter Water fits on the steady state fractionation trend with HNLC WW as Si-source, what is a strong indication of Si uptake in WW. The ML and WW of stations B5 and A11 (located off plateau) also fall on the same fractionation trend. At A11 we observe a large deep bSiO₂ maximum (6.3 $\mu\text{mol l}^{-1}$ at 150m), indicating that WW might also have undergone seasonal Si-uptake. In contrast, bloom area WW falls completely off the mixing line between the bloom area Mixed Layer and HNLC WW (**Figure 3.1.1**) whereas it fits the steady state fractionation line. Mixing lines with HNLC WW and ML for B5 and A11 stations also cannot explain their WW Si characteristics. This suggests that subsurface Si-uptake largely dominates the fertilized bloom area WW Si(OH)₄ contents and isotopic composition. B5 and A11 stations, despite they are not exactly on the Plateau also behaves similarly. At the seasonal scale, we estimate that Si-uptake by deep diatoms could contribute up to 38% of the total bSiO₂ production of the Kerguelen bloom. This process has been so far not quantified and might have significant biogeochemical consequences for Si fluxes. It probably participates to the decoupling of Si vs. C-N cycles in the Antarctic Zone with preferential depletion of Si(OH)₄ with regard to NO₃, along with processes of silicate pump (*Dugdale et al.*, 1995) and iron-light co-limitation (*Takeda*, 1998; *Hutchins and Bruland*, 1998). Further details on these calculations can be found in Fripiat et al. (2011).

Organic biomarkers

Lipid biomarkers provide information about particulate organic matter (POM) composition and the change in relative contribution of different organisms with depth. Furthermore, their natural $\delta^{13}\text{C}$ isotopic signature can help understanding processes controlling the fate of this organic matter and identifying possible sources. Recent studies on suspended (Rontani et al., 2009) and sinking particles through the water column (Wakeham et al., 2009) emphasise the the importance of biomarker studies to document the fate of organic matter through the whole oceanic water column. To our knowledge only one study reports on sterols and their $\delta^{13}\text{C}$ in suspended particles in Southern Ocean surface water (see O'Leary et al., 2001).

Samples were taken during the SAZ-Sense expedition (Jan.-Feb. 2007; R/V Aurora Australis) and the BONUS-Goodhope (BGH) expedition (Feb.-Mar. 2008; R/V Marion Dufresne). Particulate matter was sampled from the whole water column using In Situ Large Volume Filtration Systems. Whenever possible, two particle size classes were collected: > 53 μm (i.e. particles representative of sinking particles) and 53 > > 1 μm (i.e., suspended particles). Till now our focus has been on the BGH expedition, but it is planned to analyse also the SAZ-Sense in the coming months.

Total lipids were extracted using a modified Bligh and Dyer method and separated into 3 fractions according to their polarity (neutral lipids, glycolipids and polar lipids; **Figure 3.1.2**).

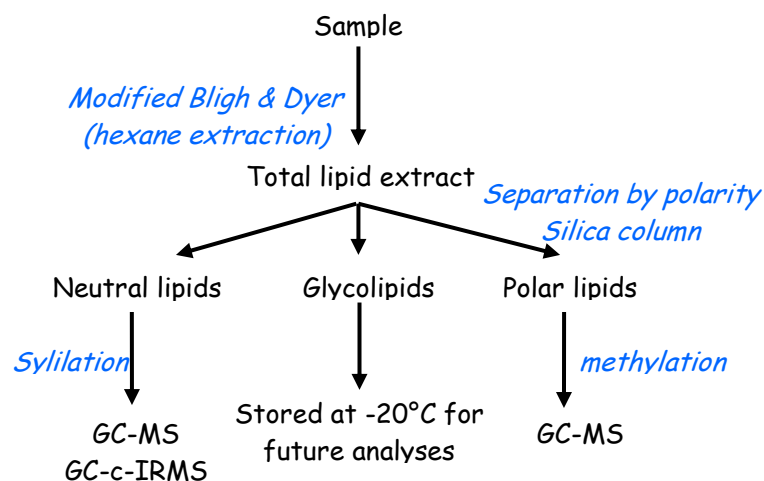


Figure 3.1.2: Extraction of lipid fractions via a modified Bligh & Dyer method. Quantitative recovery is $\leq 70\%$, and $\delta^{13}\text{C}$ standard deviation for 69 GC-c-IRMS analyses of squalane, the internal standard, is 0.90‰ ($-21.24 \pm 0.90\text{‰}$; compare with $\delta^{13}\text{C}$ value for squalane analysed via EA-IRMS: $-20.18 \pm 0.12\text{‰}$).

Glycolipids were stored at -20°C in acetone. Polar lipids from surface water were methylated and analyzed by GC-MS for identification (work in progress). The neutral lipid fraction for the BGH stations were silylated and analyzed by GC-MS and GC-c-IRMS. Data treatment focused on sterol content. The applied method also allows analysing for alkenones and alkyl-alkanoates (these are part of the neutral phase). These are coccolithophorid-specific markers, which combined with $\delta^{13}\text{C}$ information offer great potential as paleo-proxies (Riebesell et al., 2000; Benthien et al., 2007). Presently we need to solve a co-elution problem of alkyl-alkanoates and alkenones, and therefore these results are not shown here.

Results for the BONUS-GoodHope expedition

Using large volume in-situ pumps particulate matter samples were obtained from the whole water column at 5 super stations along the Greenwich Meridian (from the Cape Basin to the northern Weddell Gyre) (**Figure 3.1.3**).

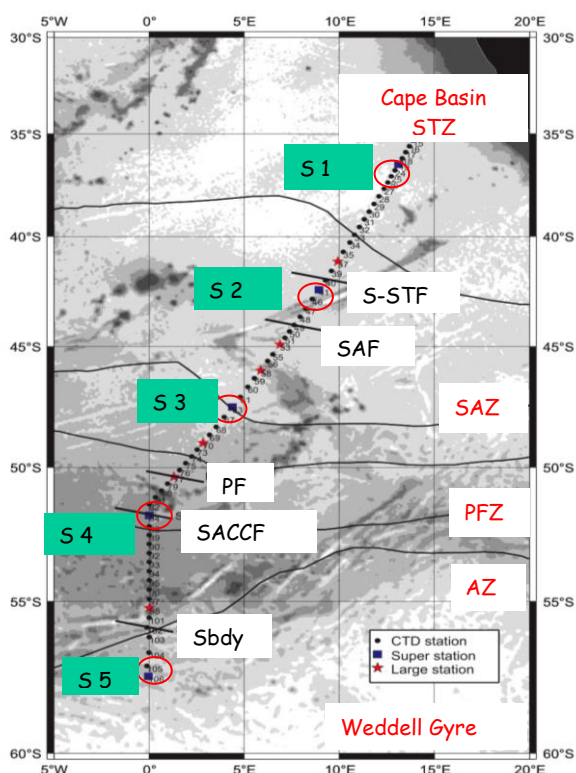


Figure 3.1.3: BONUS-GoodHope cruise. Location of stations sampled for specific compound analysis; STZ = SubTropical Zone, S-STF = South-SubTropical Front, SAZ = SubAntarctic Zone, SAF = SubAntarctic Front, AZ = Antarctic Zone, PF = Polar Front, PFZ = Polar Front Zone, SACCf = Southern ACC Front, Sbdy = Southern Boundary of the ACC).

Via the GC-MS library and literature matching individual sterols were identified. While these were common in most samples, they varied in terms of relative quantity and $\delta^{13}\text{C}$ signature. We focused on 5 of these compounds:

- (1) Phytol which is a chlorophyll proxy (it is found in plants, and esterified to chlorophyll to confer its solubility). In our samples phytol comes either from degradation of chlorophyll during chemical treatment, or was naturally formed from chlorophyll degradation.
- (2) Brassicasterol (22E)-Ergosta-5,22-dien-3 β -ol is commonly considered a diatom biomarker. However, this compound is relatively ubiquitous and can be present in other phytoplankton species as well.
- (3) Dinoergosterol (to be confirmed; 26,27-dinoregosta-5,22-dien-3 β -ol acetate) mostly associated with dinoflagellates but as for the brassicasterol, relatively ubiquitous and found in various phytoplankton species.
- (4) Cholesterol (cholest-5-en-3 β -ol) a major zooplanktonic sterol. Is an ubiquitous component.
- (5) Sitosterol (stigma-5-en-3 β -ol) mainly found in heterotrophic eukaryotes.

Figure 3.1.4 shows depth profiles (0 to 1000 m) of sterol concentrations normalized to POC content (in ‰). Phytol, brassicasterol and dinosterol as phytoplankton indicators contribute significantly to the POC content on the upper layer. Phytol shows a strong attenuation between 100 to ~ 300 m (Fig. 3A). This compound is possibly degraded by (i) photodegradation and / or by hydroperoxide induced oxidation of the chlorophyll phytol chain in senescent bloom, (ii) by marine invertebrate feedings, (iii) aerobic biodegradation of phytol -we do not cite anaerobic degradation because the studied site is not a oxygen minimum zone OMZ- (Rontani and Volkman, 2003). Work is in progress to identify possible causes of variability in degradation, attenuation of phytol and other compounds with depth. Brassicasterol and dinosterol show significant contents even at depths > 1000. Compared to phytol and dinosterol, Brassicasterol contributes more to POC pool.

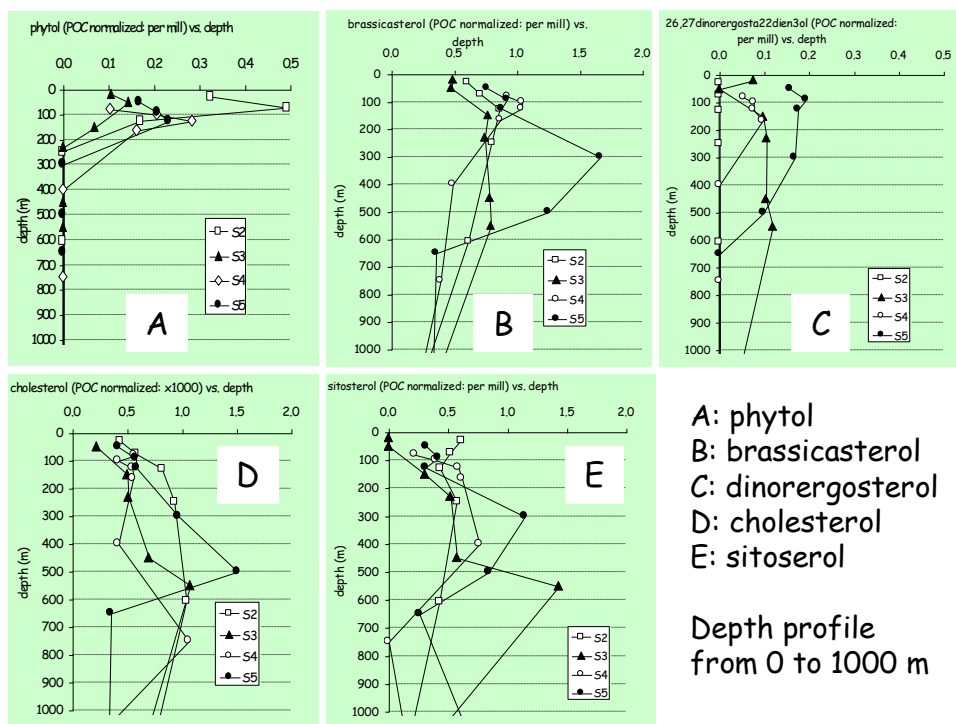


Figure 3.1.4: BONUS-GoodHope cruise. Depth profiles (0 to 1000 m) of the different normalized sterol concentrations; normalization was against POC concentration and values are in ‰.

The $\delta^{13}\text{C}$ isotopic compositions of sterols are systematically lighter than $\delta^{13}\text{C}$ -POC, as shown for cholesterol in **Figure 3.1.5**. This implies that bulk POC must consist also of carbon compounds with heavier $\delta^{13}\text{C}$ signatures (these could be proteins, amino-acids, carbohydrates, glycolipids, DNA, etc.).

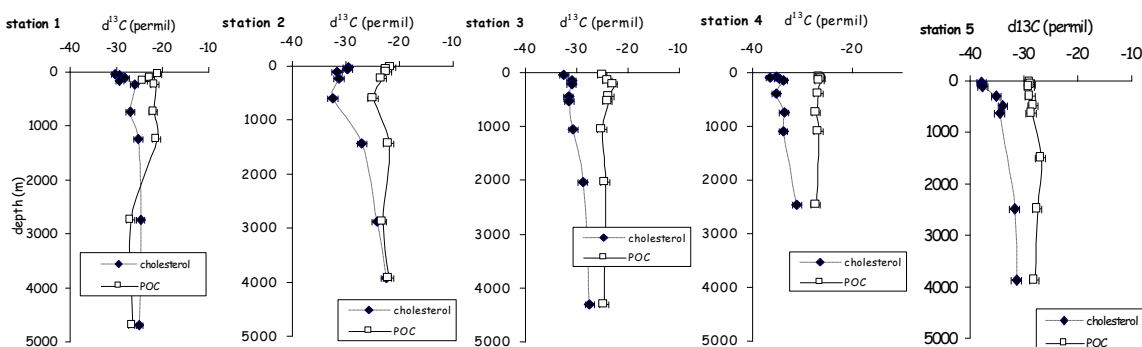


Figure 3.1.5: BONUS-GoodHope cruise. Depth profiles of $\delta^{13}\text{C}$ -POC and $\delta^{13}\text{C}$ -cholesterol for super stations 1 to 5. Circles = $\delta^{13}\text{C}$ -cholesterol; squares = $\delta^{13}\text{C}$ -POC

The isotopic variability of sterol- $\delta^{13}\text{C}$ exhibits with depth is much larger than the one for $\delta^{13}\text{C}$ -POC (**Figure 3.1.6**). This could reflect effects induced by heterotrophs and chemo-lithotrophs (degradation / synthesis).

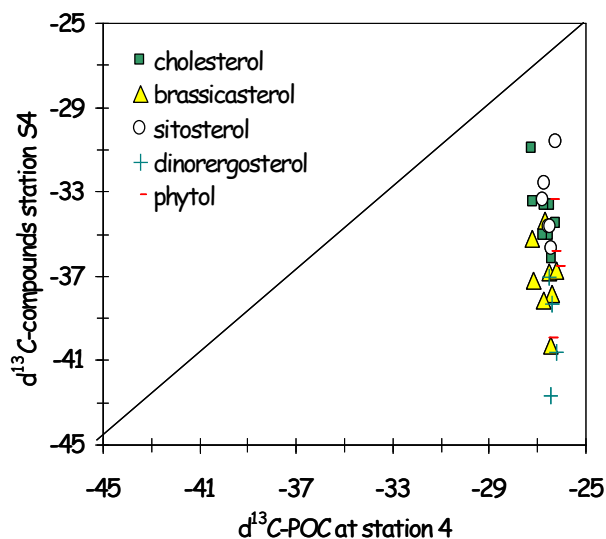


Figure 3.1.6: BONUS-GoodHope cruise. Super station 4; $\delta^{13}\text{C}$ -POC vs. $\delta^{13}\text{C}$ for individual sterols.

$\delta^{13}\text{C}$ -cholesterol increases with decreasing cholesterol content, with surface waters showing the lightest $\delta^{13}\text{C}$ -cholesterol values (**Figure 3.1.7**). Several explanations can be invoked, such as differences in particle sinking rates, differences in source regions for surface and deep suspended matter, and also a changing ratio of particle degradation vs. synthesis.

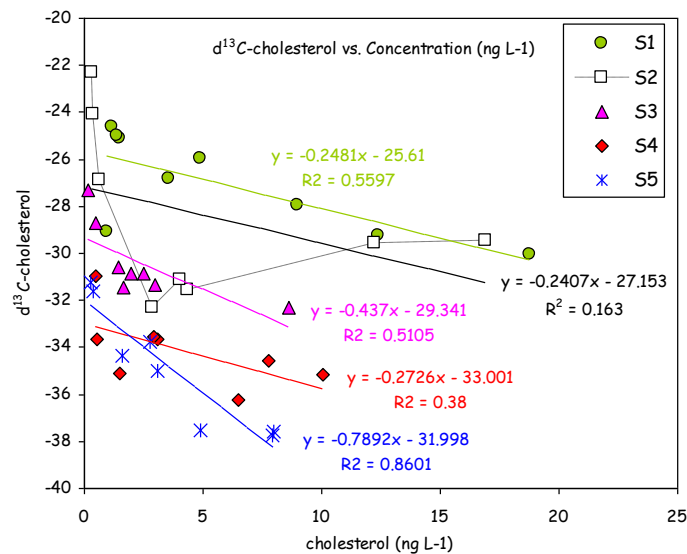


Figure 3.1.7: BONUS-GoodHope cruise. $\delta^{13}\text{C}$ variation of cholesterol vs. concentration of cholesterol.

Figure 3.1.8 shows the $\delta^{13}\text{C}$ values for two sterols plotted vs. $\delta^{13}\text{C}$ -POC. The isotopic signature of the sterols is clearly lighter than the one for bulk POC. It also is clear that $\delta^{13}\text{C}$ -sterol values become lighter southward, following $\delta^{13}\text{C}$ -POC, as related with seawater temperature and increasing pCO_2 (see also **Figure 3.1.5**).

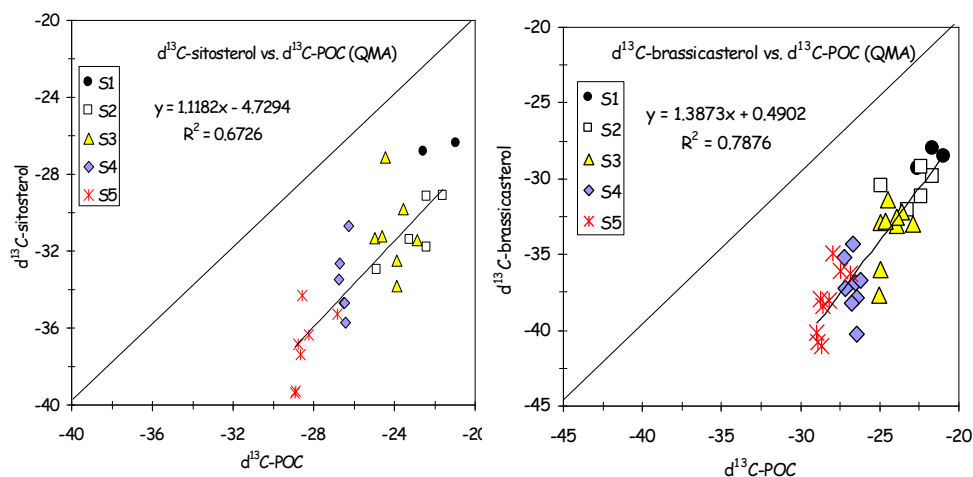


Figure 3.1.8: BONUS-GoodHope cruise. $\delta^{13}\text{C}$ -sitosterol vs. $\delta^{13}\text{C}$ -POC and $\delta^{13}\text{C}$ -brassicasterol vs. $\delta^{13}\text{C}$ -POC. Regression and R^2 values are for the combined data set.

In summary these results clearly highlight the potential of these biomarkers to shed further light on the fate of organic matter in the water column. These results were presented recently at several conferences (ASLO meeting Nice, Jan. 2009; Isocompound conference, Potsdam, June 2009; AGU Chapman conference on the Biological Carbon Pump of the Oceans, Brockenhurst, UK, Sept. 2009). They also are part of a PhD thesis (Cavagna, 2010) and will be presented in a paper (Cavagna et al., in prep.)

3.2 Remineralisation

In oceans, a large part of dissolved and particulate organic carbon produced through primary production in the surface waters is exported to the deep waters. During its downward transfer, the sinking organic carbon is submitted to degradation, eventually resulting in regeneration of nutrients and CO₂ release, with only 1% of the C export estimated to reach the seafloor (Hansell, 2002; Lee et al., 2004). That organic material sinks out of the upper layer as particulate organic carbon (POC) in the form of faecal pellets, marine snow or sinking phytoplankton (Turner, 2002) but also as dissolved organic carbon (DOC) (Ducklow et al., 2001). The efficiency of the carbon transfer and ultimately the quantity of carbon sequestered in the deep ocean (Boyd and Newton, 1999) will depend first on the magnitude of the primary production and on the ecosystem structure (Buesseler, 2007). The vertical transport of the organic material is also influenced by particle characteristics such as size, morphology, sinking rate or mineral ballasting and by grazing (Wassmann, 1998). Finally, the strength of the remineralization process through the water column determines the fate of the sinking carbon. The degradation of the organic matter (OM) happens not only in the surface layer but through the whole water column, and especially within the mesopelagic zone (also called "twilight" zone, ~100-1000 m; Hansell, 2002). Bacteria are able to remineralize the sinking particulate and dissolved organic matter by synthesizing enzymes which decompose polymeric substrates to make them directly available by the cell. A fraction of the C-uptake will be respired into CO₂ (bacterial respiration, BR) while the other fraction will serve to produce biomass (bacterial production, BP). The carbon fluxes through bacteria are particularly difficult to estimate properly, due to methodological limitations for *in situ* measuring of bacterial activity (respiration and then bacterial growth efficiency, BGE).

Methodological developments (see Willems, 2008)

Heterotrophic bacterial growth efficiency (BGE), i.e. the ratio between the carbon consumed and the bacterial biomass produced, is a key factor to understand flows of organic matter (OM) in aquatic ecosystems. Still, various approaches to determine BGE exist. Each of them involves: (1) the measurement of bacterial consumption of available organic matter (OM) and (2) the estimation of bacterial production (BP). Bacterial production is usually determined by radiotracer incorporation (³H-thymidine or leucine) though BP can also be estimated from changes in bacterial abundances. Bacterial consumption of OM can be assessed by following dissolved organic carbon (DOC) or O₂ consumption. These different methodological approaches have been applied to estimate BGE in bio-assay experiments. The evolution of the phylogenetic composition (FISH) and viability (BacLight) of the bacteria was also assessed. Results show that BGE estimated from DOC consumption were 1 to 4 times higher than BGE estimated from O₂ consumption. However, the most significant variability was due to the incubation time. **Figure 3.2.1** shows that BGE increased significantly with increasing incubation times, independently of the methodological approach. Indeed, a "bottle effect" during incubation may induce changes in bacterial viability as well as in community composition. At time 0 only a low percentage (19-24%) of bacterial cells was viable, but their fraction increased after 48h of incubation to reach up to 59%.

Fluorescent *in situ* hybridisation results indicate a modification of the major phylogenetic groups with incubation time (**Figure 3.2.2**). The proportion of *Archaea* decreased with time and among *Eubacteria*, the contribution of the gamma-*proteobacteria* group increased from 47 to 67%. Consequently, the results obtained after long incubation times may not be representative of the initial bacterial assemblages. It is therefore essential to estimate the BGE by continuously measuring O₂ over a short period of time by using optodes for instance.

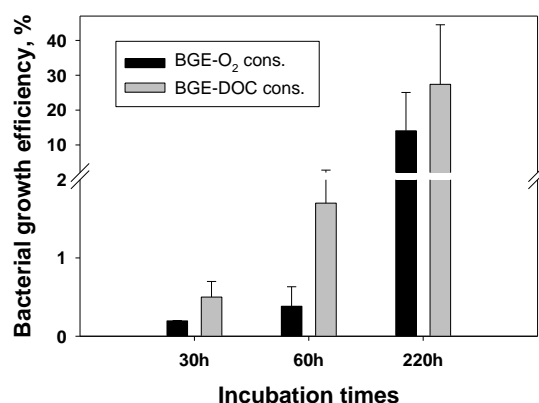


Figure 3.2.1: Bacterial growth efficiency (%) estimated by two methodological approaches (O₂ consumption, DOC consumption) for three incubation durations (30, 60 and 220h).

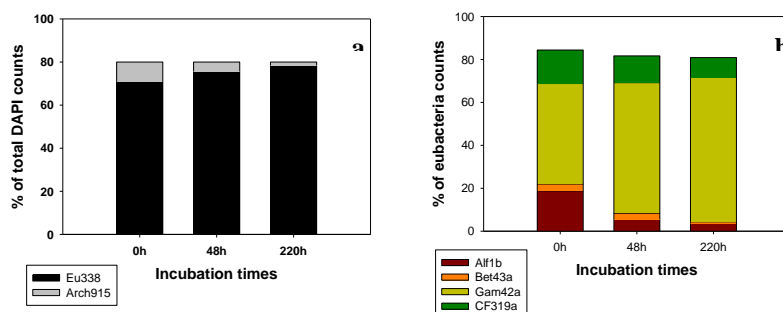


Figure 3.2.2: Major phylogenetic groups for the 3 incubation durations. (a) Contribution of *Eubacteria* (EUB338) and *Archaea* (Arch915) in the total DAPI counts (b) Contribution of alpha-*proteobacteria* (ALF1b), beta-*proteobacteria* (BET42a), gamma-*proteobacteria* (GAM42a) and *Cytophaga-Flavobacterium* (CF319a) in the total *Eubacteria*.

Laboratory experiments (see Becquevort et al. 2007)

The direct and/or indirect control of Fe availability on the degradation and remineralisation of OM was investigated via laboratory controlled experiments using *Phaeocystis antarctica* and Antarctic bacteria. The quality of dissolved as well as of particulate matter derived from *P. antarctica* improved and was rapidly degraded by bacteria in high Fe conditions. A high fraction of organic carbon consumed by bacteria was incorporated into biomass, as suggested by high bacterial growth efficiency.

Very little accumulation of DOM was observed and therefore the potential C export will mainly be due to *Phaeocystis* colonies and aggregates sedimentation. Contrastingly, in Low Fe conditions, this organic matter was slowly degraded. In this case, the persistence of DOC could participate to carbon exportation by the advection of surface water masses to greater depth. A large fraction of carbon consumed by bacteria was remineralized and respired as indicated by the low bacterial growth efficiency pointing to a lower relative potential export. By inducing increased bacterial degradation and preventing the accumulation of dissolved organic carbon, the positive effect of Fe supply on the carbon biological pump may partly be decreased.

Field observations (see publications Becquevort et al., 2009 ; Dumont, 2009 ; Dumont et al., 2009, Dumont et al., 2011; Dumont et al., in prep.)

Remineralisation of organic matter was investigated in the contrasted natural environments in the Southern Ocean. These results concern, on the one hand, the sea ice habitat where elevated concentrations of organic matter are trapped during ice formation, accumulate during winter and are released in the surface ocean at the time of ice melting. On the other hand, they address the cycling and fate of the organic matter exported below the ocean surface layer. The distribution of organic matter (OM) and its interactions with the microbial network were studied, with a special attention to the factors which regulate the biological carbon pump of the Southern Ocean. Data were collected from a) late winter to summer in the Western Pacific sector, Western Weddell Sea and Bellingshausen Sea during three sea ice cruises ARISE, ISPOL-drifting station and SIMBA-drifting station and b) summer in the Sub-Antarctic and Polar Front Zone during the oceanographic cruise SAZ-Sense. The sea ice covers were typical of first-year pack ice with thickness ranging between 0.3 and 1.2 m, and composed of granular and columnar ice. Sea ice temperature ranging between -8.9°C and -0.4°C, brines volume ranging between 2.9 to 28.2% and brines salinity from 10 to >100 were observed. These extreme physicochemical factors experienced by the micro-organisms trapped into the semi-solid sea ice matrix therefore constitute an extreme change as compared to the open ocean. At all seasons, high concentrations of dissolved and particulate organic matter were measured in sea ice as compared to the water column. Dissolved monomers (saccharides and amino acids) were accumulated in sea ice, in particular in winter. During spring and summer, polysaccharides constitute the main fraction of the dissolved saccharides pool. High concentrations of transparent exopolymeric particles (TEP), mainly constituted with saccharides, were present and their gel properties greatly influence the internal habitat of sea ice, by retaining the nutrients and by preventing the protozoa grazing pressure, inducing therefore an algal accumulation. The composition as well as the vertical distribution of OM in sea ice was linked to sea ice algae. The bacteria distribution in the sea ice was not correlated with those of algae and organic matter. Indeed, the utilization of the accumulated organic matter by bacteria seemed to be limited by an external factor such as temperature, salinity or toxins rather than by the nature of the organic substrates, which are partly composed of labile monomeric saccharides. Thus the disconnection of the microbial loop leading the OM accumulation was highlighted in sea ice.

At the time of ice melting, this accumulated OM can be used by planktonic microbial communities. Indeed, dissolved organic and inorganic nutrients from sea ice have a positive effect on the growth of pelagic micro-organisms.

Bacterial remineralization was investigated during the summer SAZ-Sense cruise (Jan.-Feb. 2007) in the sub-Antarctic and Polar Front Zones (SAZ and PFZ) of the Australian sector. Measurements of bacterial biomass (BB), ectoproteolytic activity (EPA) and bacterial production (BP) were undertaken over the epipelagic (0-100 m) and mesopelagic (100-700 m) depth zones. Bacterial phylogenetic composition (FISH) and viability (SYTOX) were also determined. All these parameters were related with the on concentrations of dissolved organic matter, saccharides and chlorophyll a (Chl-a) (Dumont et al., 2011).

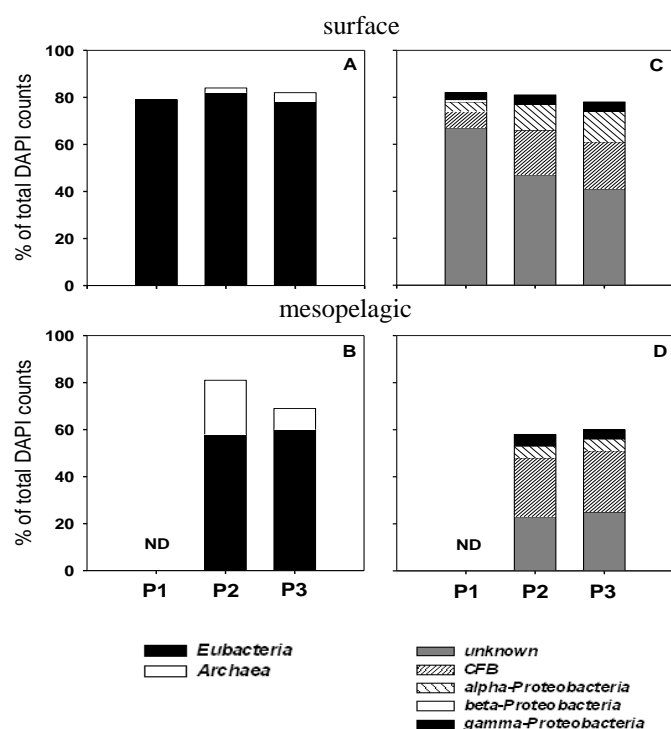


Figure 3.2.3: SAZ-Sense cruise. Major bacterial phylogenetic groups as determined by FISH at the 3 process stations (P1, SAZ-West; P2, PFZ; P3, SAZ-East). Probe data are given as % of cells detectable after DAPI staining. Distribution of total DAPI counts between *Eubacteria* and *Archaea* in surface (A) and mesopelagic (B) layers; distribution of *Eubacteria* in the main groups in surface (C) and mesopelagic (D) layers.

Bacterial biomass and associated processes were higher in the surface layer of the SAZ-West compared to SAZ-East. Interestingly, results at the Polar Front show maximum values in subsurface waters. Picoplanktonic cells stained with DAPI hybridized with the probe EUB338 specific for *Eubacteria* using *in situ* hybridization with oligonucleotide probes, accounted for between 70 and 83% of total cell count in the surface layer (**Fig. 3.2.3A**) and between 51 and 65% in the mesopelagic layer (**Fig. 3.2.3B**). The proportions of *Archaea* ranged from 0 to 25% of total DAPI counts, with highest values observed in mesopelagic waters, particularly in the PFZ (Figure 13B). Among the *Bacteria*, the *Cytophaga/Flavobacteria* subgroup dominated (**Fig. 3.2.3C, D**).

Bacterial parameters followed Chl-*a* and organic matter distributions. Dissolved organic carbon (DOC) concentrations ranged from 47 to 86 μM and were higher in the upper 100 m of water column compared to deeper waters. Higher surface DOC concentrations (84 μM) were observed in the SAZ-East, compared to the SAZ-West (56 μM) and the Polar Front (55 μM). At the PF a subsurface maximum (at about 50m deep; 75 μM) was present, roughly coinciding with a deep chlorophyll maximum (DCM) (at approx. 75 m; 0.23 $\mu\text{g l}^{-1}$). Concentrations of dissolved saccharides showed a rather similar trend with depth and accounted for between 2.4% and 25.6% of DOC. The contribution of saccharides to DOC did not show any particular trend with depth or region.

Table 3.2.1: SAZ-Sense cruise. Bacterial carbon demand (BCD) for the surface (0-100 m), the mesopelagic (100-700 m) and the 0–700 m water column, using $\text{TCF} = 0.86 \times 10^{18}$ cells mol^{-1} and $\text{BGE} = 0.15$. The min. values are based on $\text{TCF} = 0.5 \times 10^{18}$ cells mol^{-1} and $\text{BGE} = 0.38$; the max. values are based on $\text{TCF} = 2.0 \times 10^{18}$ cells mol^{-1} and $\text{BGE} = 0.09$; all values are given in $\text{mg C m}^{-2} \text{d}^{-1}$. Also shown are column integrated Primary Production (PP; from Westwood et al., 2011) and Export Production at 100 m (EP100m; from Jacquet et al., 2011b) (data are from Dumont et al., 2011)

Station	PP	EP _{100m}	BCD _{0-100m} (min-max)	BCD _{100-700m} (min-max)	BCD _{0-700m} (min-max)
2	277	118±26	269 (62-1041)	150 (35-590)	419 (97-1632)
P1 d3			536 (123-2078)	135 (31-522)	671 (154-2600)
P1 d5			378 (87-1465)	207 (48-804)	586 (134-2269)
P1 av.	1304±300	122±15	457±112	171±51	629±60
P2 d1			364 (83-1410)	161 (37-625)	525 (120-2035)
P2 d2			291 (67-1127)	237 (57-967)	528 (124-2095)
P2 d3			249 (57-966)	701 (161-2718)	951 (218-3684)
P2 d6			375 (85-1444)	161 (38-641)	536 (123-2085)
P2 av.	475±169	94±17	320±60	315±260	635±211
9	625	540±20	174 (40-673)	149 (35-585)	323 (74-1257)
10	539	66±18	202 (46-784)	150 (34-580)	352 (81-1365)
12	950	56±22	320 (73-1240)	113 (31-523)	433 (104-1763)
P3 d1			894 (205-3467)	144 (37-622)	1038 (242-4089)
P3 d3			571 (131-2214)	187 (47-733)	759 (178-2947)
P3 d5			1105 (280-4254)	233 (76-881)	1338 (357-5136)
P3 av.	749±542	49±9	857±269	188±45	1045±290
21	-	-	921 (211-3569)	105 (24-408)	1026 (236-3978)
24	-	-	1091 (250-4227)	177 (41-688)	1268 (291-4915)

Bacterial abundance, biomass and activities decreased drastically below 100 to 200 m. Nevertheless, depth-integrated rates showed that mesopelagic bacteria (residing in the 100 to 600m depth layer) contributed a non-negligible fraction of up to 53±7%, 43±14% and 33±19% of water column (0 to 700 m) bacterial biomass (BB), ectoproteolytic activity (EPA) and bacterial production (BP), respectively.

We evaluated the coupling between primary production and bacterial carbon demand (BCD). The latter was obtained from BP and bacterial growth efficiency (BGE) using different published values for the conversion factors. Calculated min. – max. BCD values are shown in **Table 3.2.1** and are compared with primary production data (i.e. gross prim. prod.) obtained by (Westwood et al., 2011) and export production (obtained by Jacquet et al., 2011b).

Only the minimal and average estimations of BCD would be in agreement with primary production and this holds for surface waters as well as for the upper 700 m. Minimal BCD estimates for SAZ-East, PFZ and SAZ-West would use on average 13, 12 and 21% of the primary production, respectively. Average BCD values, however, indicate up to 58, 52 and 85% of primary production is consumed by bacteria in the SAZ-East, PFZ and SAZ-West. The significance of the applied conversion factors and BGE value for the C budget estimated and the use of a constant value for the whole season and all depths is of course questionable.

BCD was also compared with estimates of C-export based on the ²³⁴Th deficit method and with mesopelagic remineralization estimated from excess particulate barium contents (**Table 3.2.2**). In the SAZ, only the lower estimates of BCD are compatible with C-export out of the surface layer. In the PFZ, however, estimates of BCD largely exceed C export. Overall, mesopelagic BCD values were higher than mesopelagic remineralization estimated from Ba_{xs} contents, but the similarity in spatial distributions of both parameters persists with highest values in the PFZ.

Table 3.2.2: SAZ-Sense cruise. Comparison of mesopelagic organic carbon remineralization (MR, data from Jacquet et al., 2011a) with gross primary production (GPP) and new production (NP, data from Cavagna et al., 2011), bacterial carbon demand (BCD, data from Dumont et al., 2011) and export production (EP, data from Jacquet et al., 2011b); r-ratio (in %) = ratio of MR over EP.

All fluxes in mmolC m ⁻² d ⁻¹							
Station	Area	Column integrated PP ⁽¹⁾	NP ⁽²⁾ <i>euphotic layer</i>	BCD ⁽³⁾ <i>100-600 m</i>	EP ⁽⁴⁾ <i>100 m</i>	MR <i>100-600 m</i>	r-ratio= MR/EP %
Process 1	SAZ West	108.7 ± 25	27 ± 25	14 ± 4.1	10.15 ± 1.28	2.1 ± 0.4	21 ± 5
Process 2	PFZ	39.6 ± 14.1	8.7 ± 1.8	27.1 ± 21.4	7.82 ± 1.46	5.0 ± 1.6	64 ± 24
Process 3	SAZ East	62.4 ± 45.2	10.2 ± 1.8	15.9 ± 3.8	4.08 ± 0.79	3.7 ± 0.4	91 ± 20
<i>Casts transit stations</i>							
5	SAZ West	23.1	-	10.7	9.80	3.1	32
36	SAZ West	31.9	-	-	10.55	-	-
64	SAZ East/ PFZ	52.1	-	13.7	4.45	3.7	84
66	SAZ East	44.9	-	12.2	5.52	4.3	78
71	SAZ East	79.2	-	13.6	4.69	6.1	130
93	SAZ East/ STZ	214.3	-	8.8	4.69	3.0	64
108	STZ	-	-	15.8	-	1.0	-

⁽¹⁾ PP= Primary Production; data from Westwood et al., this volume

⁽²⁾ NP= New Production; data from Cavagna et al., this volume

⁽³⁾ BCD= Bacterial C Demand; data from Dumont et al., this volume

⁽⁴⁾ EP= Export Production; data from Jacquet et al., this volume

Particulate Ba_{xs} in the twilight zone (the 100–600 m) proved to be significantly controlled by the vertical distribution of bacterial activity, with higher particulate Ba contents in situations where significant bacterial activity extended deeper in the water column.

This is reflected by the negative correlation between the ratio of mixed layer integrated BP / BP integrated over the upper 600m vs. mesopelagic Ba_{xs} content (**Figure 3.2.4**).

Note that such a type of correlation was also observed during KEOPS (Jacquet et al., 2008), what confirms the link between mesopelagic Ba_{xs} and bacterial remineralisation. However, despite this co-variation, the magnitude of the carbon fluxes as estimated from particulate Ba and bacterial activity did not match well, with carbon demand based on bacterial activity largely exceeding organic carbon remineralization estimated from Ba_{xs} . BCD exceeds the organic carbon remineralization rate based on Ba_{xs} by five-fold on average. We note however that Ba_{xs} -based remineralization rates are in the same range (but usually lower, as expected) than new production and also C-export, while BCD values are clearly in excess of carbon export (**Table 3.2.2**).

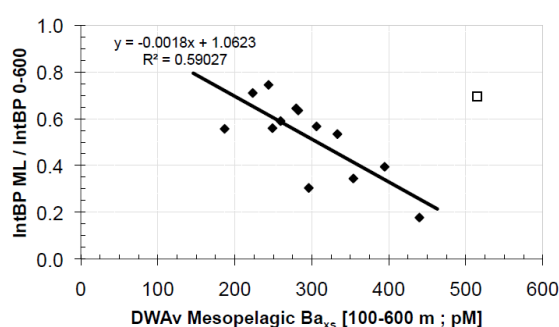


Figure 3.2.4: SAZ-Sense cruise. Regression of the ratio of mixed layer (ML) integrated BP over upper 600 m integrated BP (data from Dumont et al., 2011) versus depth weighted average (DWA) mesopelagic Ba_{xs} (pM; 100-600 m; data from Jacquet et al., 2011a). Open square is cast #58 at P2; this station is not included in the regression.

We also note that Ba_{xs} based remineralization rates are within about a factor 2 of the POC flux sampled by drifting sediment traps deployed at 150 m (Ebersbach et al., 2011), giving further credence to the calculated carbon remineralization rate values.

Possible reasons for the discrepancy between BCD and remineralisation obtained from the Ba_{xs} proxy are: (i) BCD is *in fine* satisfied by dissolved organic C availability; such DOC if not originating from the upper water column but rather supplied, for instance, by advection, would not be accounted for by the Ba_{xs} proxy. (ii) The bacterial growth efficiency (BGE) is a key factor to calculate BCD and could have been underestimated. The oceanic BGE values reported in literature vary widely and are in general rather poorly constrained (see Burd et al., 2010). Published BGE values generally concern free-living bacteria and do not concern the bacteria associated with aggregates. The latter, however, likely have higher BGE values (Azam and Long, 2001). A better matching of BCD and Ba_{xs} -based remineralization would require a BGE value > 0.15 . (iii) Finally it is important to consider that the mesopelagic Ba_{xs} proxy reflects processes integrated over a period of days to weeks (Cardinal et al., 2005; Jacquet et al., 2008b), while BCD is based on $< 8h$ incubations. Thus, part of the discrepancy may also result from differences in the characteristic time scales covered by both methodological approaches.

In **Figure 3.2.5** we compare the mesopelagic Ba_{XS} inventories for the SAZ-Sense cruise with the ones we obtained for the same area during SAZ'98 (summer 1998; Cardinal et al., 2001) and CLIVAR-SR3 (spring 2001; Cardinal et al., 2005; Jacquet et al., 2007). A clear seasonal trend is apparent from this graph, with mesopelagic Ba_{XS} contents increasing from late spring over mid summer to late summer. These data also highlight the consistency of the Ba_{XS} signal over the past decade with mesopelagic remineralisation increasing in the PFZ.

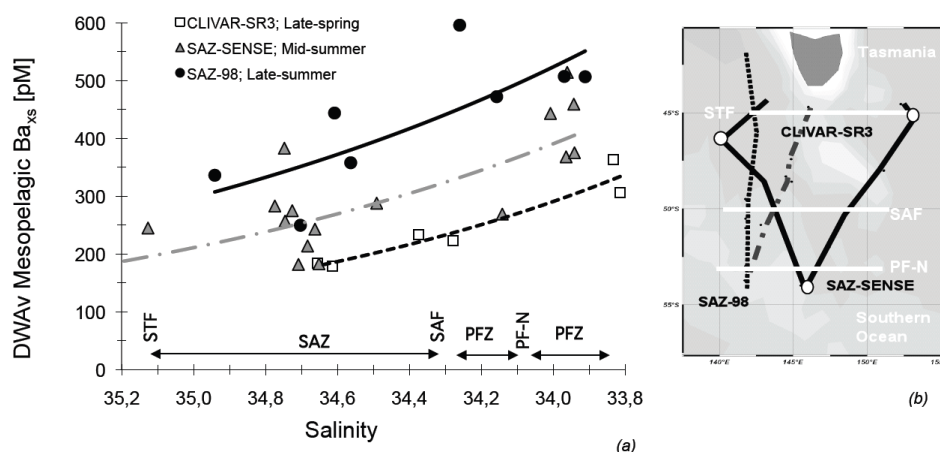


Figure 3.2.5: (a) Latitudinal distribution of depth weighted average (DWAv) mesopelagic Ba_{XS} (pM) vs. salinity at 150 m; salinity is taken here as a proxy for latitudinal position eliminating temporal and spatial variability in position of the fronts and water masses. Shown are data for the CLIVAR-SR3 cruise (squares, late-spring; Cardinal et al., 2005); the SAZ-SENSE cruise (triangles, mid-summer; Jacquet et al., 2011a) and the SAZ-98 cruise (circles, late-summer; Cardinal et al., 2001; 2005); regression lines (power functions) are shown to highlight the trend. Since for the earlier SAZ-98 and CLIVAR-SR3 cruises DWAv Ba_{XS} values shown are for the 100-450 m depth interval, we considered the same interval for the SAZ-Sense data plotted in this graph, for internal consistency. The difference with DWAv Ba_{XS} values for the 100-600m interval is minor (see text); (b) cruise tracks. STF = Subtropical Front; SAZ = Subantarctic Zone; SAF = Subantarctic Front; PFZ = Polar Front Zone; PF = Polar Front.

Role of Fe in mesopelagic remineralisation

Remineralisation has been studied in a system under Fe-repletteness (i.e., the KEOPS naturally fertilized plateau area; Jacquet et al., 2008b) and the EIFEX artificially fertilised eddy (Jacquet et al., 2008a). In both cases, a large diatom bloom is induced by Fe supply. The proximal Fe-limited HNLC areas were studied as well. The results for KEOPS and EIFEX are remarkably similar in terms of remineralisation efficiency, being the ratio between export production (from integrated ^{234}Th deficit at 100m) over mesopelagic remineralisation (from meso- Ba_{XS} proxy). For the stations under Fe influence we found a mesopelagic remineralization efficiency of $13 \pm 10 \%$ for EIFEX and $11 \pm 2 \%$ for KEOPS. In contrast, the HNLC stations have higher remineralization efficiencies: $33 \pm 8\%$ for EIFEX before the Fe release and $29 \pm 15 \%$ for KEOPS for the off-plateau area.

These results suggest that export from large diatom-dominated blooms (which are the typical phytoplankton assemblage in Fe-replete conditions) is less prone to remineralization, probably because of a faster transfer of matter (larger and denser sinking aggregates) through the water column leaving less time for mesopelagic remineralization to occur. Although this would suggest that Fe enrichment would favor deep C sequestration, it should be stressed, however, that such Fe blooms are limited in time and space because Fe becomes rapidly depleted and is quickly followed by Si limitation. Furthermore, for EIFEX the induced export event was short and the enhancement of export relative to pre-fertilization conditions, rather moderate (Jacquet et al., 2008).

Our results for the SAZ-Sense cruise do not fully corroborate the above findings. We observed that the iron-replete Sub-Antarctic Zone east of the Tasman Plateau (station P3 in **Figure 2.2.2**) has not only a slightly lower export ratio ($EP/GPP = 6\%$; see above, **Figure 2.3.6**) but also a higher mesopelagic remineralization efficiency (on average 91% of the carbon exported from the upper 100 m) compared to the SAZ area West of the plateau (station P1 in **Figure 2.2.2**), where the remineralization efficiency was on average only 21%. These differences in remineralization efficiencies combined with differences in export ratios (see above) resulted in the Fe-limited SAZ-West being more efficient in deep ocean (>600 m) carbon sequestration than the Fe-replete SAZ-East (**Figure 3.2.6**). In this case effects of grazing pressure, inhibition of nitrate uptake by ammonium, shading, were invoked to explain the differences in carbon fluxes between Fe-replete and Fe-limited systems.

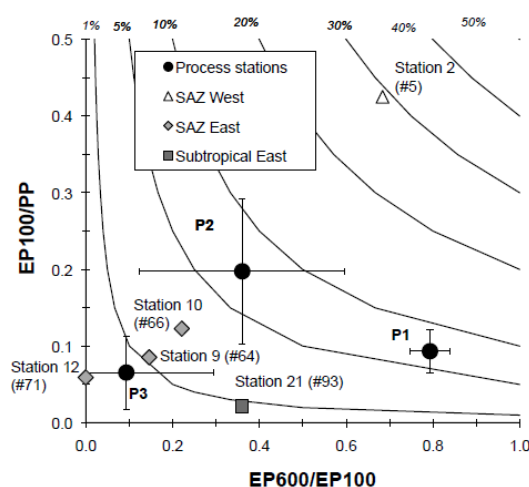


Figure 3.2.6: SAZ-Sense cruise. Y-axis: EP_{100}/GPP = POC flux from upper 100 m (EP_{100}) as a fraction of gross primary production (GPP); X-axis: EP_{600}/EP_{100} = POC flux at 600 m as a fraction of POC flux at 100 m. Isolines represent the modeled 0.05, 1, 5, 10, 20 and 30% of GPP export to depths >600 m. From Jacquet et al. (2011a).

In **Table 3.2.3**, we have summarized qualitative results regarding export, organic matter remineralisation and potential for deep ocean carbon storage for the SAZ'98, CLIVAR-SR3, KEOPS and EIFEX cruises. We note that the conditions for highest deep carbon sequestration are present for Antarctic Zone in spring under Fe-replete conditions.

Table 3.2.3: Overview of carbon flux strengths (qualitative scaling) as a function of season, zone (latitude), depth and Fe content. SAZ: Subantarctic Zone; SAF: SubAntarctic Front; (I)PFZ: (Inter)Polar Front Zone; AZ: Antarctic Zone; SIZ; Seasonal Ice Zone

	Primary Production	New Production	Export from surface	Mesopelagic Remineralisation	Deep carbon sequestration
Season					
Spring		high (i)	weak (ii)	moderate (iii)	moderate
Summer		moderate (iv)	n.a.	moderate to high	weak
Zone					
SAZ-SAF		moderate (i, iv)	moderate (ii)	weak (iii, v)	moderate
PFZ-IPFZ		weak (i, iv)	weak (ii)	high (iii, v)	weak to moderate
AZ-SIZ		high (i)	high (ii)	moderate (iii, v)	moderate to high
Fe					
replete	high (vi)	weak (vii)	moderate (viii, ix, x)	weak (ix, x)	moderate
deplete	weak (vi)	moderate (vii)	weak (viii, ix, x)	moderate (ix, xj)	weak

(i) Savoye et al., 2004a (CLIVAR-SR3)

(ii) Savoye et al., 2004b (CLIVAR-SR3)

(iii) Cardinal et al., 2005 dsr1 (CLIVAR-SR3)

(iv) Elskens et al., 2002 (SAZ98)

(v) Cardinal et al., 2001 (SAZ98)

(vi) Lefèvre et al., 2008 (KEOPS)

(vii) Mosseri et al. 2008 (KEOPS)

(viii) Savoye et al., 2008 (KEOPS)

(ix) Jacquet et al., 2008 dsr2 (KEOPS)

(x) Jacquet et al., 2998 gbc (EIFEX)

The work presented above is a contribution to Deliverable # 9b "Carbon fluxes due to mineralization in the mesopelagic zone"

More information regarding these data can be found in the following papers:

- KEOPS export: Savoye et al. (2008 ; DSR II)
- KEOPS remineralisation: Jacquet et al. (2008 ; DSR II)
- EIFEX export and remineralisation: Jacquet et al. (2008; GBC)
- CLIVAR-SR3 export: Savoye et al. (2004; GRL)
- SAZ98 and CLIVAR-SR3 remineralisation: Cardinal et al. (2001; 2005; DSR I)
- SAZ-Sense production: Cavagna et al. (2011; DSR II)
- SAZ-Sense export: Jacquet et al. (2011b; DSR II)
- SAZ-Sense: OM remineralisation based on bacterial activity: Dumont et al., (2011; DSR II and on mesopelagic Ba_{xs} inventories: Jacquet et al. (2011a; DSR II)

3.3. Impact of mesopelagic processes on nutrient profiles

3.3.1. High resolution dissolved Ba profiles

The multiple end-member mixing approach, called Optimum Multi - Parameter method and well known from literature was improved as follows: (1) mixing ratios are not estimated directly but instead are described by 2D splines and spline coefficients are estimated (this results in a reduction of unknowns to be estimated and consequently in a more robust method); (2) thanks to this parameter reduction it is possible also to optimize the end-member characteristics (simultaneously with the spline coefficients); (3) adequate inclusion of data variability in a statistical analysis of results facilitates identification and quantification of non-conservative processes. This work has led to a publication by de Brauwere et al. (2007), in JGR-Oceans. Reconstructed mixing fractions using the POMP method for the PFZ and SAZ along WOCE SR3 line are shown in **Figure 3.3.1**.

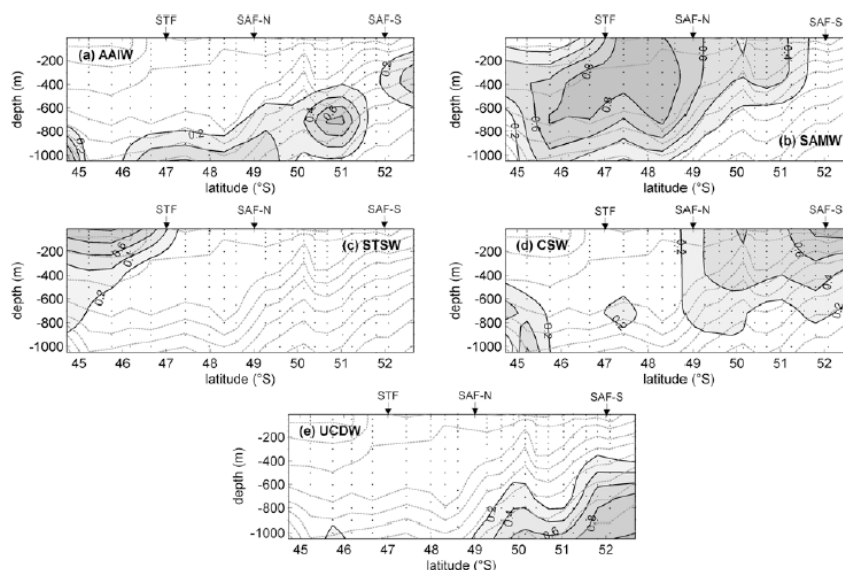


Figure 3.3.1: Mixing fractions associated with (a) Antarctic Intermediate Water, (b) Subantarctic Mode Water, (c) Subtropical Surface Water, (d) Circumpolar Surface Water and (e) Upper Circumpolar Deep Water, estimated using the POMP method for the spring 2001 situation along SR3 line south of Tasmania. Density isolines are plotted as dotted gray lines and range from 26.6 (upper north corner) to 27.6 (lower south corner) with increments of 0.1. From de Brauwere et al. (2007).

The improved method, called POMP (Parametric OMP), is being applied to dissolved Ba profiles from SAZ'98 (1998), CLIVAR-SR3 (2001); KEOPS (2005) and CIVA-1 (1992), and will be applied to dissolved Ba results we recently obtained for the Weddell Sea (ANT XXIII expedition, 2005; see **Figures 3.3.2 and 3.3.3**). By comparing the Ba fields reconstructed with the POMP method, which reflect the effect of mixing only, with the observed Ba fields, the impact of non-conservative processes (i.e. uptake, release) may be evidenced. For SAZ'98 (SAZ and PFZ south of Tasmania during, summer 1998) the approach pointed to the occurrence north of the PF of regions where dissolved barium at mesopelagic waters could not be reconstructed by mixing only. This result indicates non-conservative processes to operate, such as uptake of dissolved Ba followed by the release of particulate excess Ba in mesopelagic waters.

In **Figures 3.3.2 and 3.3.3** we show the dissolved Ba field obtained for a north south transect (SE-NW) through the Weddell Sea and the section across the Weddell Gyre along the Greenwich Meridian (Polarstern ANT XXII/3 expedition, 2005; collaboration with Mario Hoppema, AWI, Bremerhaven; Hoppema et al., 2010)

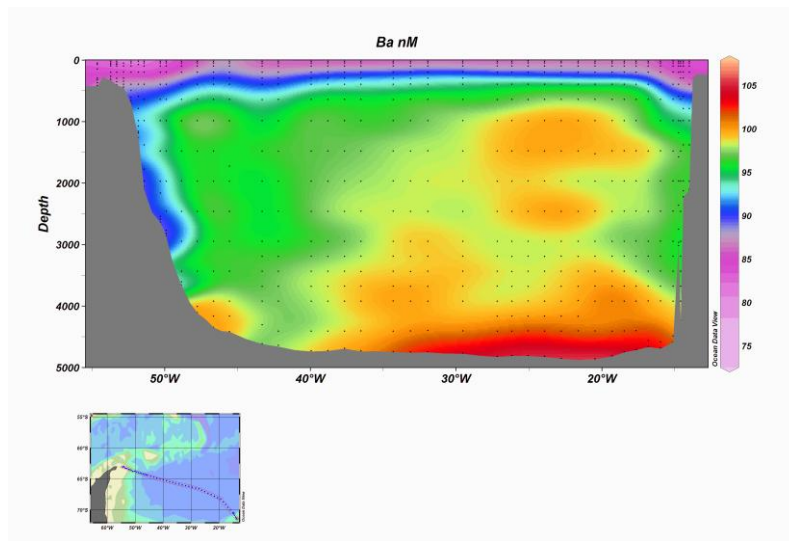


Figure 3.3.2: Polarstern ANT XXII/3 expedition (2005). Dissolved Ba transect through the Weddell Sea; Hoppema et al. (2010). The Southern Ocean data base of dissolved barium (Ba_d) has been augmented significantly with two sections across the Weddell Gyre sampled by the icebreaker FS Polarstern during February and March 2005.

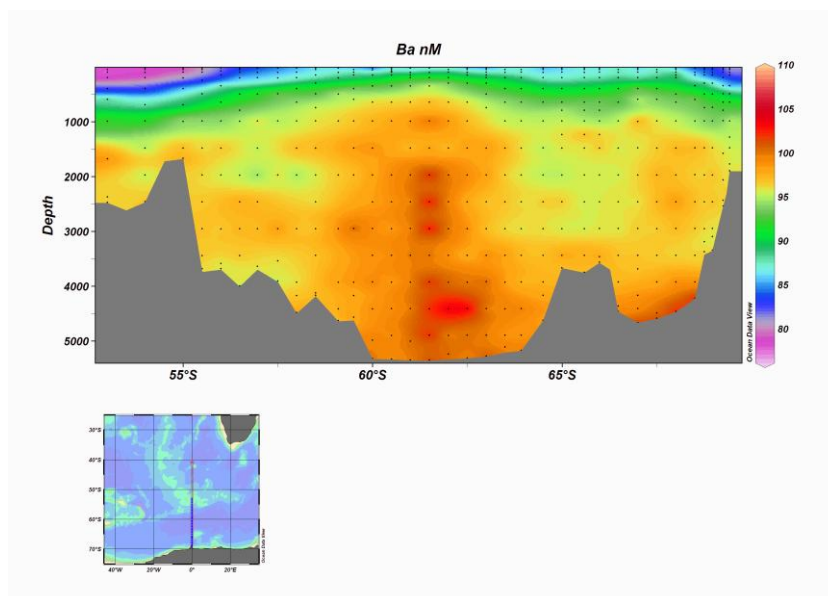


Figure 3.3.3: Polarstern ANT XXII/3 expedition (2005). Dissolved Ba transect through the Weddell Gyre along the Greenwich Meridian; Hoppema et al. (2010).

Compared to the inflowing water into the Weddell Gyre and also to the surface water, the deep water of the Weddell Basin was characterized by a Ba_d enrichment. We tentatively identified sea-ice formation as the process that forms particulate Ba in the form of barite.

The particulates rain down the water column and dissolve in deeper water where undersaturation of barite prevails. In the bottom layer, an enhanced enrichment of Ba_d occurs, exhibited as a Ba_d maximum, which is caused by Ba efflux from the sediments. In recently formed Weddell Sea Bottom Water, a Ba_d minimum is observed (see left part of the section in **Figure 3.3.2**; i.e., off Joinville Island), imposed by the shelf water component of bottom water, which has relatively low Ba_d concentration. Like in other Southern Ocean regions a strong correlation exists between Ba_d and dissolved silicate all through the water column, though the relationship is different from that at 30°E (CIVA-1 cruise, 1994; unpublished results; **Figure 3.3.3**). The slope of the Ba_d versus silicate regression is larger and the Ba_d intercept at zero silicate smaller at 30°E. In the Weddell region the higher Ba level points to a smaller Ba over Si uptake ratio in the Weddell Sea upper waters, as compared to the ACC elsewhere or a mechanism retaining Ba within the Gyre system (Hoppema et al., 2010).

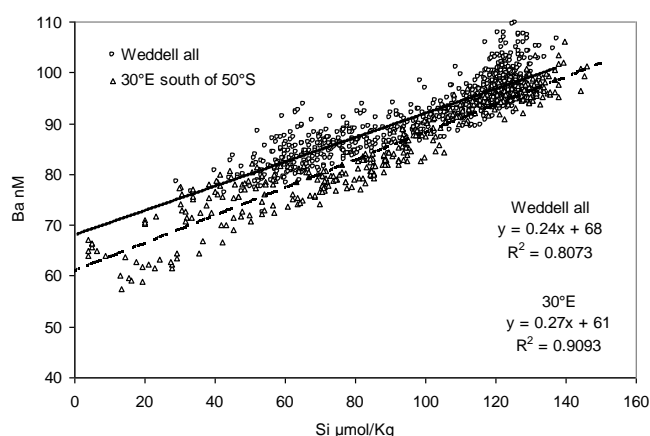


Figure 3.3.4: Polarstern ANT XXII/3 expedition (2005) and CIVA-1 (1994). Dissolved Ba (nM) vs silicate (µM).

Recently dissolved Ba has been analysed also for the 2008 BONUS-GoodHope transect (Cape basin to 58°S, Greenwich Meridian), closing an entire section between Cape Town and Antarctica along Greenwich.

3.3.2 Results for silicon stable isotope profiles

Complete open oceanic $\delta^{30}\text{Si}_{\text{Si(OH)}_4}$ profiles have been published for the first time in the framework of CLIVAR-SR3 expedition (Cardinal et al., 2005) and it was highlighted that largest isotopic shifts with depth occur in the upper mesopelagic zone. Since then we acquired many more profiles for other S.O. sites (EIFEX, KEOPS, Bonus-GoodHope expeditions). In the **Figure 3.3.5** we compare the upper 1000m profiles for two north-south transects: along 142°E (CLIVAR-SR3, spring 2001) and along ~0°E (Bonus-GoodHope, summer 2008).

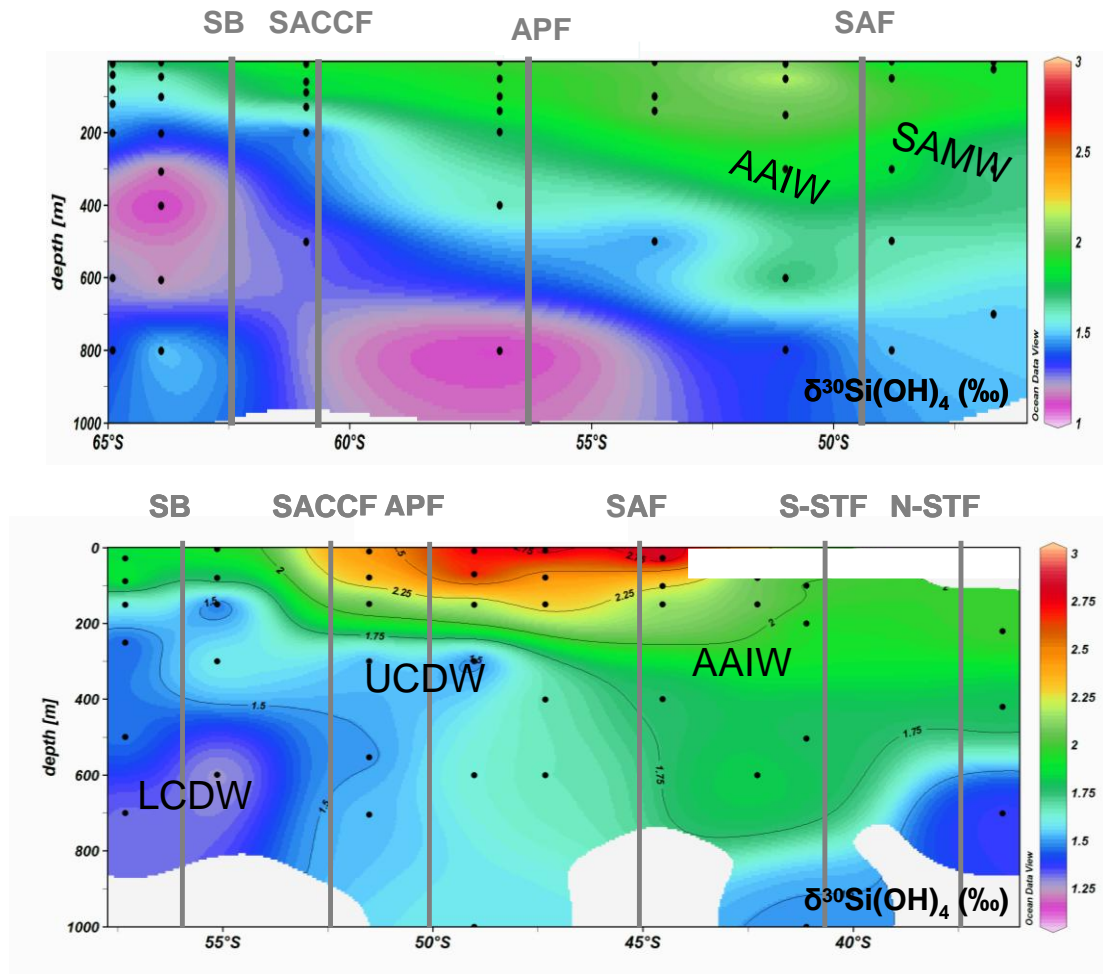


Figure 3.3.5: Latitudinal variations of $\delta^{30}\text{Si}_{\text{Si}(\text{OH})_4}$ in the upper 1000m along 145°E (upper panel; CLIVAR-SR3; spring 2001; data from Cardinal et al., 2005) and along the Greenwich Meridian (lower panel; BONUS-GoodHope; summer 2008; data from Fripiat et al., submitted). Main water masses are: LCDW, Lower Circumpolar Deep Water; UCDW, Upper Circumpolar Deep Waters; AAIW, Antarctic Intermediate Water; SAMW, Subantarctic Mode Water. Vertical lines indicate the positions of the Fronts: SB, Southern Boundary; SACCF, South Antarctic Circumpolar Current Front; APF, Antarctic Polar Front; SAF, Subantarctic Front; S-STF and N-STF, South and Northern branch of Subtropical Front.

The Si-isotopic signatures of the different water masses in the mesopelagic zone are very similar between the two cruises while surface water Si isotopic signatures are variable. In **Table 3.3.1** we summarize Si isotopic compositions and concentrations for the Antarctic Zone. The summer ML $\delta^{30}\text{Si}_{\text{Si}(\text{OH})_4}$ values during KEOPS (2.4 ± 0.3 ‰; Fripiat et al., 2011) as well as those obtained during EIFEX (2.6 ± 0.1 ‰; out-patch values; Cavagna et al., 2011) are larger than the spring isotopic values we reported for the Australian sector: 1.9 ± 0.1 ‰ (Cardinal et al., 2005). This is consistent with the ML becoming more depleted in $\text{Si}(\text{OH})_4$ with progress of the growth season, paralleled by a ^{30}Si enrichment of the $\text{Si}(\text{OH})_4$ pool, and this because of preferential ^{28}Si -uptake by diatoms and their sinking out of the ML. Varela et al. (2004) reported a similar observation during a bloom propagating from the APF southward through the Pacific sector of the AZ (see also **Table 3.3.1**). Also our results for the 2008 BONUS-GoodHope cruise corroborate this.

Table 3.3.1: Average $\delta^{30}\text{Si}_{\text{Si}(\text{OH})_4}$, and $\delta^{30}\text{Si}_{\text{bSiO}_2}$ for different water masses of the Antarctic Zone ($\pm 1\text{sd}$). ML: Mixed Layer; WW: Winter Water; UCDW: Upper Circumpolar Deep Water; LCDW: Lower Circumpolar Deep Water. (a) January – February 2005 (data from Fripiat et al., 2011); (b) January – March 2004 (data from Cavagna et al., 2011); (c) October – December 2001 (1 profile at 61°S from Cardinal et al., 2005); (d-e) AESOPS October 1997 – March 1998, SOFEX January – February 2002 (data from Varela et al., 2004).

	KEOPS ^a		EIFEX ^b	CLIVAR SR3 ^c	AESOPS ^d	SOFeX ^e	
	plateau	out plateau	out patch				
ML	$\delta^{30}\text{Si}_{\text{Si}(\text{OH})_4}$ (‰)	2.6 ± 0.2	2.2 ± 0.2	2.6 ± 0.1	1.8 ± 0.2	2.5 ± 0.9	2.1 ± 0.7
	$\text{Si}(\text{OH})_4$ ($\mu\text{mol l}^{-1}$)	2.1 ± 0.6	27.2 ± 0.2	10.3 ± 2.4	28.5 ± 0.5	50 - <10	60 - <10
WW	$\delta^{30}\text{Si}_{\text{Si}(\text{OH})_4}$ (‰)	1.9 ± 0.1	1.5 ± 0.0	1.6 ± 0.2	1.3 ± 0.2		
	$\text{Si}(\text{OH})_4$ ($\mu\text{mol l}^{-1}$)	34.2 ± 1.9	52.5 ± 3.3	37.3 ± 2.8	60.9 ± 9.3		
UCDW	$\delta^{30}\text{Si}_{\text{Si}(\text{OH})_4}$ (‰)		1.3 ± 0.2	1.3 ± 0.2	1.3 ± 0.1		
	$\text{Si}(\text{OH})_4$ ($\mu\text{mol l}^{-1}$)		78.4 ± 8.5	75.5 ± 3.2	89.8 ± 8.8		
LCDW	$\delta^{30}\text{Si}_{\text{Si}(\text{OH})_4}$ (‰)		1.1 ± 0.2		1.1		
	$\text{Si}(\text{OH})_4$ ($\mu\text{mol l}^{-1}$)		111.3 ± 3.5		117.2		
$\delta^{30}\text{Si}_{\text{bSiO}_2}$ (‰)							
ML		2.3 ± 0.1	1.2 ± 0.2	1.5 ± 0.4	0.8 ± 0.2	1.2 ± 2.1	1.0 ± 1.6
under ML		1.9 ± 0.1	1.0 ± 0.1		0.7 ± 0.2		

In contrast, UCDW and LCDW signatures are extremely homogeneous for the three campaigns, while WW exhibits moderate variability. As discussed in the section on Task 2.1 above, we have shown that WW results from a mixing between UCDW and ML. The intensity of the mixing varies, as well probably as the ML Si isotopic signatures and Si contents. Mixing is therefore the main process controlling Si characteristics in the upper mesopelagic zone (~WW), while dissolution does not appear to be significant (Fripiat et al., 2011).

De La Rocha et al. (2000) were the first to report changes in Si isotopic composition and Si content for the deep ocean along the thermohaline circulation, with deep water $\delta^{30}\text{Si}_{\text{Si}(\text{OH})_4}$ becoming progressively lighter and $\text{Si}(\text{OH})_4$ contents increasing due to dissolution of sinking diatoms. This process has recently been modeled using a Global Circulation Model (Reynolds, 2009). At the S.O. basin's scale we do not see such changes since for deep waters the isotopic shift between the North Atlantic and the North Pacific is limited to only 0.3 ‰. This probably explains why Si-isotopic signatures of UCDW and LCDW are homogeneous, because their Si characteristics are related to bSiO_2 dissolution but at the time-scale of global circulation rather than the one associated with dissolution of diatoms sinking out of local surface waters. Our data indicate a wide spatial biogeochemical uniformity of the Antarctic Zone regarding the silicon cycle.

This work is a key contribution to Deliverable # 11 "Conservative vs. non-conservative signatures of mesopelagic waters".

4. Modelling biogeochemical cycles in the modern Southern Ocean (WP4)

Objective and methodological approach

The overall objective of the BELCANTO project was to develop and test a fully coupled ice-ocean biogeochemical model, applicable to the Southern Ocean extended to latitude 30°S. The chosen methodology includes the parallel development of the NEMO -LIM -SWAMCO (*Nucleus for European Modelling of the Ocean, Louvain-la-Neuve-sea-Ice-Model, Sea WAter Microbial COmmunity model*) model with an implicit description of sea-ice biogeochemistry and of the LIM-SIMCO model that includes an explicit description of sea-ice biogeochemistry. This involves both separate upgrading and testing of the different models involved in the integrated mathematical model (The physical NEMO and LIM models and the biogeochemical SWAMCO and SIMCO models) and the implementation of their coupling. Here we present progress achieved in terms of development and performance of these different models.

4.1. 3D-NEMO-SWAMCO with implicit sea-ice biogeochemistry

4.1.1. Improvement and tests of NEMO-LIM (Nucleus for European Modelling of the Ocean and Louvain-la-neuve-sea-Ice-Model)

Treatment of the boundary condition in the case of an Antarctic zoom in the NEMO model:

In the BELCANTO project, we are using a version of the NEMO-LIM ice-ocean model covering the region located southward of 30°S. As the boundary condition imposed at 30°S could cause trouble inside the domain of interest, two boundary condition treatments have been tested here: the open and the closed boundary conditions (de Montety, 2006). To determine which method is the most accurate, the results of two regional experiments (using either open or closed boundary conditions) are compared to these of a global simulation at the same resolution. The latest has been taken as reference, because in this version the exchanges at 30°S are explicitly computed by the model and there is of course no need of imposing any particular condition at this latitude. The experiment results have been analysed after 24 years of simulation and deal with the capability of reproducing the final state and variability for different variables.

It turned out that the simulation with the open boundary conditions (OBC) yields realistic results, as compared to those based on closed boundary conditions, both for the temperature, salinity, mixed layer depth and sea-ice extent, volume and concentration. The errors are always much smaller with the open boundary conditions, see for example the sea-ice concentration simulated in the three experiments in **Figure 4.1.1**. Also, the accuracy of the results near the northern boundary is not deteriorated by the OBC method. Moreover, the variability reproduced by the experiment with the OBC is very close to the one for the global simulation, whereas the differences are much higher between the other regional simulation and the global experiment.

To conclude, the boundary conditions arising from a reduction of the model domain compared to the global version are treated in a more realistic way by using open boundary conditions than by using closed boundary conditions.

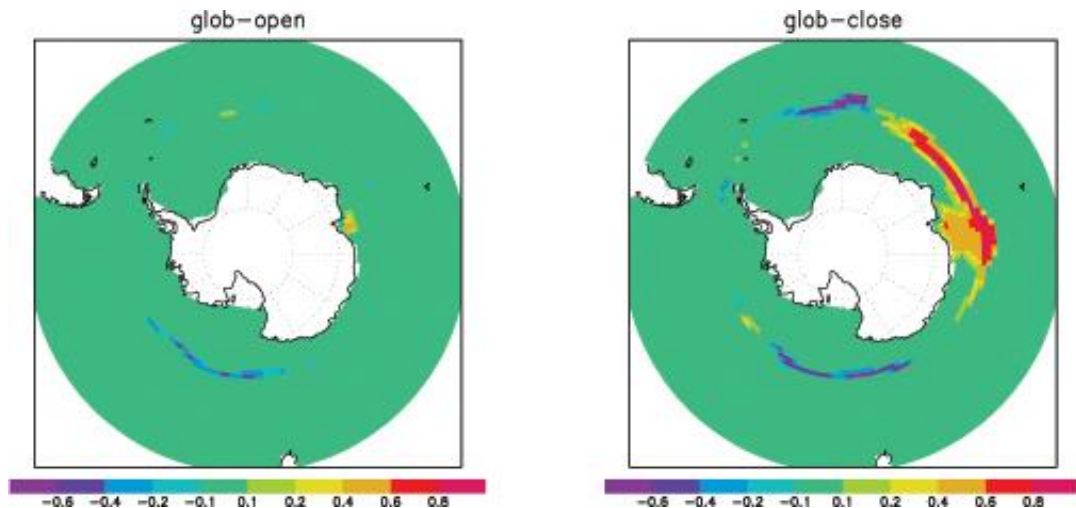


Figure 4.1.1: Differences of the sea-ice concentration at the end of the simulation (September 2002) between the open and the global simulations (left panel) and between the closed and the global experiments (right panel).

Improvement of the summer mixed layer depth in the Southern Ocean:

Because of the importance of seasonal mixed layer depth evolution for the physical and biological processes, we have investigated its representation in the NEMO-LIM model. We have first compared the simulated mixed layer depth to a recent climatology based on observation in the Southern Ocean (de Boyer Montegut et al, 2004). It is shown that the mixed layer depth is underestimated year round (compare yellow curve with black curve in **Figure 4.1.2**). During the austral summer the differences between the model results and the observations reach about 30 meters averaged over the latitudes 60°S to 45°S and for the period 1980-2000. To solve this problem different strategies have been tried out, such as for instance changing the vertical diffusion or modifying the tuning of several parameters. However, this did not solve the discrepancy between the model results and observation. Finally, we have decided to add a parameterization of the Langmuir circulation (Ming Li and Chris Garrett, 1997). This circulation is driven by the wind and generates a deepening of the mixed layer depth. Implementation of this parameterization in the NEMO-LIM model did significantly increase the simulated mixed layer depth (green curve compared to the yellow one in figure 5). In particular, the summer value has nearly doubled (45 m compared to 24 m) and reaches almost the observed depth value (51 m).

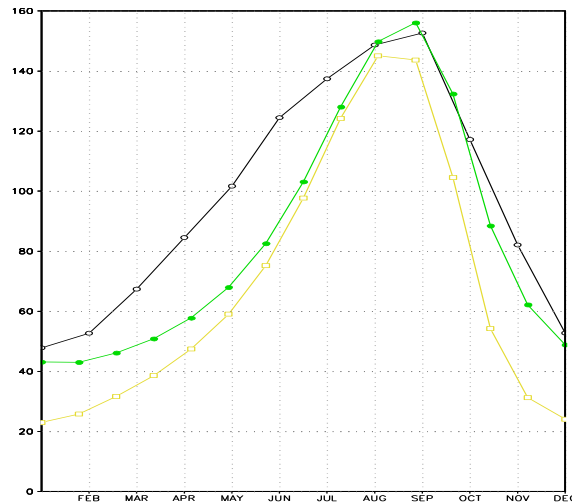


Figure 4.1.2: Monthly evolution of the mixed layer depth, averaged over all longitudes and over 45°S to 60°S, for the climatology (de Boyer Montegut et al, 2004, black curve), the simulation with the Langmuir parametrization (green curve) and without this parameterization (yellow curve). The model results are averaged over the period 1980-2000.

An analysis of the atmospheric processes driving the large-scale winter sea-ice variability in the Southern Ocean:

The response of Southern Ocean sea-ice to atmospheric variability was investigated using both model and observational data (Lefebvre and Goosse, 2008a). The model results are derived from a simulation performed with the coupled ocean-sea-ice model ORCA-LIM, driven by the NCEP/NCAR (National Centers for Environmental Prediction-National Center for Atmospheric Research) re-analysis of daily near-surface air temperatures and winds and by monthly climatologies for precipitation, cloud cover and relative humidity. Our results show that, in line with previous investigations (both observation and model) the classical modes of atmospheric variability do not explain a large part of the winter sea-ice variability integrated over the entire Southern Ocean. In the regression between the ice extent and the atmospheric pressure, the dominant mode is a static, non-symmetric wave 3 pattern (**Figure 4.1.3**). However, the sea-ice extent in the Southern Ocean does not seem to behave as a single entity: its variability is the result of the combination of regional sea-ice changes. Consequently, each sector has to be examined separately. In short, three processes seem to be important in explaining local sea-ice extent variability: the variability of the air temperature, the meridional and the zonal ice velocity.

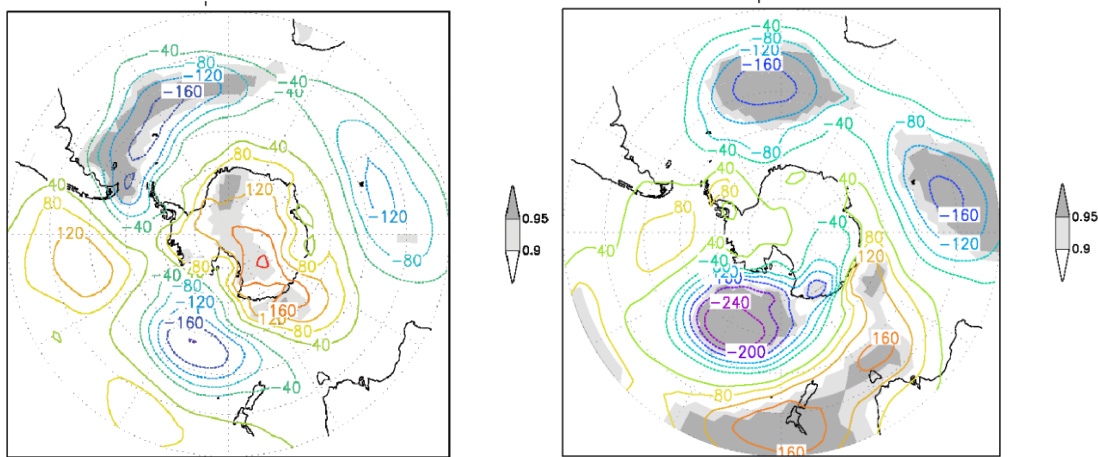


Figure 4.1.3: The regression of the surface pressure (NCEP-NCAR, in Pa, 1979-2004, averaged over August and September) onto the September sea-ice extent (observed: left; modelled: right) integrated over the whole Southern Ocean. The significance level is shown in grey shading.

4.1.2. 3D NEMO-LIM-SWAMCO simulations of the spatial distribution of the iron supply to phytoplankton in the Southern Ocean

Recognizing the role of iron (DFe) as essential micronutrient for phytoplankton growth in the HNLC waters of the Southern Ocean, we implemented the 3D coupled ice-ocean-biogeochemical model NEMO-LIM-SWAMCO in the ocean domain south of latitude 30°S to explore processes governing the spatial distribution of the iron supply to phytoplankton. Model scenarios include potential iron source functions (atmospheric deposition, iceberg calving and continental sediments; **Fig.4.1.4**) as well as iron storage within sea ice, all formulated as based on a literature review. Models, forcing functions and configuration (boundary and initial conditions) are detailed in Lancelot et al. (2009).

Five 11-yr simulations were conducted with the fully coupled NEMO-LIM-SWAMCO model, covering the period from September 1989 to December 2000. Here, we analyse the simulation results for the 1997-2000 period only, since the first 8 years are considered as a spin up allowing near-surface values to reach a quasi-equilibrium state. The nominal simulation (FULL) is obtained in NEMO-LIM-SWAMCO when all the iron sources (atmospheric, iceberg melting and sedimentary inputs; **Fig. 4.1.4**) are taken into account and the mechanism of sea-ice iron sequestration and release in the ocean surface layer is activated.

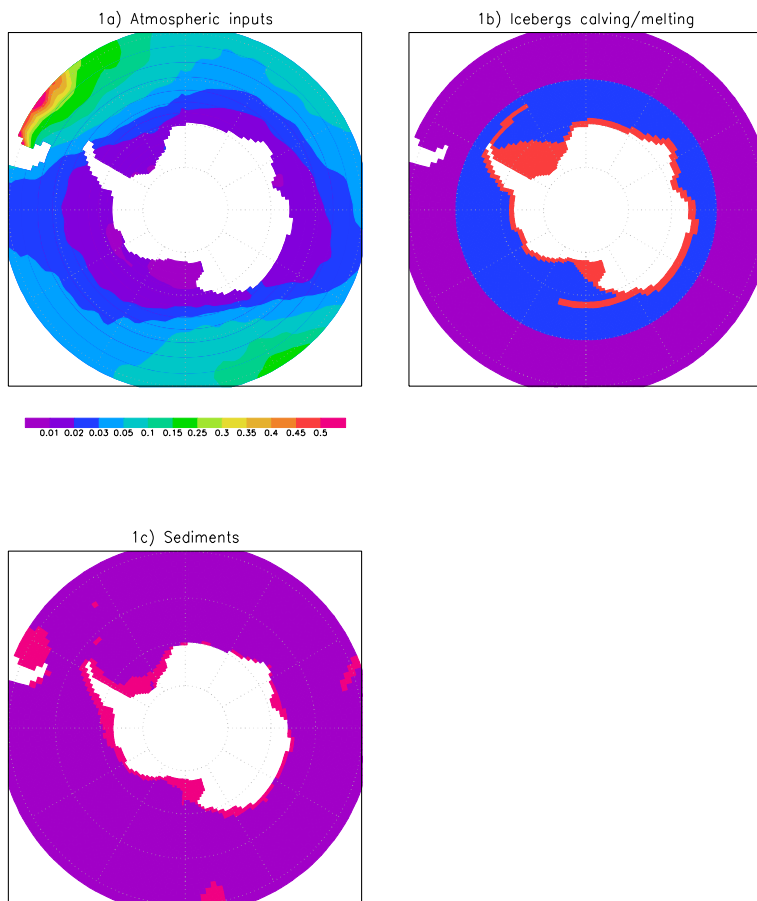


Figure 4.1.4: Distribution of Fe sources ($\text{pmol Fe m}^{-2}\text{s}^{-1}$) in the model domain. (a) Atmospheric inputs; (b) iceberg calving/melting; (c) sediments. The fluxes from iceberg melting amount to $0.22 \text{ pmol Fe m}^{-2}\text{s}^{-1}$ close to the continent (in red) and to $0.22 \cdot 10^{-2} \text{ pmol Fe m}^{-2}\text{s}^{-1}$ further to the north (in blue). The sediment fluxes are equal to $5 \text{ pmol Fe m}^{-2}\text{s}^{-1}$ (in purple). Note that the colour scale is not linear.

Model performance is verified by comparison of simulations with the global iron database of Moore and Braucher (2008) and SeaWiFS-derived Chl a (see details in Lancelot et al., 2009).

The contribution of each iron source to the model results is discussed by comparing the nominal simulation with sensitivity experiments in which one iron source or the mechanism of sea-ice iron sequestration and release in the surface layer is switched off.

A. Iron and chlorophyll a distributions in the modern Southern Ocean: 3D NEMO-LIM-SWAMCO simulations

The simulated surface oceanic DFe fields (**Fig.4.1.5**) show a seasonal cycle characterized by large-amplitude variations. During austral summer, the simulated DFe is extremely low in surface waters due to a fast biological uptake (not shown). The highest surface DFe concentrations are simulated in winter (**Fig. 4.1.5a**) due to DFe release by heterotrophic processes and to the deepening of the upper mixed layer when surface waters are merging with iron-rich waters from below.

Examination of **Fig. 4.1.5a** reveals a clear contrast between winter DFe of coastal and deep ocean regions. For instance, DFe $> 0.5 \mu\text{mol Fe m}^{-3}$ are simulated in the Weddell Sea while concentrations $< 0.2 \mu\text{mol Fe m}^{-3}$ are suggested offshore (**Fig. 4.1.5**).

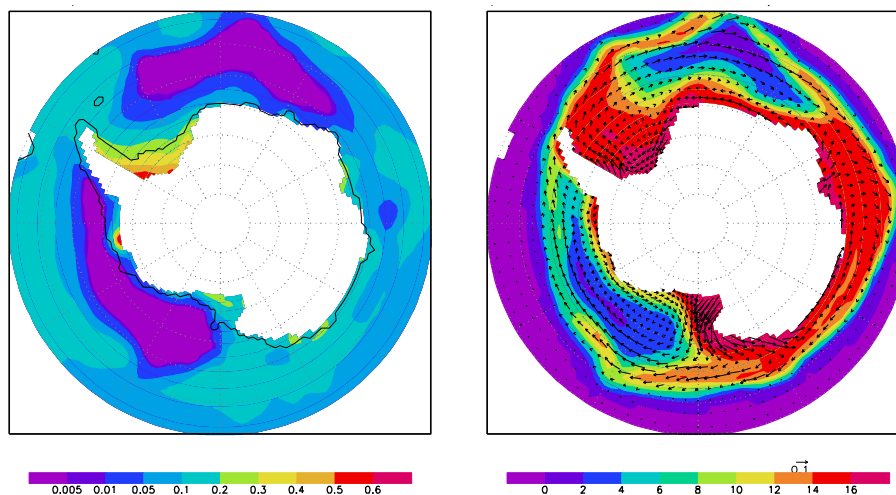


Figure 4.1.5: Simulated DFe ($\mu\text{mol Fe m}^{-3}$) in (a) surface waters and (b) sea ice, averaged for winter (July-August-September) and covering the 1997-2000 period. The contour line corresponds to the 1200 m isobath. Note that the colour scale is not linear.

Another remarkable feature of the model simulations is the strong regional variability of DFe in surface waters in winter. Interestingly, the deep ocean off the shelves of the Bellingshausen and Amundsen seas as well as in the Atlantic-Indian sector are characterized by extremely low DFe concentrations ($< 0.05 \mu\text{mol Fe m}^{-3}$; **Fig. 4.1.5a**). Nearly no observation is available in those regions during the austral winter. However, some information on surface ocean DFe concentrations in winter can be obtained by analysing the DFe values reported for the base of the upper mixed layer (around 200m) during spring and summer. At this depth, low DFe values of 0.1 to 0.2 $\mu\text{mol Fe m}^{-3}$ have been observed in many locations around Antarctica: in the Weddell sector (Boye et al., 2001; Croot et al., 2004; de Jong et al., 1998), in the Western Pacific Ocean sector (Sohrin et al.; 2000; Sedwick et al., 1999), in the Ross Sea sector (Coale et al., 2005) and in the Bellingshausen-Amundsen Seas (de Baar et al., 1999). However, only a few extremely low values ($\sim 0.05 \mu\text{mol Fe m}^{-3}$) have been recorded (Croot et al., 2004; Coale et al., 2005), suggesting that the simulated DFe in these two regions is underestimated. Such an underestimation most likely results from the too simple parameterization used to describe the transfer of ocean DFe to sea ice. When sea ice forms, DFe is indeed taken up from surface waters, independently of concentration. For areas where the simulated DFe concentrations are too low, nearly all DFe contained in the surface waters ends up being incorporated in the ice, leaving DFe concentrations close to zero at the ocean surface. Consistent with this, the simulated Fe accumulation in sea-ice (**Fig. 4.1.5b**) reflects surface water Fe concentrations in winter when ice cover is at maximum (**Fig. 4.1.5a**). Regions characterized by very low DFe concentrations in the water column (**Fig. 4.1.5a**) are associated with simulated low iron concentrations in sea ice ($< 6 \mu\text{mol Fe m}^{-3}$; **Fig. 4.1.5b**).

This is in accordance with the average DFe concentrations recently measured in the Bellingshausen Sea ($4.83 \pm 5.12 \mu\text{mol Fe m}^{-3}$; F. Masson, J. de Jong and V. Schoemann, unpublished data). The highest simulated DFe concentrations occur above the continental shelves (**Fig. 4.1.5b**), where the modeled surface ocean DFe concentration is high enough to sustain ocean-to-ice iron fluxes during ice growth and which are close to the maximum ($16.5 \mu\text{mol Fe m}^{-3}$). In agreement with this, elevated mean iron sea-ice concentrations of 12-18 and $14.8 \mu\text{mol Fe m}^{-3}$ have been measured in winter in the East Antarctic (Lannuzel et al., 2007) and Weddell Sea (Lannuzel et al., 2008) pack ice, respectively. However lower DFe mean concentrations ($2.12\text{-}5.78 \mu\text{mol Fe m}^{-3}$) were reported in coastal sea ice of Terra Nova Bay (Ross Sea; Grotti et al., 2005).

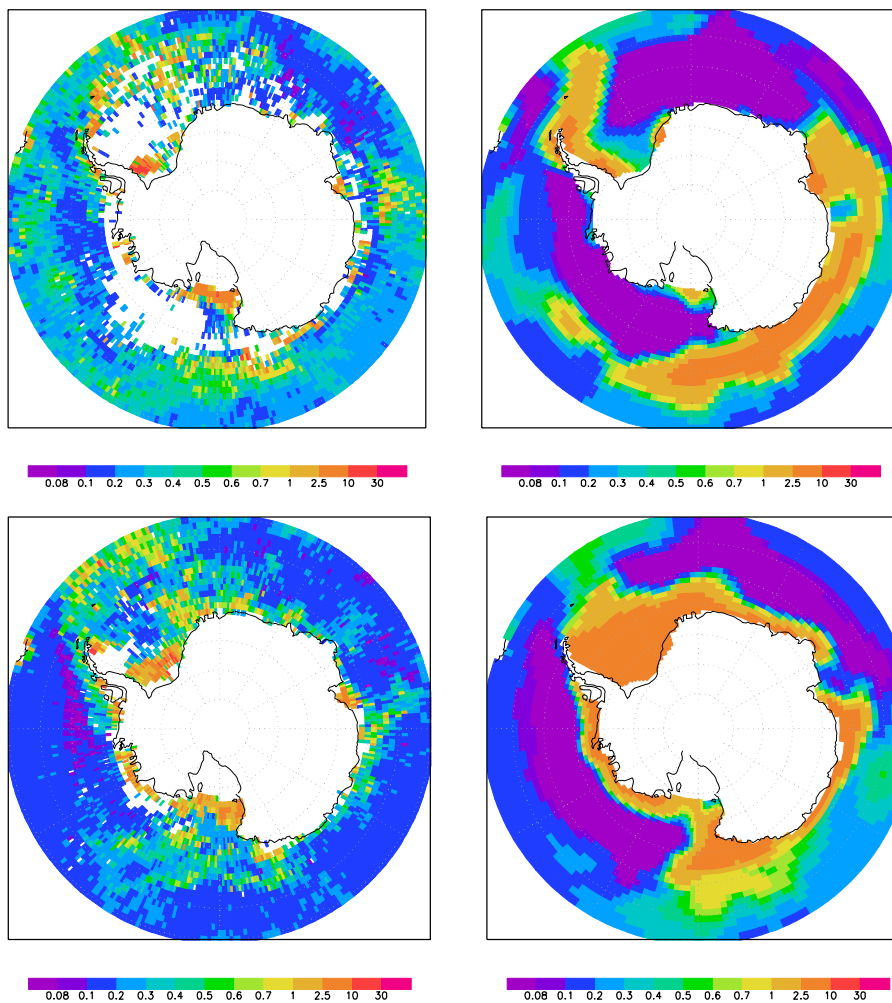


Figure 4.1.6: SeaWiFS-derived (Acker and Leptoukh, 2007) and simulated surface Chl a (mg m^{-3}) averaged for (a-b) Spring (December) and (c-d) Summer (February) over the 1997-2000 period. Note that the color scale is not linear.

The NEMO-LIM-SWAMCO distribution of surface Chl a in Spring (December) and Summer (February) for the years 1997-2000 corresponds reasonably well to SeaWiFS-derived observations for the same period (**Fig. 4.1.6**).

The highest simulated surface Chl a concentrations ($> 2.5 \text{ mg m}^{-3}$) are obtained close to the receding ice-edge and above the continental shelves, mainly off East Antarctica, in the Ross Sea and in the western Weddell Sea, as is generally observed for the Southern Ocean (Fitch and Moore, 2007; Arrigo et al., 2008). In contrast, observations and simulations reveal extremely low Chl a concentrations ($< 0.1 \text{ mg m}^{-3}$) in the Bellingshausen-Amundsen Seas and in the eastern Weddell Sea. A comparison with the winter distribution of surface and sea-ice DFe (**Fig. 4.1.5**) suggests that for these regions, characterized by shallow mixed layer depths in summer (not shown), it is low iron availability rather than light that limits phytoplankton growth in spring and summer (**Fig. 4.1.6**). As a consequence of the dominant limitation by iron, the observed and simulated circumpolar asymmetry of summer surface Chl a (**Fig. 4.1.6**) mimics the distribution field of simulated DFe in winter (**Fig. 4.1.5**).

Despite missing SeaWiFS data, due to clouds, it is clear that the spatial extent of the predicted bloom is larger than the observed extent, leading in many areas to simulated surface Chl a being higher than observed (**Fig. 4.1.6**). Such an overestimation of Chl a in the Southern Ocean is shown in many models (see for example Fig.3 in Moore et al., 2004; Fig. 4. in Aumont and Bopp, 2006; Fig.9b in Dutkiewicz et al., 2005). The bias has been attributed to several factors such as an unrealistic representation of nutrient trapping in the surface layer (Dutkiewicz et al., 2005) or an underestimation of in situ observed Chl a derived from SeaWiFS (this underestimation can reach up to a factor 3 in some regions; Preunkert et al., 2007). In our model, limitations in some process description, such as the absence of krill grazing pressure, might well explain the predicted too high surface Chl a in e.g. the West Antarctic Peninsula Scotia-Weddell Sea and East Antarctica, where significant swarms are commonly reported (Atkinson et al., 2004). Moreover, the similar geographical patterns between sea ice DFe in winter (**Fig. 4.1.5b**) and surface Chl a in spring/summer (**Fig. 4.1.6**) suggest that the chosen parameterization for iron capture in sea-ice determines the position and spatial extent of regions of the marginal ice zone with very high or very low Chl a and hence explains the small discrepancy between the modelled and observed areas of high and low Chl a (**Fig. 4.1.6**). Furthermore, in regions characterized by both high and low phytoplankton concentration, the model results tend to be spatially more homogenous, as compared to SeaWiFS-derived Chl a. This lack of spatial heterogeneity in our simulation might be due to the relatively low model resolution, which does not allow resolving structures such as fronts or the local influence of topography that is associated with excessive diffusion.

B. Processes governing iron distribution in the modern Southern Ocean : sensitivity analysis

The influence of the iron accumulation process in sea ice and its release after melting as well as the contribution of the different iron sources to the simulated complex geographical pattern of surface DFe and Chl a, are assessed from model sensitivity tests obtained by turning off separately each iron source or process. A first-order estimate of the contribution of each mechanism is then obtained by computing the difference between the FULL experiment and the corresponding sensitivity

experiment (Figs. 4.1.7- 4.1.8). Hence, the non-linear interactions between the different mechanisms are not considered.

Influence of the various sources of iron

As expected from the forcing field (Fig. 4.1.4a), the effect of iron dust deposition on surface DFe (Fig. 4.1.7a) is globally low at high latitudes, in agreement with conclusions of Wagener et al. (2008). Interestingly however, the surface DFe enrichment due to atmospheric input (Fig. 4.1.7a) does not decrease in parallel with the forcing (Fig. 4.1.4a) but shows maximum values ($\sim 0.01 \mu\text{mol Fe m}^{-3}$) in a quasi circumpolar band around 60°S and close to the continent around 45°E . Relatively strong vertical movements are simulated by the model in those regions, indicating that the pattern of Fig. 4.1.7a is not related to the forcing itself but rather to the transport by ocean currents of dust iron from distant sources.

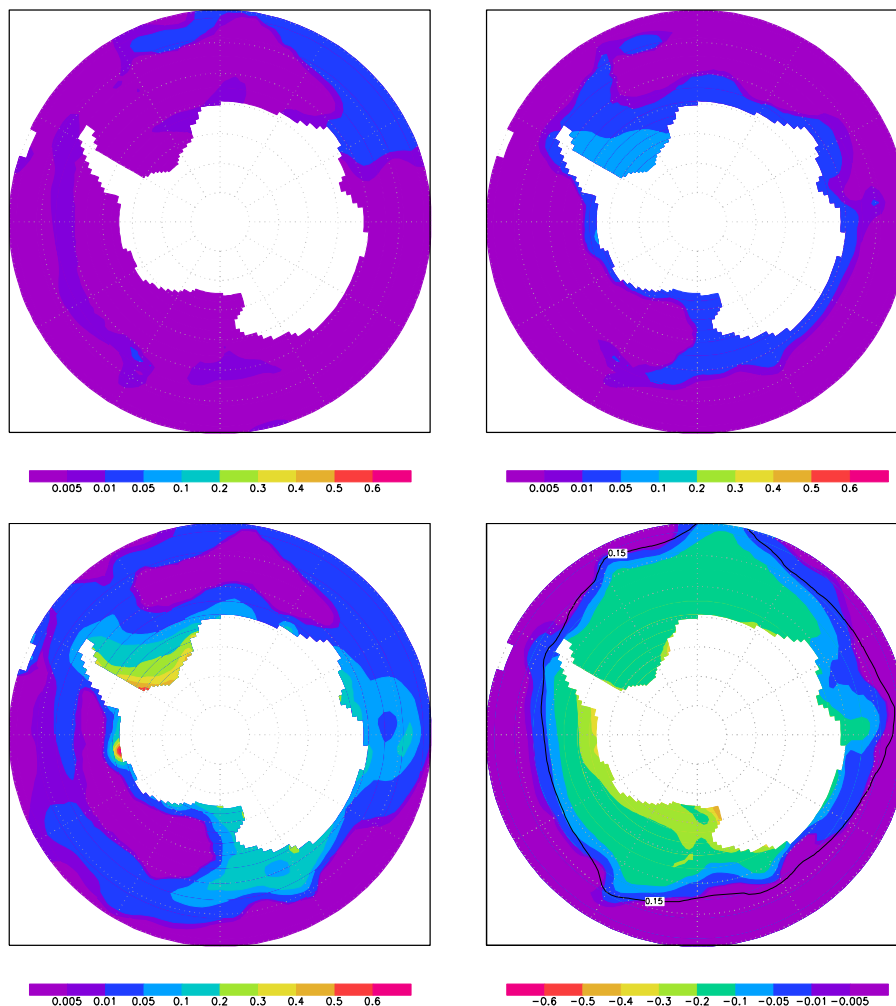


Figure 4.1.7: Simulated effect of iron inputs from (a) atmosphere, (b) iceberg melting, (c) sediments, on iron concentration ($\mu\text{mol Fe m}^{-3}$); (d) simulated effect of iron capture in sea-ice on the winter (September) distribution of surface ocean DFe. The contribution of each component is obtained by subtracting results from the FULL experiment and the corresponding sensitivity experiment (Table 1). The September ice edge is displayed in

contour. Values are averaged over the 1997-2000 period. Note that the colour scale is not linear.

The contribution of icebergs is comparatively more significant than dust deposition, amounting to $0.1 \mu\text{mol Fe m}^{-3}$ close to the coast of Antarctica (**Fig. 4.1.7b**). Contrasting with the geographical pattern associated with iron dust influence, the maximal iron releases from icebergs are predicted on the continental shelves and in bands located in the northern limbs of the Ross and Weddell Gyres, i.e., where the largest iceberg melting is observed (Gladstone et al., 2001). This suggests that ocean currents play a minor role in the horizontal redistribution of iron originating from iceberg melting.

Iron from sedimentary source has clearly the largest influence on the simulated surface DFe concentration (**Fig. 4.1.7c**). For many areas neglecting this iron source has an an order of magnitude larger impact than dust deposition and iceberg melting (**Fig. 4.1.7a,b,c**). The largest differences ($>0.2 \mu\text{mol Fe m}^{-3}$) are found on the continental shelves due to the entrainment of iron from sedimentary sources by vertical currents and intense mixing in winter. Iron is then transported horizontally from the shelf areas to the Antarctic circumpolar current, mainly by the Ross and Weddell gyres,. The surface divergence and the associated vertical currents in the model also play a role in the local maximum located around 60°S , by inducing an upwelling of iron from deeper waters, as already mentioned in the analysis of the effect of iron dust deposition. Interestingly, model simulations are pointing two wide "iron-desert" zones in the eastern Weddell Sea and in the Bellingshausen-Amundsen Seas (**Fig. 4.1.7c**) which only receive a very small fraction of the iron released from the sediments.

All the sensitivity experiments point to the major role of iron in limiting the simulated phytoplankton growth in the Southern Ocean (**Fig. 4.1.8a,b,c**): every tested source of iron contributes to an increase in the summer concentrations of surface Chl a that appears clearly related to the amount of iron provided and the subsequent changes in the iron winter stock (**Fig. 4.1.7a,b,c**).

The margin sediments constitute the major iron source to phytoplankton, with a 2 to 10 times larger enhancement of simulated Chl a in February, than obtained by activating iceberg melting (**Fig. 4.1.8bc**). Yet the added contribution of iron from iceberg melting can not be neglected, since it induces an increase in surface Chl a of more than 1 mg m^{-3} in some regions of the Weddell Sea, off the west coast of the Antarctic Peninsula and in the outer Ross Sea (**Fig. 4.1.8b**). In contrast, the impact of dust on the Chl a distribution at high latitudes appears very minor (**Fig. 4.1.8a**), as expected from **Fig. 4.1.7a**.

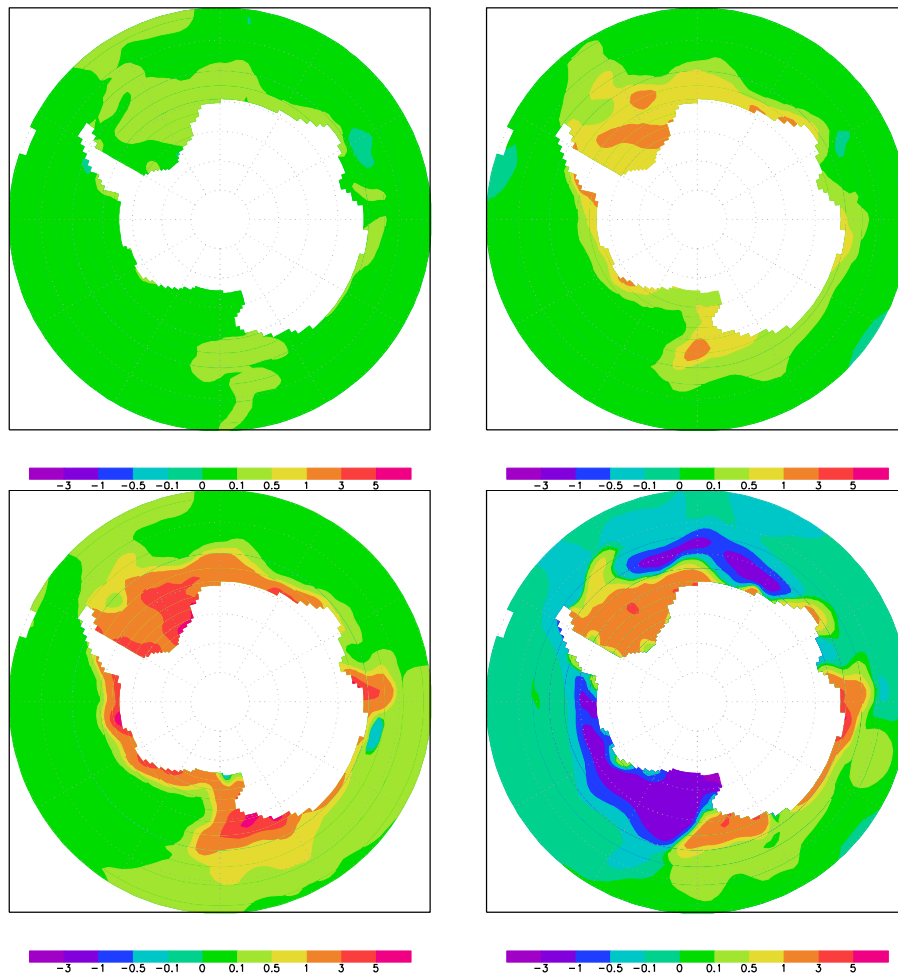


Figure 4.1.8: Simulated effect of iron inputs from (a) atmosphere, (b) iceberg melting, (c) sediments and of (d) the capture of iron in sea-ice and release when melting on the spatial distribution of surface Chl-a (mg m^{-3}) in December (a) and February (b,c,d). The contribution of each component is obtained by subtracting results from the FULL experiment and the corresponding sensitivity experiment (Table 1). The September ice edge is displayed in contour. Values are averaged over the 1997-2000 period. Note that the colour scale is not linear.

Role of iron sequestration in sea ice

Taking into account the iron capture and its storage by sea ice has a strong negative impact on the surface ocean DFe simulated in winter (**Fig. 4.1.7d**). The largest changes are simulated close to the coast, where ice production is significant and hence large ocean-to-ice iron fluxes take place. For instance, in the western Ross Sea more than 10 m of ice per square meter are formed every year, leading to an annual mean iron uptake in sea ice from the ocean of $9 \text{ pmol Fe m}^{-2} \text{ s}^{-1}$ ($0.8 \text{ } \mu\text{mol Fe m}^{-2} \text{ d}^{-1}$; **Fig. 4.1.9b**) i.e. of the same order of magnitude as epibenthic iron fluxes (**Fig. 4.1.4c**). The sea ice formed around the continent is then transported northward as shown by the high sea ice DFe simulated in the northern limbs of the Ross and Weddell gyres (**Fig. 4.1.5b**). Ice motion then ensures a transport of iron from the continental shelf to the deep ocean regions. This physical process also contributes to depleting oceanic DFe in the vicinity of the shelves, where ice-ocean iron exchanges

are activated (Fig. 4d). On the shelves the iron loss due to its capture in the ice is compensated by inputs from sediments and iceberg melting, still allowing relatively high Fe concentrations at the ocean surface (**Fig. 4.1.5a**) as well as in the sea ice (**Fig. 4.1.5a**). Contrasting with this, many offshore regions show a net annual iron flux from sea ice to ocean (**Fig. 4.1.9b**). Hence, iron transport by sea ice and its subsequent release through melting acts as a net source of iron for phytoplankton in those regions (**Fig. 4.1.9a**). The DFe ice-ocean fluxes are quite low in some regions such as the central Amundsen-Bellinghshausen Sea ($<0.1 \text{ pmol Fe m}^{-2}\text{s}^{-1}$; **Fig. 4.1.9a**) and do not compensate the absence of a large source of iron and of direct inflow of iron-rich waters there (**Fig. 4.1.4**). The magnitude of the annual mean iron flux is largest in the Indian and western Pacific sector off Victoria Land as well as on the continental shelf of the Ross Sea, just off shore of the coastal polynia (**Fig. 4.1.9a**). In those regions, a net annual melting is simulated (and thus a net annual mean import of ice), inducing iron fluxes from sea ice to ocean that have the same magnitude or are even larger than those associated with wind, icebergs and sediment sources (**Fig. 4.1.4**).

In summer the iron fluxes at the ice–ocean interface are positive for the whole marginal ice domain (**Fig. 4.1.9a**), due to the release of iron accumulated in sea ice when the latter melts,. However, there is a high contrast between the relatively low values in the central Amundsen-Bellinghshausen Sea and in the eastern Weddell Sea compared to the high values in the Western Weddell Sea, the Ross Sea and off East Antarctica. This is related to the large differences in the concentration of iron in sea ice between those regions (**Fig. 4.1.5b**).

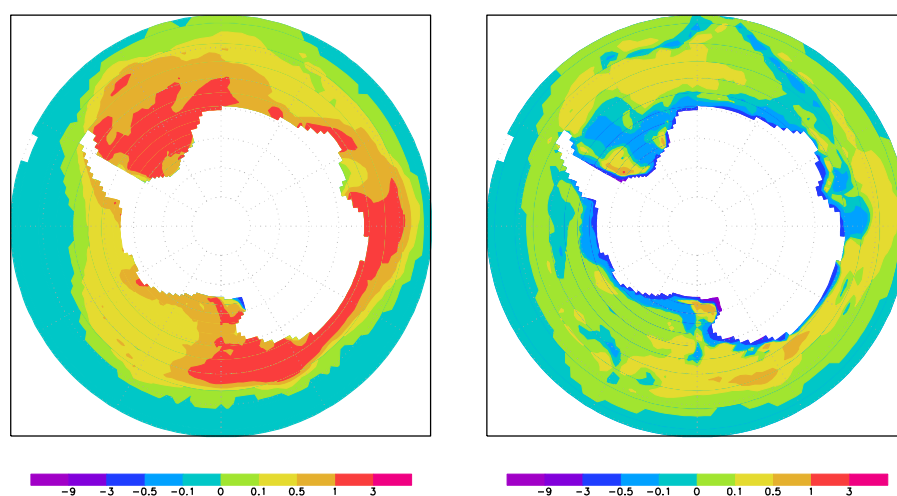


Figure 4.1.9: Simulated iron fluxes between ocean and sea-ice for (a) summer (November-December-January) and in (b) annual mean ($\text{pmol Fe m}^{-2}\text{s}^{-1}$) averaged over the 1997-2000 period. The fluxes are positive when the iron is released into the ocean. Note that the colour scale is not linear.

Iron release associated to ice melting has no remarkable impact on the summer DFe concentration in the upper ocean, since the available DFe is nearly immediately taken up by phytoplankton. This is clearly suggested by **Fig. 4.1.8d** that shows a strong increase in surface Chl-a concentration by 1 to 3 mg m^{-3} in the western Weddell Sea and off East Antarctica when the process of iron sequestration in ice and release is surface waters when ice melt is activated. However, in other regions

than the Ross Sea, Belingshausen Sea and Amundsen Sea as well as in the eastern Weddell Sea, the sequestration of iron in sea ice induces a decrease in Chl a (**Fig. 4.1.8d**). In those areas the simulated release of iron from melting ice (**Fig. 4.1.9a**) is not sufficient to balance the year long decrease of oceanic iron concentration (**Fig. 4.1.7d**) due to sea ice capture and export out of these regions (**Fig. 4.1.9**).

4.2 Development of an explicit model of sea-ice biogeochemistry

As underlined above, the process of Fe sequestration in the snow/sea ice and the Fe release in the surface layer during ice melting appears of paramount importance for describing phytoplankton blooms in the marginal ice zone and the related biogeochemical cycles. In order to consider this process we are developing the 1D LIM-SIMCO, a vertical physical-biogeochemical model of the sea ice column that will be further online coupled to the existing NEMO-LIM-SWAMCO.

4.2.1 Structure of LIM-SIMCO

The LIM-SIMCO model (**Figure 4.2.1A**) results of the coupling between several components: (i) The halo-thermodynamic sea ice model of UCL LIM (Vancoppenolle et al., 2006, 2007), (ii) a sea-ice passive tracer module, (iii) a single-wavelength simplified version of the bio-optical model of Arrigo et al. (1991), and (iv) the biogeochemical model SIMCO.

The development of the numerical code required several new developments. Firstly, the structure of the code was adapted to include the newly developed components (ii, iii, iv). The SIMCO model is a priori grid-independent. At each time step, the biologically relevant physical variables (temperature, salinity, brine volume, and light) are conservatively interpolated from the LIM grid to the SIMCO grid, while Chl-a (necessary for radiation) is interpolated from the SIMCO grid to the LIM grid.

Secondly, we formulated an original advection-diffusion equation for tracers in the vertically-varying brine network, and resolved it with a grid-independent, finite-difference, conservative finite difference numerical scheme. Boundary conditions explicitly account for bottom entrapment during growth and snow-ice formation. A remapping algorithm is applied at the end of each time step to ensure mass conservation on the time-varying grid. This scheme was successfully tested offline and then included into the model.

Thirdly, the Arrigo et al. (1991) bio-optical model has been reformulated without wavelength dependence and has been included into the code. The numerical scheme is based on absorbed visible radiation fluxes (instead of transmitted) to ensure both heat conservation and the separation between biological and physical absorption of radiation. In addition, a possibility for lateral penetration of light was included in the model.

Finally, the structure of SIMCO was defined as a function of dominant biogeochemical processes controlling iron accumulation in sea ice and to ensure an optimal coupling with SWAMCO.

Based on literature review and results gained in the Belgian ARC SIBCLIM project, we identified three key processes possibly leading to Fe accumulation in the ice (**Figure 4.2.1B**): (i) diffusion of dissolved Fe (DFe) in the brines and direct uptake by sea ice microalgae (mainly diatoms), (ii) scavenging of particulate Fe (PFe) from the water column and, (iii) direct adsorption of diffused DFe on organic matter (TOC) and sequestration under PFe form. SIMCO is thus defined by 5 state variables : 2 nutrients (DSi and DFe), 1 diatom described by 2 state variable (DASR, DAF) in accordance with SWAMCO description and 1 organic matter (TOC). The structure of SIMCO and the processes linking the state variables are described in **Figure 4.2.1B**. Equations are those described in SWAMCO and a first set of parameters has been derived from literature survey and SIBCLIM results (Becquevort et al. in prep; Schoemann et al., in prep).

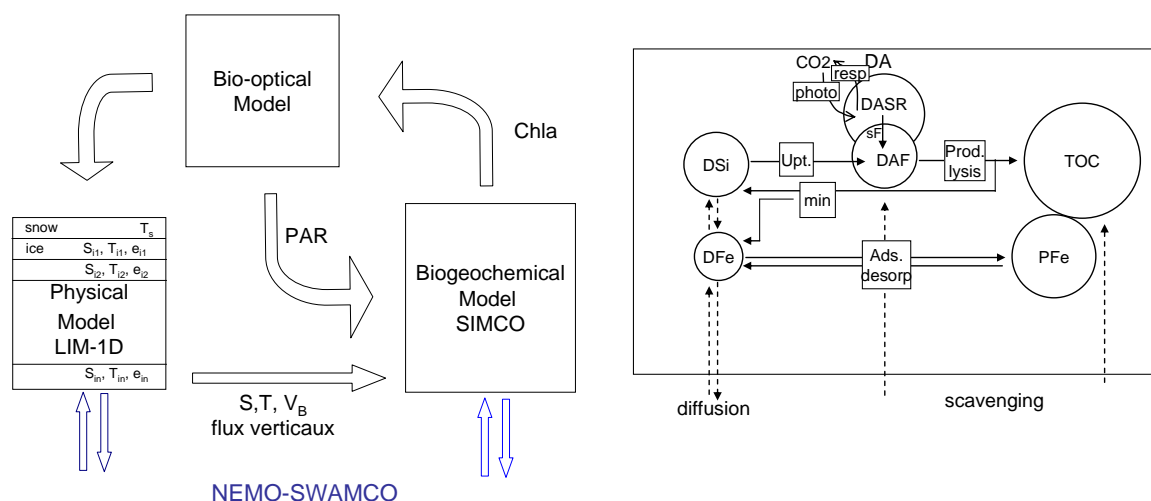


Figure 4.2.1: Schematic representation of the LIM-SIMCO model (A) and trophic resolution of SIMCO (B).

4.2.2 LIM-SIMCO implementation and results

Vertical transport of nutrients in sea ice

Nutrients are an essential component of primary production in sea ice. Present sea ice models assume a prescribed ocean-to-ice nutrient flux. However, nutrients are transported in a non-linear way by moving liquid brine through open channels in sea ice.

I

Interestingly, our 1D sea ice model (LIM-1D) is the first to include explicit brine physics and hence offers a natural way of improving the representation of nutrients. For this reason, a new scheme of nutrient transport was formulated and implemented within LIM1D. The model has been tested using a prescribed primary production rate, in order to simulate a seasonal cycle of dissolved silicates (DSi) in Antarctic sea ice. Vertical profiles of DSi compare relatively well to observations (Tison et al., 2008).

A comparison is presented here which has been made at the location of ISPOL (Ice Station POLarstern; 68°S, 55°W) Antarctic expedition in 2004, where physical and biogeochemical measurements were measured at a drifting sea ice station between 29 November and 30 December 2004. The model is forced by NCEP reanalysis of atmospheric fields which gives seasonal evolution of ice-cover and thickness (**Figure 4.2.2**) in agreement with observations.

The conclusions of our study (Vancoppenolle et al., 2009) point to significant interactions between nutrient uptake by growing algae which cannot be represented using a simple model. Nevertheless, significant errors remain, due to the simplicity of the model biological component.

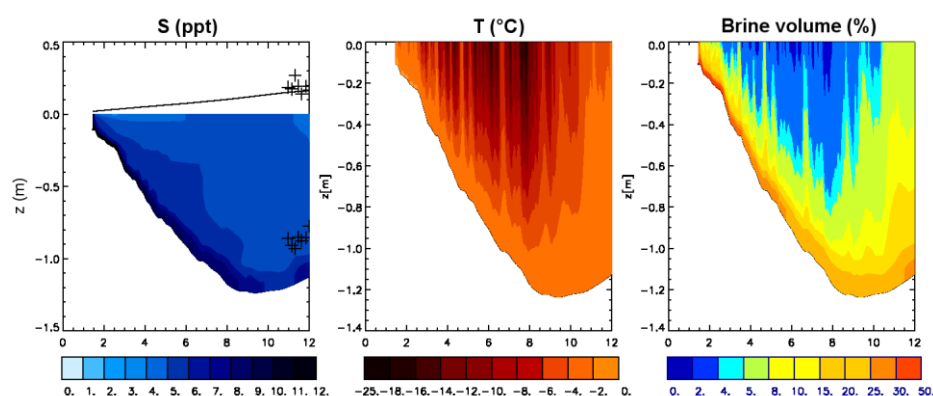
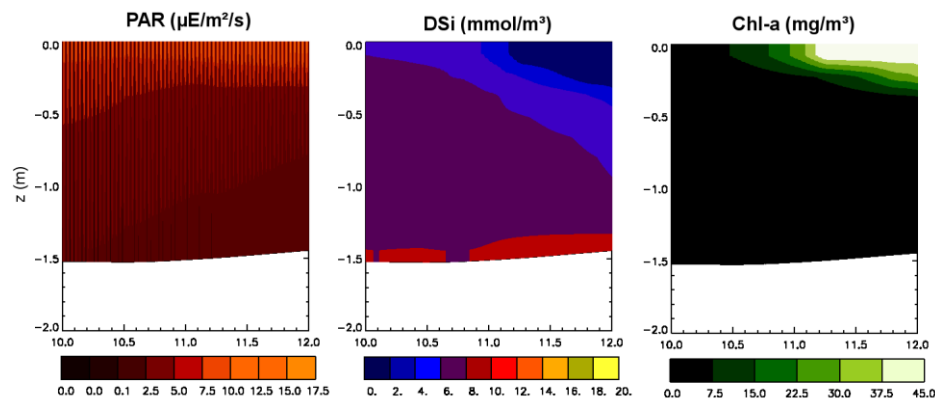


Figure 4.2.2: Simulated seasonal cycle of sea ice and snow mass balance and vertical profiles of salinity (a, ppt), temperature (b, °C), relative brine volume (c, %) on a simulation at ISPOL. On panel (a), the snow depth is also depicted. The crosses refer to ice thickness and snow depth observations made during the ISPOL field campaign (J. Tison, C. Haas and M. Nicolaus, personal communication).

Interactive biological component

For this reason, simulations have been performed with SIMCO, representing explicitly the sea ice biogeochemical processes. Shown below is a simulated phytoplankton bloom in sea ice for a summer Antarctic pack ice case study. Algae first develop on available light, then reduce nutrients near the surface and reduce light arrival at the ice base. The model is currently validated using the various data sets collected by Belgian teams (V1, ISPOL, SIMBA) and the sensitivity to model complexity is studied in order to include it in a 3D model at a reasonable cost.



A simulated surface bloom in spring Antarctic pack ice by LIM1D – SIMCO.

4.2.3 Collection of validation data set for LIM-SIMCO during the SIMBA cruise

The American-Belgian Sea Ice Mass Balance of the Antarctic (SIMBA) field study provided a large continuous physico-biogeochemical validation data set for LIM-SIMCO which will be used in the future. The Belgian part of the SIMBA program is a collaboration between the ULB, Ulg and UCL and was conducted by J.-L. Tison (ULB). The field program consisted in 3 way-in stations and a 26-day long drift station (Ice Station Belgica, ISB) from Sep 25th (JD 271) to Oct 23rd (JD 296) in an area situated between 69 and 71 °S and 90 and 95°E in the Bellingshausen Sea (see **Figure 4.2.3**). During the drift station, measurements were done at two camps (called 'Bruxelles' and 'Liège') on the SIMBA floe from JD 274 to 296. Each camp was visited 5 times.

At each visit, a series of ice cores were drilled. The measurement of ice physico-chemical characteristics (ice thickness, snow depth, freeboard, salinity, temperatures and oxygen isotopes), of biogeochemical parameters (Chl-a, nutrients, iron, bacterias, organic matter, ...) as well as climatically-significant gases (CO_2 , DMS) were done. The role of UCL on the field was to perform heat and radiation measurements, which provide boundaries for 1-D simulations of sea ice physics and biogeochemistry. To accomplish this goal, four data sets were collected. The first data set consists of ship-based observations of wind, temperature, relative humidity as well as visible and infrared radiation. The second data set consists of meteo and radiation measurements made in situ. A third data set includes 282 hourly visual observations of cloudiness and snowfall made mostly during daylight hours. The last data set covers measurements of snow depth and albedo along a line at each visit of any of the ice camps.

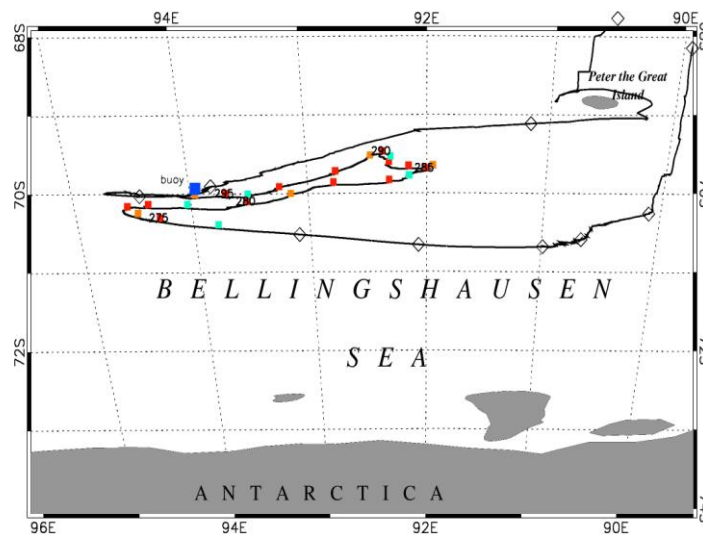


Figure 4.2.3: NB Palmer's track in the Bellingshausen Sea. Symbols indicate the ship's position every day. Colored symbols indicate daily position of the Ice Station Belgica. Numbers are Julian Day (JD). Blue (orange) squares indicate visits at the Brussels (Liège) site.

4.3. 3D-NEMO-SWAMCO with explicit sea-ice biogeochemistry

In parallel with the experiments performed with the explicit sea-ice biogeochemistry in the one-dimensional configuration (section 4.2), SIMCO is currently implemented into the 3D-NEMO-SWAMCO model. Tests are in process. Furthermore, an important part of task 4.3 was to analyse the role of the forcing on simulation results as described below.

Investigation of the potential influence of the forcing deficiencies on model results

The analysis of the NEMO-LIM-SWAMCO results shows a systematic bias: the simulated Chl-a is overestimated during the summer austral season around Antarctica and especially in the western Weddell Sea. This overestimation in the latter region is linked to a misrepresentation of the summer sea-ice cover. The simulated sea-ice concentration exhibits indeed high values in the middle of the Weddell Sea during summer (**Fig 4.3.1a**) while the model underestimated the ice concentration along the Antarctic Peninsula as in the HADSST dataset (see the sea-ice extent- defined as the 15% concentration- in black curve in **Fig. 4.3.1a**). In addition, the simulated ice thickness is smaller than the observed all year long in this region (Timmerman et al., 2004, 2005). This weakness is present in many models (Griffies et al., 2009; Timmerman et al., 2002, 2004, Mathiot, 2009). One potential cause is the deficiencies of the forcing in this region. We have thus performed several simulations using different forcings as well as some idealized experiments.

Firstly, the ECMWF reanalysis (ERA40) (Uppala et al., 2005) has been employed to force the model during the period 1992-2001. When the whole data set (surface air temperature, surface wind stresses) is used, the sea-ice cover is underestimated all over the year and in particular during the summer austral season (**Fig. 4.3.1b**). In order to distinguish whether the warm ECMWF temperature or the strong ECMWF

surface wind was responsible to the low sea-ice concentration (**Fig. 4.3.1b**), additional simulations with fields from NCEP/NCAR and ECMWF reanalyses have been conducted. It appears that the Antarctic sea-ice cover simulated by the model is very sensitive to the surface wind. By reducing the magnitude of the surface wind stresses, we succeeded in simulating a higher sea-ice cover. Unfortunately, the geographical distribution was less realistic than the one obtained with the NCEP/NCAR forcing.

Secondly, we have pursued our investigations in a different way. Idealized experiments have then been performed by modifying the orientation of the NCEP/NCAR surface wind or adding a component to the wind forcing in the Weddell Sea. The addition of a zonal component of 1 m/s towards the west in the Weddell Sea has clearly improved the sea-ice concentration in this region with a maximum close to the Peninsula (**Fig. 4.3.1c**). So it is possible to improve the sea-ice cover simulated by the model by adding a zonal component to the surface wind forcing. This conclusion points out possible deficiencies of the forcing due to a poor representation of the influence of the Antarctic Peninsula.

Thirdly, in order to test the previous hypothesis, we have decided to use a higher resolution (40 km) wind forcing, which should describe in a more realistic way the topographic effects. The outputs of the regional atmospheric model MAR (Gallée and Schayes, 1994) have been employed for the available period 1980-1993. Once the wind field was interpolated in the ORCALIM grid, the model has been run with this new forcing.

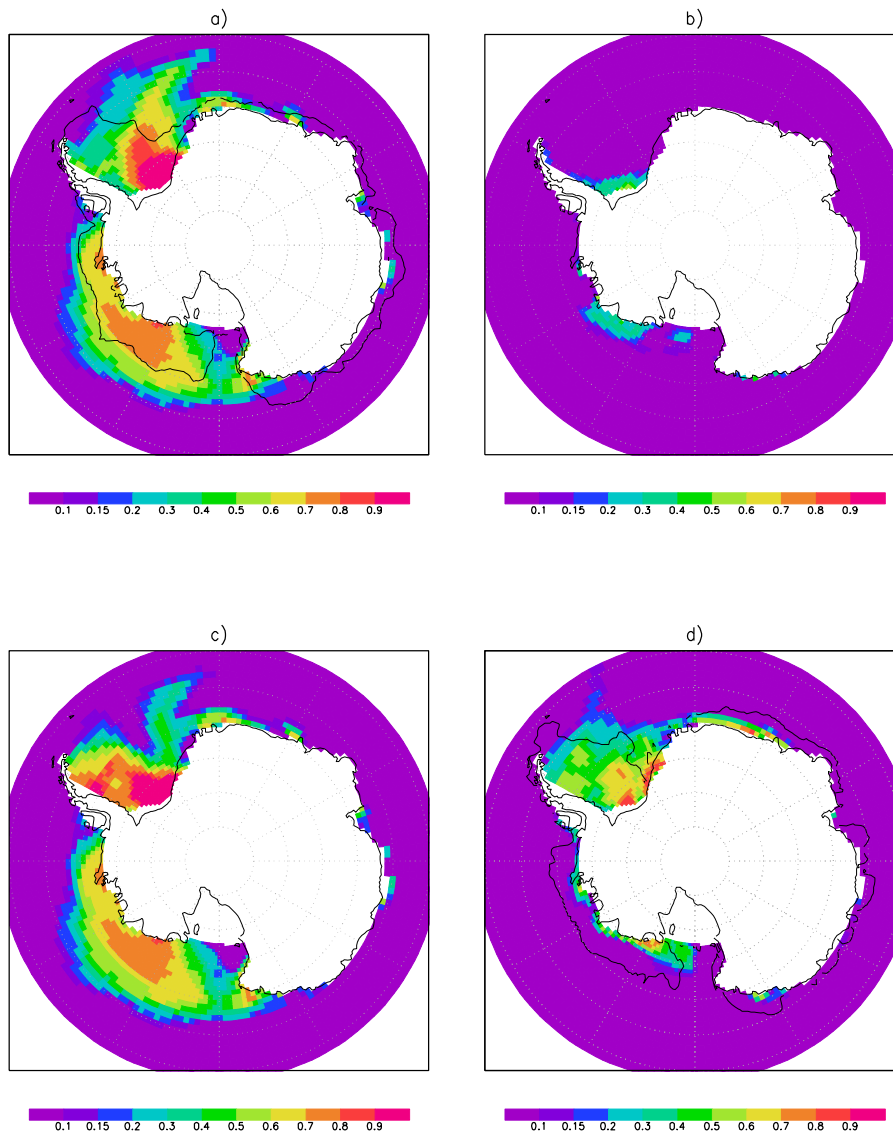


Figure 4.3.1: Simulated summer (February) sea-ice concentration averaged over 5 years for the simulation forced by (a) NCEP/NCAR reanalysis (Kalnay et al., 1996) (period 1997-2001), (b) ECMWF reanalysis (Uppala et al., 2005) (period 1997-2001), (c) NCEP/NCAR reanalysis with an additional zonal wind component of 1 m/s towards the west in the Weddell Sea (period 1997-2001), (d) MAR surface wind forcing (Gallée and Schayes, 1994) (period 1989-1993) with NCEP/NCAR air temperature and air humidity. The sea-ice extent from HadISST dataset (Rayner et al., 2003 and updates) is added in black contour for the same period as for the shaded information.

The simulated summer sea-ice concentration has been improved (**Fig. 4.3.1d**), the sea ice is more confined in the Weddell Sea as in the observation (see the black contour in **Fig. 4.3.1d**) with a more realistic distribution of the ice concentration. However, the maximum sea-ice concentration is still not located close to the Antarctic Peninsula as observed.

Other teams have also working on this topic; in particular, Pierre Mathiot in Grenoble studied the influence of the atmospheric forcing on the Antarctic sea-ice representation during his thesis (Mathiot, 2009).

The sensitivity experiments that he has lead in MEOM (LEGI, Grenoble, France) for DRAKKAR project with a regional configuration (PERIANT05) based NEMO with higher resolution (0,5° instead of 2° in previous result) complete and confirm result of this study. Experiments carried out with all atmospheric data provide by MAR model with PERIANT05 show that MAR wind stress improve sea ice extent, especially along Peninsula area as also shown in our experiments. Another result of these sensitivity experiments is that MAR air temperature and MAR air humidity increase significantly sea ice extent leading in that case to an underestimation of the summer ice cover. Other experiments carried out with several resolution (2°, 0,5° and 0,25°) with ERA40 atmospheric fields seems to conclude that resolution do not solve this underestimation of sea ice extent in summer (Mathiot, 2009).

Analysis of meteorological and radiation forcing applied to large-scale sea ice models

Ice-ocean large-scale models work relatively well in the Arctic but are less accurate in the Southern Ocean, for two reasons. First, physical processes specific of Antarctic sea ice are not well known and hence not well represented in sea ice models. Second, the forcing applied to models, consisting of atmospheric reanalyses, probably includes more errors than in the Arctic. However, the latter are not quantified. Hence, it is relatively difficult to diagnose the errors in the simulations coming from model parameterizations and to improve the models.

We thus started to diagnose errors in the radiation and meteorological forcings. As an absolute reference, we collected a large amount of data from research ships frequently cruising in the Southern Ocean: Polarstern (Germany), N.B. Palmer and L.M. Gould (USA) and Aurora Australis (Australia). The data, spanning the years 1982-2009, have recently been released separately. Our collection is hence entirely original. An example of application is shown in **Figure 4.3.2**.

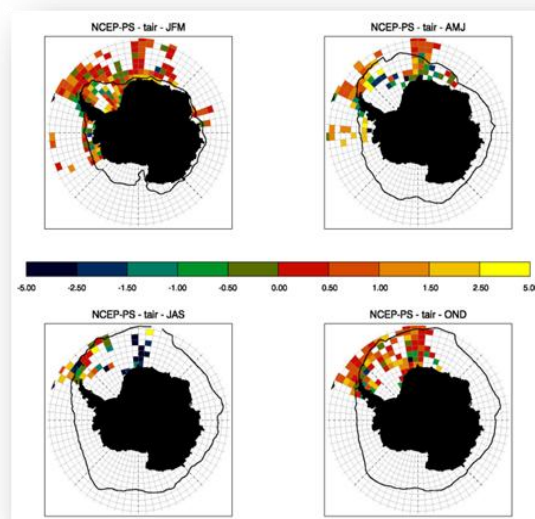


Figure 4.3.2: Seasonal bias (NCEP Reanalysis-Observation) in temperature over the Southern Ocean for the Polarstern observation data set.

4.4 Impact of future climate change (WP5)

Analysis of the projected regional sea ice changes in the Southern Ocean during the 21st century:

Using the set of simulations performed with atmosphere-ocean general circulation models (AOGCMs) for the Fourth Assessment Report of the International Panel on Climate Change (IPCC AR4), the projected regional distribution of sea ice for the 21st century has been investigated (Lefebvre and Goosse, 2007b). Averaged over all those model simulations, the current climate is reasonably well reproduced. However, there are a lot of models that have a sea ice extent that significantly differs from the observed extent. Some of them also have a wrong regional distribution of sea-ice, simulate trends over the last 30 years with the wrong sign in most of the sectors compared to observations and/or have a too large variability of the total extent. Furthermore, simulated key elements of the climate system like the strength of the ACC are in many models far outside the observational variability.

Over the 20th century, the multimodel average simulates a stronger warming around the peninsula compared to other regions, which is in qualitative agreement with observations. This is probably related to the positive trend in the Southern Annular Mode (SAM) index over the 20th century, in both observations and in the multimodel average. Despite the simulated positive future trend in SAM, such a regional warming is absent in the projected temperature change for the end of the 21st century. The maximum warming is indeed located over the continent, over the Weddell and the Amundsen-Bellingshausen Seas. In those latter regions the warming is associated with a large reduction of the ice cover in the multimodel average (**Figure 4.4.1**).

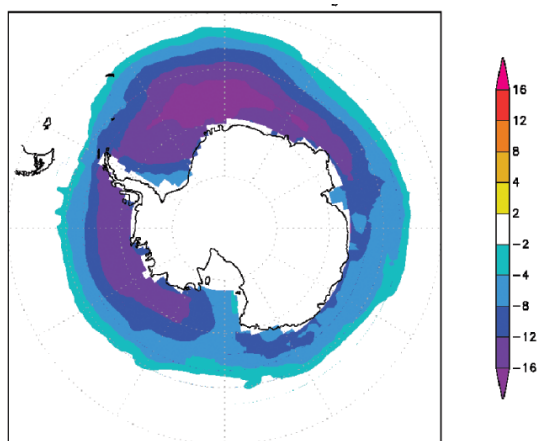


Figure 4.4.1: The difference in sea-ice concentration between the 2071-2100 period in the scenario SRES A1B and the 1979-2004 period averaged over the 16 discussed AOGCMs.

3. POLICY SUPPORT

In addition to the above statements directly drawn from BELCANTO scientific results, there are several activities and publications which are relevant to policy support in the framework of the expertise developed by BELCANTO. In Belgium, we have been involved in the following actions:

- Nine BELCANTO scientists are contributors to the Chapter 3 "The role of the ocean in global change" of the report published in 2005 and edited by BELSPO: "Belgian global change research 1990-2002: Assessment and integration report" (Wollast et al., 2005).
- BELCANTO scientists have been consulted regularly in 2008-2009 by BELSPO during the feasibility study of the R/V *New Belgica*, a project that would shape marine Belgian research on a long-term perspective. We have provided inputs regarding which infrastructure and technical specifications would be required for such new research vessel, taking into account international research prospective for the next two decades in oceanography. Some BELCANTO scientists have also been consulted by BELSPO in 2009 to provide their opinion on the *European Strategy Forum on Research Infrastructures* (roadmap 2008), which includes the European icebreaker project, R/V *Aurora Borealis*.
- Experts from BELCANTO have been involved in the evaluation of the proposals for the *Antarctic InBev-Baillet Latour Fellowship Award*. The award of €150,000 is designed to promote research activities in, or in the vicinity of, the Princess Elisabeth Antarctica research station.
- 22 Belgian Antarctic scientists (among which eight members of BELCANTO) published an open letter in national newspapers *Le Soir* and *De Standaard* in September 2007 (Becquevort et al., 2007a,b). This letter was addressed to the new Minister of Belgian Science Policy and was related to the under-funding of Belgian Antarctic Research. In this letter we acknowledged the great opportunities offered by the new Belgian Antarctic Base *Princess Elisabeth* but at the same time urged for an increased funding of Belgian polar research. We draw the attention of the public and policy makers on the contradiction of having new infrastructures and, at the same time, a decrease of Antarctic research functioning budget (-15% compared to 2000-2005). Two years later, this concern is more than ever relevant at a time when programs are ending with no clear vision on their follow-up and when some junior and senior scientists are facing difficult position due to job insecurity. The risk of losing (part of) the know-how developed at an international level by Belgian Antarctic oceanography in climate change research (which was a priority the last years) is high. There is a need to have a consistent and sustainable polar research policy implemented on a longer term.
- BELCANTO scientists have contributed for the text and illustrations of the report edited by BELSPO "Belgium and Antarctica Exploration, Science and Environment" (Vancauwenberghe, 2009).

Through different ways, BELCANTO partners have frequently been requested to provide advice on international research policies.

Examples are:

- BELCANTO partners have been invited to evaluate many research Antarctic proposals from other countries. Noteworthy, most of the funding agencies ask the reviewers to evaluate the relevance of these research projects with respect to their own policy's strategy. These evaluations are anonymous and confidential so cannot be developed further here but we list below the funding agencies that have used BELCANTO scientists expertise to select research projects during the time frame of BELCANTO III: *Australian Antarctic Division*, *European Cooperation in Science and Technology* (COST Office, Brussels), *Netherlands Organization for Scientific Research* (NWO), *Swiss National Science Foundation* (FNSNF), *Natural Environmental Research Council* (NERC, UK), *IPY Canadian Federal Programme*, *Research Council of Norway*, *Netherlands Organisation for Scientific Research (N.W.O)*, *Deutsche Forschungsgemeinschaft (DFG)*
- H. Goosse (partner UCL) was an invited speaker and session chair at the International Symposium "Polar Environment and Climate: The Challenges – European Research in the context of the International Polar Year" organized by the European Commission (5-6 March 2007). The aims of this symposium were to provide an overview of current research activities and to identify future research needs at the European level for polar research. These needs were discussed in round tables and published along with extended abstracts in the Conference Proceedings (Goosse and Murray, 2007; Goosse and Lefebvre, 2007). They have been used to prepare subsequent FP7 calls where polar research was a top priority (e.g. topic ENV.2008.1.1.1.1. *Sea-Level Rise: Trends in contributions from continental ice, processes and links to climate change*).
- Belcanto partner Vrije Universiteit Brussel is a participant in the extension (2010-2013) of the Antarctic Climate and Ecosystem CRC programme.
- BELCANTO partners are contributing author of the Chapters 8 « Climate models and their evaluation » and 9 « Understanding and attributing climate change » of the 4th assessment report (AR4) of the Intergovernmental Panel on Climate Change (IPCC) "Climate Change 2007: The Physical Science Basis (WG1-AR4)". They have also contributed to Chapter 4 "The next 100 years" of the "Antarctic Climate Change and the Environment" report published by the Scientific Committee on Antarctic Research (Scott Polar Research Institute). SCAR's AGCS team was indeed asked to take the lead in the preparation of a report on Antarctic Climate Change and the Environment (ACCE), to consider the past and possible future changes in the physical environment of the Antarctic and the impact on the biota.

4. DISSEMINATION AND VALORISATION

- Since 2005 BELCANTO has produced 61 peer-reviewed publications (including *Science* and *Nature*) and 6 non-peer-reviewed publications (section 5). Eight further manuscripts are currently in revision or in preparation. BELCANTO partners were contributed to some 76 communications (oral, posters) at international symposia since 2006 (section 5 below). Furthermore, 7 PhD and 5 MSc theses were finalised within the frame of the project.
- Results are available from the following data bases (with or without restricted access):
 - KEOPS (<http://www.obs-vlfr.fr/proof/vt/op/ec/keops/keo.htm>)
 - SAZ-Sense (<http://www.cmar.csiro.au/datacentre/saz-sense/>)
 - BONUS-GoodHope (http://www.obs-vlfr.fr/proof/bonusgh/bgh_plan.php)
- A logo has been created and the website has been redesigned (<http://www.co2.ulg.ac.be/belcanto/>). The website is regularly updated although we could not do it as often as wished. This is especially true in the last two years because of a peak activity due the International Polar Year with the webmaster (B. Delille) being extremely often on field trip in polar regions.
- In parallel to the website, a blog "Polar Belgium" was launched by ULg partner B. Delille (<http://www.polarbelgium.blogspot.com/>). It aimed at providing real time information for the large public on the IPY campaigns in which we participated (SIMBA, BONUS-GoodHope cruises).
- We have contributed to the set up and content of the BELSPO Belgian Polar platform (<http://www.belspo.be/antar>).
- We have participated to the cluster BE-POLES activities which was initiated by BELSPO and aimed to promote the national and international profile of Belgian polar research. It clustered all Belgian polar researchers, funded or not within the Belspo research programmes and run from 2006 to 2008:
 - We contributed to the BE-POLES workshop: *Belgian Research in Polar Regions* (23-24 March 2006; a general audience of scientists and non-scientists) with oral and poster presentations

Interviews

- D. Cardinal was interviewed for a national radio broadcast program on BONUS-GoodHope oceanographic campaign by D. Mussche for the program "*Musique et autres muses*" under the theme "*Au fil de l'eau*", Musique 3 channel (RTBF), 5 Feb. 2008 (15').
- Becquevort S., A. Borges, D. Cardinal, F. Dehairs, B. Delille, H. Goosse, C. Lancelot, V. Schoemann et al. Meer geld voor Zuidpool. De Standaard, 2 septembre 2007.
- Becquevort S., A. Borges, D. Cardinal, F. Dehairs, B. Delille, H. Goosse, C. Lancelot, V. Schoemann et al. Station belge dans l'Antarctique : « émission zéro » pour un gain maximal ? Le Soir, 4 septembre 2007.

5. PUBLICATIONS

In preparation

- Cavagna A.-J., F. Dehairs, Véronique Woule-Ebongué, Bruno Delille, whole water column distribution and C-isotopic composition of cholesterol and brassicasterol from the Cape basin to the northern Weddell Gyre. *Biogeosciences*, special BONUS-GoodHope volume, to be submitted.
- Dehairs et al., Dissolved barium and silicate during the BONUS-GoodHope cruise and other Southern Ocean cruises. *Biogeosciences*, special BONUS-GoodHope volume, to be submitted.
- Dumont I., Schoemann V., Lannuzel D., de Jong J., Delille B., Tison J-L., Becquevort S., Impacts of Antarctic pack ice melting on planktonic microbial communities in the Western Weddell Sea. In prep.
- Dumont I., F. Masson, V. Schoemann, J-L. Tison and S. Becquevort. Impacts of Antarctic pack ice melting on planktonic microbial communities in the Western Weddell Sea. In prep.
- Fripiat F., A.-J. Cavagna, F. Dehairs, S. Speich, L. André and D. Cardinal, Silicon pool dynamics and biogenic silica export in the Antarctic Circumpolar Current inferred from Si-isotopes. *Biogeosciences*, special BONUS-GoodHope volume, to be submitted.
- Fripiat F., A.-J. Cavagna, F. Dehairs, L. André and D. Cardinal, A conceptual approach for describing the processes controlling Si-isotopic composition in the Southern Ocean: A paleoceanography perspective. *Ocean Sciences*, special BONUS-GoodHope volume, to be submitted.
- Masson F., Becquevort S., de Jong J., Dumont I., Tison J-L. and Schoemann V. Effect of organic ligands on iron bioavailability to pelagic and sympagic communities in the Bellingshausen sea. In prep.
- Masson F., de Jong J., Dumont I., Tison J-L., Becquevort S. and Schoemann V. Spatial distribution of Fe in the Antarctic pack ice zone, Bellingshausen sea. In prep.
- Masson F., de Jong J., Dumont I., Tison J-L., Becquevort S. and Schoemann V. Temporal evolution of iron distribution and its interactions with organic matter in the Antarctic pack ice zone, Bellingshausen sea. In prep.
- Schoemann, V., C. Hassler, F. Masson, I. Dumont, D. Lannuzel, A. Bowie, and S. Becquevort. The effect of organic ligands on Fe bioavailability to natural plankton communities of the Southern Ocean. In prep. for *Marine Chemistry*.

Submitted & in revision

- Fripiat F., K. Leblanc, M. Elskens, A.-J. Cavagna, L. Armand, L. André, F. Dehairs, and D. Cardinal, Summer efficient silicon loop across the Polar Front and SubAntarctic Zones despite contrasted diatom Si-affinity, *Marine Ecology Progress Series*, in review.
- Bowie A.R., F.B. Griffiths, F. Dehairs and T.W. Trull, Oceanography of the subantarctic and polar frontal zones south of Australia during summer: setting for the SAZ-Sense study. *Deep-Sea Research II*, Topical volume (SAZ-Sense expedition), in review.

- de Jong, J., V. Schoemann, D. Lannuzel, J.-L. Tison, H.W.J. and de Baar and. Iron inputs into the Antarctic Circumpolar Current from continental shelf sources: towards a dissolved iron budget for the Southern Ocean. *Journal of Geophysical Research*, submitted.
- Delille, B., M. Vancoppenolle, B. Tilbrook, D. Lannuzel, V. Schoemann, S. Becquevort, N.-X. Geilfus, G. Carnat, A.V. Borges, D. Delille, C. Lancelot, L. Chou, G. S. Dieckmann and J.-L. Tison. Southern Ocean CO₂ sink: the contribution of the marine cryosphere, *submitted to Science*.

2011

- Cavagna A.-J., M. Elskens, F.B. Griffiths, S.H.M. Jacquet and F. Dehairs, Contrasting regimes of nutrient availability and ecosystems functioning in the SAZ and PFZ south of Tasmania. *Deep-Sea Research Part II*, Topical volume (SAZ-Sense expedition), accepted.
- Cavagna A.-J., F. Fripiat, F. Dehairs, D. Wolf-Gladrow, N. Savoye, L. André and D. Cardinal, 2011. Silicon uptake and supply during a Southern Ocean iron fertilization experiment (EIFEX) tracked by Si isotopes. *Limnology and Oceanography*, 56, 147-160.
- Dumont I., V. Schoemann, S. Jacquet, F. Masson and S. Becquevort, 2011. Bacterial remineralization in epipelagic and mesopelagic waters in Subantarctic and Polar Front zones south of Tasmania. *Deep-Sea Research Part II*, Topical volume (SAZ-Sense expedition) accepted.
- Fripiat F., A.-J. Cavagna, L. André, N. Savoye, F. Dehairs and D. Cardinal, 2011. Isotopic constraints on the Si-biogeochemical cycle of the Antarctic Zone in the Kerguelen area (KEOPS). *Marine Chemistry*, 123, 11-22.
- Hassler, C.S., V. Schoemann, C.A.M. Nichols, E.C.V. Butler and P.W. Boyd, 2011. Saccharides enhance iron bioavailability to Southern Ocean phytoplankton. *Proceedings of the National Academy of Sciences USA*, 108 (3), 1076-1081, 10.1073/pnas.1010963108.
- Jacquet, S.H.M., F. Dehairs, I. Dumont, S. Becquevort, A.-J. Cavagna and D. Cardinal, 2011a. Twilight zone organic carbon remineralization in the PFZ and SAZ south of Tasmania, *Deep-Sea Research Part II*, Topical volume (SAZ-Sense expedition), accepted.
- Jacquet, S.H.M., P. Lam, F. Dehairs and T. Trull, 2011b. ²³⁴Th-determined shallow export flux from the Subantarctic and Polar Frontal Zones of the Southern Ocean, *Deep-Sea Research Part II*, Topical volume (SAZ-Sense expedition), accepted.
- Lannuzel, D., T. Remenyi, P. Lam, A. Townsend, E. Ibsanmi, E. Butler, T. Wagener, V. Schoemann and A. Bowie, 2011. Distributions of dissolved and particulate iron in the sub-Antarctic and Polar Frontal Southern Ocean (Australian sector). *Deep-Sea Research Part II*, Topical volume (SAZ-Sense expedition), accepted.
- Lecomte, O., T. Fichfet, M. Vancoppenolle and M. Nicolaus, 2011. A new snow thermodynamic scheme for the Louvain-la-Neuve sea ice model (LIM). *Annals of Glaciology*, in press, 10pp.
- Petrou, K., M.A. Doblin, P.J. Ralph, C.S. Hassler, K. Shelly, V. Schoemann, S. Wright and R. van den Enden, 2011. Iron-limitation and high light on phytoplankton

2010

- Breitbarth, E., E. P. Achterberg, M.V. Ardelan, A. R. Baker, E. Bucciarelli, F. Chever, P. L. Croot, S. Duggen, M. Gledhill, M. Hassellöv, C. Hassler, L. J. Hoffmann, K. A. Hunter, D. A. Hutchins, J. Ingri, T. Jickells, M. C. Lohan, M. C. Nielsdóttir, G. Sarthou, V. Schoemann, J. M. Trapp, D. R. Turner, Y. Ye., 2009. Iron biogeochemistry across marine systems – progress from the past decade. *Biogeosciences*, 6, 1075-1097.
- Hoppema M., F. Dehairs, J. Navez, C. Monnin, C. Jeandel, E. Fahrback and H.J.W. de Baar, 2010. Dissolved barium distributions in the Weddell Gyre: Impact of circulation and biogeochemical processes. *Marine Chemistry*, 122,118-129.
- Lannuzel, D., V. Schoemann, B. Pasquer, J.T.M. de Jong, J.-L. Tison, P. van der Merwe and A.R. Bowie, 2010. Distribution of dissolved iron in Antarctic sea ice: Spatial, seasonal, and inter-annual variability. *Journal of Geophysical Research - Biogeosciences*, 115, doi:10.1029/2009JG001031.
- Vancoppenolle M., Goosse H., de Montety A., Fichet T., Tremblay B. and Tison J.-L., 2010. Modelling brine and nutrient dynamics in Antarctic sea ice: the case of dissolved silica. *Journal of Geophysical Research - Oceans*, 115, doi:10.1029/2009JC005369.

2009

- Becquevort S, I Dumont, J-L Tison, D Lannuzel, M-L Sauvée, L Chou and V Schoemann, 2009. Biogeochemistry and microbial community composition in sea ice and underlying seawater off East Antarctica during early spring. *Polar Biology*, 32 (6): 879-895, DOI :10.1007/s00300-009-0589-2.
- Delille, B., A.V. Borges and D. Delille, 2009. Influence of giant kelp beds (*Macrocystis pyrifera*) on diel cycles of pCO₂ and DIC in the Sub-Antarctic coastal area. *Estuarine, Coastal and Shelf Science*, 81(1):114-122.
- Dumont, I., V. Schoemann, D. Lannuzel, L. Chou, C. Lancelot, J-L.Tison, B. Delille, J.T.M. de Jong and S. Becquevort, 2009. Distribution and characterization of dissolved and particulate organic matter in Antarctic sea ice. *Polar Biology*. 32 (5): 733-750, DOI :10.1007/s00300-008-0577-y.
- Fripiat, F., R. Corvaisier, J. Navez, M. Elskens, V. Schoemann, K. Leblanc, L. André and D. Cardinal, 2009. Determination of the rates of production and dissolution of biosilica in seawater using high resolution sector field inductively coupled plasma mass spectrometry (HR-SF-ICP-MS). *Limnology and Oceanography: Methods*. 7:470-478.
- Goosse H., W. Lefebvre, A. de Montety, E. Cressin and A. Orsi, 2009. Consistent past half-century trends in the atmosphere, the sea ice and the ocean at high southern latitudes. *Climate Dynamics*, DOI 10.1007/s00382-008-0500-9.
- Hassler, C. and V. Schoemann, 2009. Bioavailability of organically bound iron to model phytoplankton of the Southern Ocean. *Biogeosciences*, 6, 2281–2296.
- Hassler, C.S. and V. Schoemann, 2009. Discriminating between intra- and extracellular metals using chemical extractions-the case of iron. *Limnology and Oceanography: Methods*, 7:479-489.
- Jongma, J.I., E. Driesschaert, T. Fichet, H. Goosse and H. Renssen, 2009. Facilitation of Southern Ocean sea ice formation in a three dimensional climate model with interactively coupled icebergs. *Ocean Modelling*, 26, 104–113.

- Lancelot, C., A. de Montety, H. Goosse, S. Becquevort, V. Schoemann, B. Pasquer and M. Vancoppenolle, 2009. Spatial distribution of the iron supply to phytoplankton in the Southern Ocean: a model study. *Biogeosciences*, 6, 2861–2878.
- Takahashi, T., C.S. Sutherland, R. Wanninkhof, C. Sweeney, R.A. Feely, D.W. Chipman, B. Hales, G. Friederich, F. Chavez, A. Watson, D.C.E. Bakker, U. Schuster, N. Metzl, H. Yoshikawa-Inoue, M. Ishii, T. Midorikawa, C. Sabine, M. Hoppema, J. Olafsson, T. Arnarson, B. Tilbrook B., T. Johannessen, A. Olsen, R. Bellerby, Y. Nojiri, C.S. Wong, B. Delille, N. R. Bates and H.J.W. de Baar, 2009. Climatological Mean and Decadal Change in Surface Ocean pCO₂, and Net Sea-air CO₂ Flux over the Global Oceans. *Deep-Sea Research II*, 56, 554-577.
- Vancoppenolle M., Fichefet T., Goosse H., Bouillon S., Madec G. and Morales Maqueda M.A. 2009a. Simulating the mass balance and salinity of Arctic and Antarctic sea ice. 1. Model description and validation. *Ocean Modelling*, 27, 33-53, doi:10.1016/j.ocemod.2008.10.005.
- Vancoppenolle M., T. Fichefet and H. Goosse, 2009b. Simulating the mass balance and salinity of Arctic and Antarctic sea ice. 2. Sensitivity to the ice salinity processes. *Ocean Modelling*, 27, 54-69.

2008

- Abraham K., S. Opfergelt, F. Fripiat, A.-J. Cavagna, J.D.J. De Jong, S. Foley, L. André and D. Cardinal, 2008. $\delta^{30}\text{Si}$ and $\delta^{29}\text{Si}$ determinations on USGS BHVO-1 and BHVO-2 reference materials via new configuration on Nu Plasma Multi-Collector ICP-MS. *Geostandards and Geoanalytical Research*, 32, 193-202.
- Borges, A.V., B. Tilbrook, N. Metzl, A. Lenton and B. Delille, 2008. Inter-annual variability of the carbon dioxide oceanic sink south of Tasmania. *Biogeosciences*, 5, 141-155.
- Boyd PW, Jickells T, Law CS, Blain S, Boyle EA, Buesseler KO, Coale KH, Cullen JJ, de Baar HJW, Follows M, Harvey M, Lancelot C, Levasseur M, Pollard R, Rivkin RB, Sarmiento J, Schoemann V, Smetacek V, Takeda S, Tsuda A, Turner S and Watson AJ, 2007. A synthesis of mesoscale iron-enrichment experiments 1993-2005: key findings and implications for ocean biogeochemistry, *Science*, 315, 612-617.
- Dehairs F., A. de Brauwere, M. Elskens, U. Bathmann, S. Becquevort, S. Blain, K. Buesseler, E. Buitenhuis, M. Gehlen, G. J. Herndl, C. Klaas, R. Lampitt, D. Lefèvre, U. Passow, H. Ploug, F. Primeau, L. Stemmann and T. Trull, 2008. Controls on Organic Carbon Export and Twilight Zone Remineralisation. *Oceanography* 21(3): 92-95.
- de Jong J., V. Schoemann, J.-L. Tison, D. Lannuzel and N. Mattielli, 2008. High-accuracy determination of iron in seawater by isotope dilution multiple collector inductively coupled plasma mass spectrometry (ID-MC-ICP-MS) using nitilotriacetic acid chelating resin for pre-concentration and matrix separation. *Analytica Chimica Acta*, 623, 126-139. doi:10.1016/j.aca.2008.06.013.
- Jacquet, S.H.M., F. Dehairs, N. Savoye, I. Obernosterer, U. Christaki, C. Monnin and D. Cardinal, 2008. Mesopelagic organic carbon remineralization in the Kerguelen Plateau region tracked by biogenic particulate Ba. *Deep-Sea Research II*, 55, 868-879.

- Jacquet, S.H.M, F. Dehairs, N. Savoye, I. Vöge, D. Cardinal and V.H. Strass, 2008. Mesopelagic C remineralization in the Southern Ocean during the European Iron Fertilization Experiment (EIFEX). *Global Biogeochemical Cycles*, 22, GB1023, doi:10.1029/2006GB002902, 1-9.
- Lannuzel, D., V. Schoemann, J. de Jong, L. Chou, B. Delille, S. Becquevort and J.-L. Tison, 2008. Iron study during a time series in the western Weddell pack ice. *Marine Chemistry*, 108, 85-95.
- Lefebvre W. and H. Goosse, 2008a. An analysis of the atmospheric processes driving the large-scale winter sea-ice variability in the Southern Ocean. *Journal of Geophysical Research*, 113, C02004, doi:10.1029/2006JC004032.
- Lefebvre W. and H. Goosse, 2008b. Analysis of the projected regional sea-ice changes in the Southern Ocean during the 21st century. *Climate Dynamics*, 30, 59-76 DOI 10.1007/s00382-007-0273-6.
- Massom R. A., S. E. Stammerjohn, W. Lefebvre, S. A. Harangozo, N. Adams, T. A. Scambos, M. J. Pook and C. Fowler, 2008. West Antarctic Peninsula sea ice in 2005. Extreme ice compaction and ice edge retreat due to strong anomaly with respect to climate. *Journal of Geophysical Research*, 113, C02S20, doi:10.1029/2007JC004239.
- Remy J.-Ph., S. Becquevort, T. Haskell and J.-L. Tison, 2008. Impact of the B-15 iceberg "stranding event" on the physical and biological properties of sea ice in McMurdo Sound. *Antarctic Science*, 20 (6): 593-604.
- Swingedouw D., T. Fichefet, P. Huybrechts, H. Goosse, E. Driesschaert and M.F. Loutre, 2008. Antarctic ice-sheet melting provides negative feedbacks on future climate warming. *Geophysical Research Letters*, 35, L17705, doi:10.1029/2008GL034410.

2007

- Becquevort, S., Lancelot, C. and V. Schoemann, 2007. The role of iron in the bacterial degradation of organic matter derived from *Phaeocystis antarctica*. *Biogeochemistry*. 83:119-135.
- Blain S., B. Quéguiner, L. Armand, S. Belviso, B. Bombled, L. Bopp, A. Bowie, C. Brunet, C. Brussaard, F. Carlotti, U. Christaki, A. Corbière, I. Durand, F. Ebersbach, J.-L. Fuda, N. Garcia, L. Gerringa, B. Griffiths, C. Guigue, C. Guillemin, S. Jacquet, C. Jeandel, P. Laan, D. Lefèvre, C. Lo Monaco, A. Malits, J. Mosseri, I. Obernosterer, Y.-H. Park, M. Picheral, P. Pondaven, T. Remenyi, V. Sandroni, G. Sarthou, N. Savoye, L. Scouarnec, M. Souhaut, D. Thuiller, K. Timmermans, T. Trull, J. Uitz, P. van Beek, M. Veldhuis, D. Vincent, E. Viollier., L. Vong and T. Wagener, 2007. Effect of natural iron fertilization on carbon sequestration in the Southern Ocean, *Nature*, 446, 1070-1074.
- Cardinal D., N. Savoye, T.W. Trull, F. Dehairs, E.E. Kopczynska, F. Fripiat and L. André, 2007. Silicon isotopes in spring Southern Ocean diatoms: large zonal changes despite homogeneity among size fractions. *Marine Chemistry*, 106, 46-62.
- de Brauwere A., S.H.M. Jacquet, F. De Ridder, F. Dehairs, R. Pintelon, J. Schoukens and W. Baeyens, 2007. Seasonal water mass distribution in the Southern Ocean derived from a parametric analysis of mixing water masses, *Journal of Geophysical Research - Oceans*, 112, C02021, doi:10.1029/2006JC003742.

- de Jong, J., V. Schoemann, J.-L. Tison, S., Becquevort, F., Masson, D., Lannuzel, J., Petit, L. Chou, D., Weis and N., Mattielli, 2007. Precise measurement of Fe isotopes in marine samples by multi-collector Inductively Coupled Plasma Mass Spectrometry. *Analytica Chimica Acta*, 589, 105-119.
- Elskens M, A., de Brauwere, C. Beucher, R. Corvaisier, N. Savoye, P. Treguer and W. Baeyens, 2007. Statistical process control in assessing production and dissolution rates of biogenic silica in marine environments. *Marine Chemistry*, 106, 272-286.
- Fripiat F., D. Cardinal, J.-L. Tison, A. Worby and L. André, 2007. Diatom-induced silicon isotopic fractionation in Antarctic sea ice. *Journal of Geophysical Research – Biogeosciences*, 112, G02001.
- Jacquet S.H.M., F. Dehairs, N. Savoye, M. Elskens and D. Cardinal, 2007. Barium cycling along WOCE SR3 line in the Southern Ocean. *Marine Chemistry*, 106, 33-45.
- Jacquet, S.H.M., J. Henjes, F. Dehairs, A. Worobiec, N. Savoye and D. Cardinal, 2007. Particulate Ba-barite and acantharians in the Southern Ocean during the European Iron Fertilization Experiment (EIFEX). *Journal of Geophysical Research – Biogeosciences*, 112, G04006, doi:10.1029/2006JG000394.
- Kopczynska, E.E., N. Savoye, F. Dehairs, D. Cardinal and M. Elskens, 2007. Spring phytoplankton assemblages in the Southern Ocean between Australia and Antarctica. *Polar Biology*, 31, 77-88.
- Lannuzel, D., V. Schoemann, J. de Jong, J.-L. Tison and L. Chou, 2007. Distribution and biogeochemical behaviour of iron in the East Antarctic sea ice. *Marine Chemistry*, 106, 18-32.
- Reynolds B.C., J. Aggarwal, L. André, D. Baxter, C. Beucher, M. A. Brzezinski, E. Engström, R. B. Georg, M. Land, M.J. Leng, S. Opfergelt, I. Rodushkin, H.J. Sloane, S.H.J.M. van den Boorn, P.Z. Vroon and D. Cardinal, 2007. An inter-laboratory comparison of Si isotope reference materials. *Journal of Analytical Atomic Mass Spectrometry*, 22, 561-568.
- Vancoppenolle, M., C.-M. Bitz and T. Fichefet, 2007. Summer landfast sea ice desalination at Point Barrow, Alaska: modeling and observations. *Journal of Geophysical Research*, 112, C04022, doi:10.1029/2006JC003493.

2006

- Arzel O., T. Fichefet and H. Goosse, 2006. Sea ice evolution over the 20th and 21st centuries as simulated by current AOGCM. *Ocean Modelling*, 12, 401-415.
- Lannuzel D., J.T.M. de Jong, V. Schoemann, A. Trevena, J-L Tison and L. Chou, 2006. Development of a sampling and flow injection analysis technique for iron determination in the sea ice environment. *Analytica Chimica Acta*, 556 (2): 476-483.
- Savoye N, Benitez-Nelson C, Burd A, Cochran K, Charette M, Buesseler K, Jackson G, Roy-Barman M, Schmidt S and Elskens M, 2006. An overview of techniques used to model 234-Th in the water column. *Marine Chemistry*, 100, 234-249.
- Vancoppenolle, M., T. Fichefet and C.-M. Bitz, 2006. Modeling the salinity profile of undeformed Arctic sea ice. *Geophysical Research Letters*, 33, L21501, doi:10.1029/2006GL028342.

2005

- Cardinal D., L.Y. Alleman, F. Dehairs, N. Savoye, T.W. Trull and L. André, 2005. Relevance of silicon isotopes to Si-nutrient utilization and Si source assessment in Antarctic waters. *Global Biogeochemical Cycles*, 19, GB2007, doi:10.1029/2004GB002364.
- Cardinal, D., N. Savoye, T.W. Trull, L. André, E. E. Kopczynska and F. Dehairs, 2005. Variations of carbon remineralisation in the Southern Ocean illustrated by the Baxs proxy. *Deep-Sea Research I*, 52, 355-370.
- Jacquet, S.H.M., F. Dehairs, D.B. Cardinal, J. Navez and B. Delille, 2005. Barium distribution across the Southern Ocean frontal system in the Crozet–Kerguelen Basin. *Marine Chemistry*, 95, 149- 310.
- Pasquer, B, G. Laruelle, S. Becquevort, V. Schoemann, H. Goosse and C. Lancelot, 2005. Linking Ocean Biogeochemical Cycles and Ecosystem Structure and Function: Results of the Complex SWAMCO-4 Model. *Journal of Sea Research* 53: 93-108.
- Schoemann, V., S. Becquevort, J. Stefels, V. Rousseau and C. Lancelot, 2005. Phaeocystis blooms in the global ocean and their controlling mechanisms: a review. *Journal of Sea Research*, 53 (1-2), 43-66.
- Vancoppenolle, M., T. Fichefet and C.M. Bitz, 2005. On the sensitivity of undeformed Arctic sea ice to its vertical salinity profile. *Geophysical Research Letters*, 32, L16502, doi:10.1029/2005GL023427.

Non-peer reviewed

- Dehairs, F., A. de Brauwere and M. Elskens, 2008. Organic carbon in the ocean's twilight zone, *EOS, Transactions, American Geophysical Union*, 89, 351.
- Garric, G., N. Verbrugge, S. Bouillon and M. Vancoppenolle, 2008. Preliminary assessment of sea ice in the global $\frac{1}{4}^{\circ}$ Mercator Ocean forecasting system, *Mercator Newsletter*, 28.
- Goosse H. and T. Murray, 2007. Past climate session: Report from Chairs. In: Cardinal D. and E. Lipiatou (editors), *Polar environment and climate: the challenges. European research in the context of the International Polar Year. Conference Proceedings*, Climate Change and Natural Hazards Series # 11, ISBN 92-79-06278-0, EUR 22965, pp 28-29.
- Goosse H. and W. Lefebvre, 2007. Modelling climate variability and climate changes in the Southern Ocean. In: Cardinal D. and E. Lipiatou (editors), *Polar environment and climate: the challenges. European research in the context of the International Polar Year. Conference Proceedings*, Climate Change and Natural Hazards Series # 11, ISBN 92-79-06278-0, EUR 22965, pp 84-85.
- Vancoppenolle, M., T. Fichefet, H. Goosse, S. Bouillon, C. K. Beatty and M. A. Morales Maqueda, 2008. LIM3, an advanced sea-ice model for climate simulation and operational oceanography. *Mercator Newsletter*, 28 (Vancoppenolle_et_al_Mercator08.pdf. http://www.astr.ucl.ac.be//users/vancop/PUBS/Vancoppenolle_et_al_MERCATOR08.pdf).
- Wollast R., J.-P. Vanderborcht et al., 2005. The role of the ocean in global change. In: Belgian global change research 1990-2002: Assessment and integration report. Main editors: G. den Ouden and M. Vanderstraeten, Belgian Science Policy, pp 111-134.

Reports

BELSPO, 2009. La Belgique et l'Antarctique : Exploration, science et environnement. M. Vancauwenberghe (Ed.), 83pp.

Dehairs F, C. Lancelot, L. André, H. Goosse, M. Frankignoulle, S. Becquevort, A. Borges, D. Cradinal, A. de Montety, B. Delille, M. Elskens, S. Jcquet, W. Lefebvre, B. Pasquer, N. Savoye, V. Schoemann, 2006. Assessing the sensitivity of the Southern Ocean's biological carbon pump to climate change. In: Scientific results of the Second Belgian Support Plan for a Sustainable Development Policy. Published and edited by Belgian Science Policy. 130pp.

HDR Thesis

Cardinal D., 2008. Etude des cycles biogéochimiques du carbone et du silicium par une approche multi-traceurs. Habilitation à Diriger les Recherches, Université Paul Sabatier, Toulouse, France, 154pp.

PhD Theses (finalized and in progress):

Cavagna A.-J. (2010) Type and fate of biogenic matter in the Southern Ocean using isotopic and compound-specific tracers. PhD Thesis, Vrije Universiteit Brussel, pp 187.

Dumont (2009) Importance du réseau trophique microbien de la glace de mer dans les échanges air-mer de CO₂ de l'océan Austral. PhD Thesis, Université Libre de Bruxelles, pp 200.

Fripiat F., (2009) Biogeochemical cycle of silicon in the Southern Ocean: The isotopic approach. PhD Thesis, Université Libre de Bruxelles. December 2009.

Jacquet S.H.M (2007) Barium in the Southern Ocean: Towards an estimation of twilight zone carbon mineralization. PhD thesis, Vrije Universiteit Brussel, 234 pp.

Lannuzel D. (2007). Iron biogeochemistry in the Antarctic Sea Ice Environment. PhD Thesis, Université Libre de Bruxelles, pp 143.

Masson F. Biodisponibilité du Fe complexé à la matière organique dans l'Océan Austral. PhD Thesis, Université Libre de Bruxelles. Public defense expected for summer 2010.

Pasquer B. 2005. Modélisation de la pompe biologique à carbone dans l'Océan Austral. PhD Thesis, Université Libre de Bruxelles, pp 213.

Vancoppenolle, M., 2008. Modelling the mass balance and salinity of Arctic and Antarctic sea ice. PhD Thesis, Université Catholique de Louvain, ISBN 978-2-87463-113-9.

(http://www.astr.ucl.ac.be//users/vancop/PUBS/Vancoppenolle_thesisUCL_08.pdf)

MSc Theses

Content M. (2007) : Etude de l'impact de la fonte de la glace de mer sur les efflorescences planctoniques en Antarctique. MSc Thesis, Université Libre de Bruxelles.

Fripiat F., 2005. Etude structurale et isotopique du silicium dans la glace de banquise Antarctique. MSc Thesis, Université Libre de Bruxelles, 117pp.

- Masson F. (2005) : Signatures isotopiques de l'origine du fer et des processus biologiques liés au cycle biogéochimique du fer dans la zone côtière de la mer du Nord. MSc Thesis, Université Libre de Bruxelles.
- Remy J.-P. (2005) : Etude du réseau microbien dans la glace de mer, Mc Murdo, Antarctique. MSc Thesis, Université Libre de Bruxelles.
- Terseleer Lillo N. (2009) : Travail de synthèse bibliographique et de modélisation : paramétriser et caractériser l'impact de la reminéralisation bactérienne sur l'efficacité de la pompe biologique de carbone. MSc Thesis, Université Libre de Bruxelles.
- Willems N. (2008) : Etude de de la reminéralisation bactérienne en milieux aquatiques : application de différentes méthodes. MSc Thesis, Université Libre de Bruxelles.

Colloquium proceedings and abstracts (since 2006)

2010

- Cavagna A.-J., I. Bouloubassi, D. Cardinal, B. Delille, F. Dehairs, 2010. Sterols and their $\delta^{13}\text{C}$ composition in the Southern Ocean water column (BONUS-GoodHope expedition): What can they tell us about organic matter sources and fate of sinking material? Ocean Sciences Meeting, Portland, Feb. 2010.
- Dehairs F., S.H.M. Jacquet, A.-J. Cavagna, D. Cardinal, P.J. Lam, B. Griffiths and T.W Trull, 2010. Export and twilight zone carbon remineralization efficiencies in SAZ and PFZ of the Southern Ocean, Ocean Sciences Meeting, Portland, Feb. 2010.
- Dehairs F. , D. Cardinal, A.-J. Cavagna, F. Fripiat and F. Planchon, 2010. A proxy tool-box for assessing Southern Ocean biological carbon pump efficiency, International Polar Year – Oslo Science Conference in Oslo 8-12.june 2010. International Polar Year – Oslo Science Conference, Oslo, 8-12 June 2010.
- Maiti K., K.O Buesseler, C. R Benitez-Nelson, J K. Cochran, M. Dai, F. Dehairs, P. Masque, LA. Miller, B. Moran, P.J. Morris, J.-C. Miquel, F. Peine, F. Planchon, M. Rutgers van der Loeff, P.H. Santschi, R. Turnewitsch, J.T Waples, 2010. Total and Particulate Thorium-234 Results From GEOTRACES Intercalibration Cruises. Ocean Sciences Meeting, Portland, Feb. 2010.
- Speich S., F. Dehairs, M.A. Sicre, M. Boye , E. P. Achterberg, I. Ansrorge, M. Arhan, T. Arsouze, A. Baker, K. Barnes, B. Beker, M. Bender, L. Beaufort, J. Bown, E. Bucciarelli, D. Cardinal, N. Cassar, A.-J. Cavagna, B. Chapron, B. Charriere, F. Chever, H. Claustre, R. Corvaisier, B. Delille, U. Ezat, F. Fripiat, W. Geibert, N. X. Geilfus, S. Gladyshev, M. Gonzalez, E. Grossteffan, C. Hanfland, C. Jeandel, W. Joubert, E. Key, F. Lacan, F. Le Moigne, J. Lutjeharms, P. Masque, A. Masson, L. Memery, C. Messenger, P. Monteiro, X. Perrot, J.-F. Piolle, F. Planchon, P. Pondaven, A. Radic, J. Ras, P. Riviere, M. Rouault, A. Roychoudhury, V. Rupolo, J. M. Santana, G. Sarthou, R. Sempere, S. Swart, N. Tisnerat, M.P. Torre, E. Verdeny, E. Viollier, H. Waldron, 2010. Ocean dynamics, biogeochemistry and air-sea interactions in the Southern Ocean south of Africa: results from the IPY BONUS-GoodHope transect. Ocean Sciences Meeting, Portland, Feb. 2010.

2009

- Cavagna A.-J. and F. Dehairs, 2009. Biomarkers and their $\delta^{13}\text{C}$ signature in suspended particles in the open ocean water column: the case of BONUS-GoodHope expedition (Southern Ocean). AGU Chapman Conference on the Biological Carbon Pump of the Oceans Brockenhurst, Hampshire, England 1–4 September 2009.
- Cavagna A.J., V. Woule-Ebongué and F. Dehairs, 2009. Biomarkers and their $\delta^{13}\text{C}$ in suspended particles in the open ocean water column: BONUS-GoodHope expedition (Southern Ocean). ISOCOMPOUND 2009 Conference, June 2009, Potsdam, Germany.
- Boye M., F. Dehairs, D. Cardinal, F. Lacan, 2009. An overview of the biogeochemical features of the Southern Ocean during the International Polar Year, ASLO symposium, Nice Jan. 2009.
- Boye M., Achterberg E., Bown J., Bucciarelli E., Cardinal D., Cassar N., Chever F., Dehairs F., Fine R.A., Fripiat F., Happell, J., Joubert W., Le Moigne F., Masqué P., Monteiro P., Planchon F., Sarthou G., Verdeny E., Wake B., Waldron H., 2009. A First look at GEOTRACES issues from the IPY BONUS GOODHOPE cruise in the Southern Ocean, Golschmidt symposium, Davos, 2009.
- Dehairs F., 2009. Respiration of organic carbon in the mesopelagic ocean: What is there to learn from the barite proxy and is there a control by iron ? Talk given on March 4th 2009, at CSIRO, Hobart, Tasmania.
- Dehairs F., L. André and D. Cardinal, 2009. Late summer mesopelagic carbon remineralisation in the Atlantic Sector of the Antarctic Circumpolar Current, ASLO symposium, Nice Jan. 2009
- Cavagna A.-J. and F. Dehairs, 2009. Spatial variability of neutral lipids along the Greenwich Meridian in the Southern Ocean (BONUS-GOODHOPE): Preliminary results, ASLO symposium, Nice Jan. 2009.
- Goosse H., W. Lefebvre, A. de Montety, and A. Orsi, 2009. Consistent past half-century trends in the atmosphere, the sea ice and the ocean at high southern latitudes. *Geophys. Res. Abs.*, 11, 2009.
- Jacquet S.H.M., F. Dehairs, A.-J. Cavagna, F. Planchon and D. Cardinal, 2009. Twilight zone carbon remineralization efficiency in the southern ocean. AGU Chapman Conference on the Biological Carbon Pump of the Oceans, Brockenhurst, Hampshire, UK, 1–4 September 2009.
- Planchon F., A.-J. Cavagna and F. Dehairs, 2009. ^{234}Th and POC fluxes along a transect from Cape Basin to the northern Weddell Gyre (BONUS-GOODHOPE), ASLO symposium, Nice, Jan. 2009.
- Planchon F., A.-J. Cavagna and F. Dehairs, 2009. ^{234}Th , POC and PON fluxes along a transect from Cape Basin to the northern Weddell Gyre (BONUS-GOODHOPE). AGU Chapman Conference on the Biological Carbon Pump of the Oceans Brockenhurst, Hampshire, UK, 1–4 September 2009.
- Vancoppenolle M., H. Goosse, A. de Montety, T. Fichefet, and J.-L. Tison, 2009. On the brine drainage and algal uptake controls of the nutrient supply to the sea ice interior. *Geophys. Res. Abs.*, 11, 2009.

2008

- Becquevort S., I. Dumont, J.-L. Tison, D. Lannuzel, M. L. Sauvée, L. Chou, V. Schoemann, 2008. Sea ice microenvironments during early spring in the pack ice zone, Antarctica. SCAR/IASC IPY Open Science Conference, St-Petersburg, Russia, July 2008.

- Borges, A.V., B. Tilbrook, N. Metzl, A. Lenton & B. Delille, 2008. Inter-annual variability of the carbon dioxide oceanic sink south of Tasmania), *European Geosciences Union General Assembly* 13– 18 April 2008, Vienna, Austria, poster.
- Cavagna, A.-J. , N. Cassar, F. Dehairs, P.J. DiFiore, B. Tilbrook, B. Griffiths and M. Elskens, 2008. Summer *f*-ratios and net community production in the Australian sector of the Southern Ocean: contrasting regimes of nutrient availability and ecosystems functioning. *Geophysical Research Abstracts*, Vol. 10, EGU2008-A-00000, 2008, EGU General Assembly 2008.
- Cavagna, A.-J. and F. Dehairs, 2008. Spatial variability of Sterols along the Greenwich Meridian in the Southern Ocean (BONUS-GoodHope): Preliminary results, EurOceans, final Meeting, Rome 25-27, Nov 2008
- Dehairs, F., S. Jacquet and D. Cardinal, 2008. Micro-crystalline barite accumulation in suspended matter as a proxy of mesopelagic remineralization, IMBER IMBIZO meeting Miami, FL, USA, 10-13 Nov. 2008.
- De Jong, J.T.M., V. Schoemann, D. Lannuzel, J.-L. Tison, N. Mattielli, 2008. High-accuracy determination of iron in Antarctic waters by isotope dilution MC-ICP-MS using nitrilotriacetic acid chelating resin for preconcentration and matrix separation. *Geochimica et Cosmochimica Acta*: 72 (12), A209 Suppl. S.
- Geilfus, N.-X., J.-L. Tison, G. Carnat, A.V. Borges, S. F. Ackley & B. Delille, 2008. Sea ice pCO₂ dynamics and related air-ice CO₂ fluxes during a flood-freeze cycle (Bellingshausen Sea, Antarctica). *European Geosciences Union General Assembly*, 13– 18 April 2008, Vienna, Austria, poster.
- Goosse H., W. Lefebvre, A. de Montety, and A. Orsi, 2008. Variability of the Southern Ocean ice extent and water masses characteristics during the last 100 years in a climate model using data assimilation. *Geophys. Res. Abs.*, 10, CD-ROM, 2008.
- Jacquet, S.H.M., F. Dehairs, A.J. Cavagna, I. Dumont, S. Becquevort, D. Cardinal and P. Lam, 2008. Twilight zone C mineralization under different regimes of macro- and micronutrient availabilities in the Southern Ocean, *Geophysical Research Abstracts*, Vol. 10, EGU2008-A-00000, 2008, EGU General Assembly 2008.
- Lancelot, C., A. de Montety, H. Goosse, S. Becquevort, V. Schoemann, 2008. Processes governing the supply of iron to phytoplankton in the Southern Ocean: a model study. EGU General Assembly, 15–20 April 2008, Vienna, Austria. *Geophysical Research Abstracts*, Vol. 10, EGU2008-A-08701, 2008.
- Lefebvre W. and H. Goosse, 2008. The changes in Southern Ocean stratification projected for the 21st century *Geophys. Res. Abs.*, 10, CD-ROM, 2008
- Schoemann V., J.T.M. de Jong, D. Lannuzel, J.-L. Tison, B. Dellille, L. Chou, C. Lancelot, S. Becquevort. 2008. Microbiological control on the cycling of Fe and its isotopes in Antarctic sea ice. *Geochimica et Cosmochimica Acta*: 72 (12), A837 Suppl. S.
- Swingedouw D., T. Fichefet, P. Huybrechts, H. Goosse, E. Driesschaert, and M.-F. Loutre, 2008. Antarctic ice-sheet melting provides negative feedbacks on future climate warming. *Geophys. Res. Abs.*, 10, CD-ROM, 2008

2007

- Abraham K., Opfergelt S., Cavagna A.-J., Planchon F., Fripiat F., André L., de Jong J. & Cardinal D., 2007. Solving interference on ³⁰Si with a MC-ICP-MS Nu Plasma, EGU Annual meeting, April 2007, Vienna.
- Becquevort S., I. Dumont, J.-L. Tison, D. Lannuzel, J. de Jong, B. Delille, L. Chou, C. Lancelot, V. Schoemann, 2007. Significance of sea ice microbial communities,

- during early spring in the pack ice zone, Antarctica. Symposium EUROCEANS, 25 - 27 March 2007, Athens, Greece.
- Bourquin, M., van Beek P., Reyss J-L., Souhaut M., Jacquet S.H.M., Dehairs F., M. Charrette and C. Jeandel, 2007. ^{226}Ra activities and $^{226}\text{Ra}/\text{Ba}$ ratios on the Kerguelen plateau (KEOPS project), Goldschmidt Conference, August 2007, Köln, Germany.
- Cavagna A.-J., 2007. Natural dissolved silicon isotopic signal during EIFEX (European Iron Fertilization Experiment): diatom uptake vs. mixing, EurOceans Annual meeting, Athens, April, 2007.
- Cavagna A.-J., F. Fripiat, D. Wolf-Gladrow, F. Dehairs, L. André and D. Cardinal, 2007. Natural dissolved silicon isotopic signal during EIFEX (European Iron Fertilization Experiment): diatom uptake vs. mixing, EGU Annual meeting, April 2007, Vienna.
- Delille, B., A.V. Borges, D. Lannuzel, S. Becquevort, V. Schoemann, C. Lancelot, J.T.M. De Jong, B. Tilbrook, D. Delille, and J.-L. Tison, 2007. Spring CO_2 dynamics within sea ice: abiotical versus biological control. EGU General Assembly, 15–20 April 2007, Vienna, Austria, Geophysical Research Abstracts, Vol. 9, 07604, 2007.
- Dumont I., V. Schoemann, J-L. Tison, D. Lannuzel, C. Lancelot, S. Becquevort, 2007. Distribution and characterization of dissolved and particulate organic matter in Antarctic sea ice (poster) Gordon Research Conference "Polar Marine Science", Ventura, California, 25-30 March 2007.
- Goosse, H., 2007. Polar Environment and Climate: the challenges, Brussels 5-6 march 2007. Talk: "Modelling climate variability and climate change in the Southern Ocean" (Invited speaker).
- Goosse, H., Lefebvre, W., 2007. Evolution of the ice extent in the Southern Ocean during the last 100 years, *General Assembly of the European Geosciences Union*, Vienna, Austria, 16-20/4/2007.
- Goosse, H. and Lefebvre W., 2007. Modelling climate variability and climate change in the Southern Ocean. Abstracts of the conference: "Polar Environment and Climate: the challenges", Brussels, 5- 6 March 2007, page 14.
- Goosse, H., W. Lefebvre, A. de Montety, A. Orsi, 2007. Variability of the water masses characteristics in the Southern Ocean during the last 50 years: a model-data comparison. Second International Conference on Earth System Modelling, Abstracts (CD-ROM), 2007
- Hassler, C.S., V. Schoemann, D. Lannuzel, A.R. Bowie, T. Remenyi, S. Blackburn, E.C.V. Butler, 2007. Use of model and natural phytoplankton to measure iron bioavailability in the Southern Ocean. Biogeochemistry of Trace Elements in the Environment Protection, Remediation and Human Health, Proceedings of the 9th International Conference on the Biogeochemistry of Trace Elements. 2007. Ed. Y. Zhu, N. Lepp and R. Naidu. Tsinghua University Press, Beijing. ISN 978-7-302-15627-7, 2pp.
- Henjes J., S. Jacquet, P. Assmy, D. Cardinal, F. Dehairs, N. Savoye, M. Montesor & V. Smetacek, 2007. The ecological and biogeochemical role of acantharia in the Southern Ocean, Gordon Research Conference, March 2007, Ventura, CA.
- Jacquet, S.H.M., F. Dehairs, M. Elskens, N. Savoye, A. de Brauwere, B. Delille and D. Cardinal, 2007. Mesopelagic C mineralization at the Southern Ocean's scale, EGU Annual meeting, April 2007, Vienna.
- Jacquet, S.H.M., 2007. Mesopelagic C mineralization at the Southern Ocean's scale, EurOceans Annual Meeting, Athens, April 2007.

- Jeandel, C., M. Bourquin A. Bowie, E. Bucciarelli, F. Chever, F. Dehairs, S. Jacquet, F. Lacan P. van Beek, C. Venchiarutti, Y. Zhang and S. Blain, 2007. A multiproxy approach to constrain the origin of the natural fertilisation on the Kerguelen Plateau, Goldschmidt Conference, August 2007, Köln.
- Lancelot C., A. de Montety, H. Goosse, S. Becquevort, 2007. Light and iron are controlling ecosystem dynamics and biogeochemical cycles in the present-day Southern Ocean: results of the NEMOSWAMCO model. EGU General Assembly, 15–20 April 2007, Vienna, Austria (Geophysical Research Abstracts, Vol. 9, 07604, 2007).
- Lefebvre, W., Goosse, H., 2007. An analysis of atmospheric processes driving the large-scale winter sea-ice variability in the Southern Ocean, *General Assembly of the European Geosciences Union*, Vienna, Austria, 16-20/4/2007.
- Lefebvre, W., Goosse, H., 2007. Analysis of the projected regional sea-ice changes in the Southern Ocean during the 21st century, *General Assembly of the European Geosciences Union*, Vienna, Austria, 16-20/4/2007.
- Lefebvre, W., H. Goosse., 2007. An analysis of atmospheric processes driving the large-scale winter sea-ice variability in the Southern Ocean. Geophysical Research Abstracts, 9 (CD-ROM), 2007
- Lefebvre, W., H. Goosse, 2007. Analysis of the projected regional sea-ice changes in the Southern Ocean during the 21st century. Geophysical Research Abstracts, 9 (CD-ROM), 2007
- Vancoppenolle, M., T. Fichefet, H. Goosse, 2007. LIM3, an advanced sea ice model for climate studies. Geophysical Research Abstracts, 9 (CD-ROM), 2007
- Vézina, A.F., M. Levasseur, Y. LeClainche, J. Gunson, S. Vallina, M. Vogte, C. Lancelot, I. Allen, S. Archer, R. Cropp, C. Deal, S. Elliott, M. Jin, G. Malin, V. Schoemann, R. Simò, K. Six, J. Stefels, H. Zemelink, 2007. A first appraisal of ocean DMS models and prospects for their use in climate models (SOLAS-CODIM) EGU General Assembly, 15–20 April 2007, Vienna, Austria. Geophysical Research Abstracts, Vol. 9, 03845, 2007.
- Petrou K., Shelly K., Hassler C., Schoemann V., Doblin M., Ralph P., 2007. Ocean productivity in a changing world ~ Iron-limitation of Southern Ocean Phytoplankton and implications for Antarctic meltwater productivity. Australian Marine Sciences Association - Marine Science in a Changing World, 9-13 July 2007, Melbourne.
- Schoemann V., 2007. Introductory lecture on the acclimation of polar algae to extreme conditions to the session: "Zooming in: Processes at the limits of detection 2", Gordon Research Conference "Polar Marine Science", Ventura, 25-30 March 2007.
- Schoemann V., J.T.M. de Jong, D. Lannuzel, J.-L. Tison, C. Lancelot, Dumont, I., B. Delille, L. Chou and S. Becquevort, 2007. Microbial control on the cycling of Fe and its isotopes in Antarctic sea ice. Gordon Research Conference "Polar Marine Science", Ventura, 25-30 March 2007.

2006

- Cavagna, A.-J., 2006. Tracking type, origin and transformation of biogenic matter settling through the Southern Ocean water column from Si, C, N stable isotope signatures and specific compound, EurOceans Annual meeting, March 2006, Barcelona.

- de Brauwere A., S. H. M. Jacquet, F. Dehairs, F. De Ridder, R. Pintelon, J. Schoukens and W. Baeyens, 2006. A parametric method for water mass analysis applied to the Southern Ocean, Goldschmidt Conference, Melbourne, August 2006.
- de brauwere A., 2006. Modeling of ocean mixing giving quantitative indications of large scale biogeochemical processes", DISCO XX, Dissertations Symposium on Chemical Oceanography, October 8–October 12, 2006, Honolulu, Hawaii.
- Dehairs F. & BELCANTO team, 2006. Carbon fluxes and processes in the Southern Ocean: Regional or Global importance, BE-POLES Workshop, March 23-25, 2006, Brussels.
- Delille B., V. Schoemann, C. Lancelot, D. Lannuzel, J.T.M. de Jong, B. Tilbrook, D. Delille, A.V. Borges & J.-L. Tison, 2006. Can sea ice-specific biogeochemical processes support significant air-ice CO₂ fluxes? European Geosciences Union General Assembly 02 – 07 April 2006, Vienna, Austria, 2006.
- Fripiat F., D. Cardinal, J.-L. Tison, A. Worby and L. André, 2006. Diatom-induced Si isotopic fractionation in Antarctic sea ice, AGU fall meeting, December 11-15, San Francisco, 2006.
- Fripiat F., R. Corvaisier, J. Navez, M. Elskens, L. André and D. Cardinal, 2006. New method (HR-SF-ICPMS) to measure biosilica production and dissolution in ocean surface waters, Goldschmidt Conference, Cologne, August 2007.
- Goosse H., 2006. Climate change and climate variability in Polar regions, BE-POLES Workshop, March 23-25, Brussels.
- Jacquet S.H.M., Dehairs F., Jeandel C., Reyss J.-L. , Thévenet J., Souhaut M. and P. van Beek, 2006. Radium isotopes and dissolved barium to investigate the water mass pathways on the Kerguelen Plateau (KEOPS project), *Ocean Sciences* meeting, AGU-ASLO, Hawaii, February 2006.
- Jacquet S., D. Cardinal, N. Savoye and F. Dehairs, 2006. Mesopelagic C mineralization under natural and Fe-amended conditions, *Ocean Sciences* meeting, AGU-ASLO, Hawaii, February 2006.
- Lannuzel D., V. Schoemann, J. de Jong, J.-L. Tison, B. Delille, L. Chou, 2006. Iron Distribution in Antarctic Pack Ice, AGU ocean sciences meeting, 20-24 February 2006, Honolulu, Hawaii, United States. *Eos Trans. AGU*, 87(36), Ocean Sciences Meeting, Suppl., OS16M-18.
- Lannuzel D., L. Chou, J. de Jong, J.-L. Tison, B. Delille, V. Schoemann, 2006. Pack ice: a significant source of Fe to Antarctic surface waters? EGU General Assembly, 02–07 April 2006, Vienna, Austria. *Geophysical Research Abstracts*, Vol. 8, 08918, 2006.
- Lefebvre, W; Goosse, H., 2006. An analysis of the atmospheric processes driving the large-scale winter sea ice variability in the Southern Ocean. *Geophysical Research Abstracts*, 8 (CD-ROM), 2006
- Reynolds B.C., J. Aggarwal, M.A. Brzezinski, D. Cardinal, E. Engström, R.B. George, M. Land, S. Opfergelt, and P.Z. Vroon, 2006. An inter-laboratory calibration of Si isotope reference materials. Goldschmidt Conference, Melbourne, August 2006.
- Schoemann V., D. Lannuzel, S. Becquevort, J.-L. Tison, A. Trevena, J. De Jong, B. Delille, M.-L. Sauvée, C. Lancelot, L. Chou, 2006, Impact of microbiological processes on the cycling of Fe in Antarctic sea-ice during Spring, AGU ocean sciences meeting, 20-24 February 2006, Honolulu, Hawaii, United States. *Eos Trans. AGU*, 87(36), Ocean Sci. Meet. Suppl., OS16M-30.

- Tison, J.L., de Jong J., Becquevort S., Schoemann V., Dumont I., Masson F., Lancelot C., Lannuzel D., Chou L., Delille B., Borges A., 2006. Sea Ice Biogeochemistry in a Climate Change Perspective (SIBCLim): an integrated interdisciplinary project, BE-POLES Workshop, Brussels, March 23-25, 2006,
- Tison J.-L., F. Brabant, B. Delille, V. Schoemann, S. Becquevort, T. Worby, G. Dieckmann, 2006. Temporal evolution of gas properties in decaying summer first-year sea ice in the western Weddell Sea (Antarctica): links to biological activity, AGU Fall Meeting, 11-15 December 2006, San Francisco.
- Tison J.L and Goosse H., 2006. Het verhaal van ijs en klimaat in de polaire gebieden / Une petite histoire Activity report intended for the intermediary evaluation - Document G 37 de la glace de mer et du climat des régions polaires, BE-POLES Workshop, March 23-25, 2006, Brussels.
- Vancoppenolle, M., Bitz, C. M., Fichefet, T., Goosse, H. Modeling salinity variations in sea ice with a climate modeling perspective. Geophysical Research Abstracts, 8 (CD-ROM), 2006.
- Vöge I., N. Savoye, G.M. Berg, C. Bertoia, C. Klaas, U. Bathmann, V. Strass, J. Friedrich and F. Dehairs, 2006. ^{234}Th -based export production during the European Iron Fertilization Experiment (EIFEX), *Ocean Sciences* meeting, AGU-ASLO, Hawaii, February, 2006.

6. ACKNOWLEDGEMENTS

We acknowledge the assistance of the following research institutes and research groups:

- Alfred Wegener Institute, Bremerhaven
- Institut Polaire P.E. Victor, Brest
- Antarctic Climate and Ecosystem CRC, Hobart, Australia
- Woods Hole Oceanographic Institute (research groups of K.O. Buesseler and K. Casciotti), Woods Hole, MA, USA
- Research Foundation Flanders
- Research Council Vrije Universiteit Brussel
- The EU FP6 Network of Excellence 'EurOceans'

We thank the members of the end-user committee (H. de Baar, Royal NIOZ, Texel, The Netherlands; C. Jeandel, Laboratoire d'Etudes en Géophysique et Océanographie Spatiales, OMP, Toulouse; N. Metzl, Institut Pierre Simon Laplace, Université Pierre et Marie Curie, Paris; E. Murphy, British Antarctic Survey; J.-L. Tison, Glaciologie, Université Libre de Bruxelles; T.W. Trull, Antarctic Climate and Ecosystem CRC, Hobart; M. Vancauwenberghe, Belspo) for their numerous valuable criticisms and suggestions.

7. REFERENCES

The list does not include papers of the Belcanto group listed under section 5 'Publications'

- Acker, J. G. and Leptoukh G., 2007. Online Analysis Enhances Use of NASA Earth Science Data. *Eos, Transactions, AGU*, 88 (2), 14-17.
- Armstrong R.A., C. Lee, J.I. Hedges, S. Honjo and S. G. Wakeham, 2002. A new, mechanistic model for organic carbon fluxes in the ocean based on the quantitative association of POC with ballast minerals. *Deep-Sea Research II*, 49, 219-236.
- Arrigo K.R., Worthen, D.L. and Robinson, D.H., 2003. A coupled ocean-ecosystem model of the Ross Sea: 2. Iron regulation of phytoplankton variability and primary production. *Journal of Geophysical Research*, 108 (C7): 3232, doi:10.1029/2001JC000856.
- Arrigo K.R. , van Dijken G.L. and Bushinsky S., 2008. Primary production in the Southern Ocean , 1997-2006. *Journal of Geophysical Research – Oceans*, 113, C08004, doi:10.1029/2007JC004551
- Arrigo, K., C. W. Sullivan and J. N. Kremer, 1991. A bio-optical model of Antarctic sea ice, *Journal of Geophysical Research*, 96(C6), 10581-10592.
- Atkinson, A., Siegel, V., Pakhomov, E. and Rothery, P., 2004. Long-term decline in krill stocks and increase in salps in the Southern Ocean. *Nature*, 432, 100-103.
- Aumont O. and Bopp L. 2006. Globalizing results from ocean in situ iron fertilization studies. *Global Biogeochemical Cycles*, 20, GB2017, doi:10.1029/2005GB002591
- Azam F. and R.A. Long. 2001. Sea snow microcosms. *Nature*, 414, 495 -498.
- Benitez-Nelson, C., Buesseler, K.O., Rutgers van der Loeff, M., Andrews, J., Ball, L., Crossin, G. and Charette, M.A., 2001. Testing a new small volume technique for determining Thorium-234 in seawater. *Journal of Radioanalytical and Nuclear Chemistry*, 248, 795–799.
- Benthien, A., I. Zonderaven, A. Engel, J. Hefter, A. Terbrüggen and U. Riebesell, 2007. Carbon isotopic fractionation during a mesocosm bloom experiment dominated by *Emiliana huxleyi*: Effects of CO₂ concentration and primary production. *Geochimica and Cosmochimica Acta*, 71, 1528-1541.
- Bernstein R.E. and R.H. Byrne, 2004. Acantharians and marine barite. *Marine Chemistry*, 86, 45-50.
- Bernstein R.E., R.H. Byrne and J. Schijf, 1998. Acantharians: a missing link in the oceanic biogeochemistry of barium, *Deep-Sea Research I*, 45, 491-505.
- Bidle K.D. and F. Azam, 2001. Bacterial control of silicon regeneration from diatom detritus: significance of bacterial ectohydrolases and species identity. *Limnology and Oceanography*, 46, 1606-1623.
- Bidle, K.D. and F. Azam, 1999. Accelerated dissolution of diatom silica by marine bacterial assemblages. *Nature*, 397, 508-512.
- Blain S, Quéguiner B, Armand L, Belviso S, and others. 2007. Effects of natural iron fertilisation on carbon sequestration in the Southern Ocean. *Nature*, 446: 1070-1074

- Bowie A.R., Lannuzel D., Remenyi T.A., Wagener T., Lam P., Boyd P.W., Guieu C., Townsend A.T. and Trull T.W., 2009. Biogeochemical iron budgets of the Southern Ocean south of Australia demonstrate that summertime supply decouples iron and nutrient cycles in the subantarctic zone. *Global Biogeochemical Cycles*, 23, doi:10.1029/2009GB003500.
- Boyd P. W. and Newton P. P., 1999. Does planktonic community structure determine downward particulate organic carbon flux in different oceanic provinces? *Deep-Sea Research I*, 46 (1), 63-91.
- Boyd, P. W., T. Jickells, C. S. Law, S. Blain, E. A. Boyle, K. O. Buesseler, K. H. Coale, J. J. Cullen, H. J. W. de Baar, M. Follows, M. Harvey, C. Lancelot, M. Levasseur, N. P. J. Owens, R. Pollard, R. B. Rivkin, J. Sarmiento, V. Schoemann, V. Smetacek, S. Takeda, A. Tsuda, S. Turner and A. J. Watson, 2007. Mesoscale Iron Enrichment Experiments 1993–2005: Synthesis and Future Directions. *Science*, 315, 612-617.
- Boye M., van den Berg C.M.G., de Jong J.T.M., Leach H., Croot P. and de Baar H.J.W., 2001. Organic complexation of iron in the Southern Ocean, *Deep-Sea Research I*, 48: 1477-1497.
- Brzezinski M.A and D.M. Nelson, 1989. Seasonal changes in the silicon cycle within a Gulf Stream warm-core ring. *Deep-Sea Research I*, 36, 1009-1030.
- Brzezinski M.A. and D.R. Phillips, 1997. Evaluation of ^{32}Si as a tracer for measuring silica production rates in marine waters. *Limnology and Oceanography*, 42, 856-865.
- Buesseler, K.O., Ball, L., Andrews, J., Cochran, J.K., Hirschberg, D.J., Bacon, M.P., Fler, A. and Brzezinski, M., 2001. Upper ocean export of particulate organic carbon and biogenic silica in the Southern Ocean along 1701W. *Deep-Sea Research II*, 48 (19/20), 4275–4297.
- Buesseler, K.O., Andrews, J.E., Pike, S.M., Charette, M.A., Goldson, L.E., Brzezinski, M.A. and Lance, V.P., 2005. Particle export during the Southern Ocean Iron Experiment (SOFeX). *Limnology and Oceanography*, 50 (1), 311–327.
- Buesseler K.O., Lamborg C.H., Boyd P.W., Lam P.J., Trull T.W., Bidigare R.R., Bishop J. K. B., Casciotti K. L., Dehairs F., Elskens M., Honda M., Karl D. M., Siegel D. A., Silver M. W., Steinberg D. K., Valdes J., Van Mooy B., and Wilson S., 2007. Revisiting carbon flux through the ocean's twilight zone. *Science*, 316, 567-570.
- Burd A.B., D.A. Hansell, D.K. Steinberg, T.R. Anderson, J. Aristegui, F. Baltar, S.R. Beupré, K.O. Buesseler, F. Dehairs, G. A. Jackson, D.C. Kadko, R. Koppelman, R.S. Lampitt, T. Nagata, T. Reinthaler, C. Robinson, B.H. Robison, C. Tamburini and T. Tanaka, 2010. Assessing the Apparent Imbalance Between Geochemical and Biochemical Indicators of Meso- and Bathypelagic Biological Activity: What the @\$#! is wrong with present calculations of carbon budgets? *Deep-Sea Research II*, 57, 1557–1571.
- Cardinal D., F. Dehairs, T. Cattaldo and L. André, 2001. Geochemistry of suspended particles in the Subantarctic and Polar Front Zones south of Australia: Constraints on export and advection processes. *Journal of Geophysical Research - Oceans*, 106, 31,637-31,656.
- Cardinal D., L.Y. Alleman, J. De Jong, K. Ziegler and L. André, 2003. Isotopic composition of silicon measured by multicollector plasma source mass spectrometry in dry plasma mode. *Journal of Analytical Atomic Spectrometry*, 18, 213-218.

- Casciotti K.L., Sigman D.M., Hastings M.G., Böhlke J.K. and Hilkert A., 2002 - Measurement of the oxygen isotopic composition of nitrate in seawater and freshwater using the denitrifier method. *Analytical Chemistry*, 74 (19), 4905-4912.
- Church M.J., Hutchins D.A. and Ducklow H.W., 2000. Limitation of bacterial growth by dissolved organic matter and iron in the Southern Ocean. *Applied Environmental Microbiology*, 66, 455-466.
- Cisewski, B., Strass, V. H., Losch, M. and Prandke, H., 2008. Mixed layer analysis of a mesoscale eddy in the Antarctic Polar Front Zone. *Journal of Geophysical Research - Oceans*, 113, C05017. doi:10.1029/2007JC004372.
- Coale K.H., Gordon R.M. and Wang X., 2005. The distribution and behavior of dissolved and particulate iron and zinc in the Ross Sea and Antarctic Circumpolar Current along 170°W. *Deep-Sea Research I*, 52: 295-318.
- Croot P.L., Andersson K., Oztürk M. and Turner D., 2004. The distribution and speciation of iron along 6°E, in the Southern Ocean. *Deep-Sea Research II*, 51: 2857-2879.
- Cubillos J. C., S. W. Wright, G. Nash, M. F. de Salas, B. Griffiths, B. Tilbrook, A. Poisson and G. M. Hallegraeff, 2007. Calcification morphotypes of the coccolithophorid *Emiliana huxleyi* in the Southern Ocean: changes in 2001 to 2006 compared to historical data. *Marine Ecology Progress Series*, 348, 47-54.
- de Baar H.J.W. and Boyd, P.M., 2000. The role of iron in plankton ecology and carbon dioxide transfer of the global oceans, In: R.B. Hanson, H.W. Ducklow and J.G. Field, Editors, *The Dynamic Ocean Carbon Cycle: A Midterm Synthesis of the Joint Global Ocean Flux Study*, International Geosphere Biosphere Programme Book Series, Vol. 5, Cambridge University Press, 61–140.
- De Baar HJW, Boyd PW, Coale KH, Landry MR, Tsuda A, Assmy P, Bakker CE, Bozec Y, Narber RT, Brzezinski MA, K.O. Buesseler, MA, Boyé M, Croot PL, Gervais F, Gorbunov MY, Harrison PJ, Hiscock WT, Laan P, Lancelot C, Law CS, Lévassieur M, Marchetti A, Millero FJ, Nishioka J, Noriji Y, van Oijen T, Riebesell U, Rijkenberg MJA, Saito H, Takeda S, Timmermans KR, Veldhuis MJW, Waite AM and Wong C-S, 2005. Synthesis of iron fertilization experiments: from the iron age in the age of enlightenment. *Journal of Geophysical Research - Oceans*, 110:C09S16.
- de Baar H.J.W., de Jong J.T.M., Nolting R.F., van Leeuwe M.A, Timmermans K.R., Templin M., Rutgers van der Loeff M.M. and Sildam J., 1999. Low dissolved Fe and the absence of diatoms blooms in remote Pacific waters of the Southern Ocean. *Marine Chemistry*, 66: 1-34
- de Boyer Montégut, C., Madec, G., Fischer, A. S., Lazar, A., and Ludicone, D., 2004. Mixed layer depth over the global ocean: An examination of profile data and a profile-based climatology, *Journal of Geophysical Research*, 109, doi:10.1029/2004JC002378.
- Dehairs F., D. Shopova, S. Ober, C. Veth and L. Goeyens, 1997. Particulate barium stocks and oxygen consumption in the Southern Ocean mesopelagic water column during spring and early summer: Relationship with export production. *Deep-Sea Research II*, 44, 497-516.
- de Jong J.T.M., den Das J., Bathmann U., Stoll M.H.C., Kattner G., Nolting R.F. and de Baar H.J.W., 1998. Dissolved iron at subnanomolar levels in the Southern Ocean as determined by ship-board analysis. *Analytica Chimica Acta*, 377, 113-124.

- De La Rocha C.L., M.A. Brzezinski and M.J. DeNiro, 1997. Fractionation of silicon isotopes by marine diatoms during biogenic silica formation, *Geochimica et Cosmochimica Acta*, 61, 5051-5056.
- de Montety A., 2006. Comparison between open and closed boundary conditions: a study performed with the NEMO model, Scientific Report 2006/02, Institut d'Astronomie et de Géophysique Georges Lemaître.
- Demarest, M.S., Brzezinski, M.A. and Beucher, C.P., 2009. Fractionation of silicon isotopes during biogenic silica dissolution. *Geochimica et Cosmochimica Acta*, 73, 5572-5583.
- DiFiore, P.J., D.M. Sigman, T.W. Trull, M. J. Lourey, K. Karsh, G. Cane and R. Ho, 2006. Nitrogen isotope constraints on subantarctic biogeochemistry, *Journal of Geophysical Research - Oceans*, 111, C08016, doi:10.1029/2005JC003216.
- Ducklow H.W., Steinberg D.K., Buesseler K.O., 2001. Upper ocean carbon export and the biological pump. *Oceanography* 14 (4), 50-58.
- Dugdale R.C., Wilkerson F.P., Minas H.J., 1995. The role of a silicate pump in driving new production. *Deep-Sea Research*, 42 :697-719.
- Dutkiewicz, S., Follows, M.J. and Parekh, P., 2005. Interactions of the iron and phosphorus cycles: A three-dimensional model study. *Global Biogeochemical Cycles*, 19, GB1021, doi:10.1029/2004GB002342, 2005.
- Ebersbach F., T. W. Trull, D. Davies, C. Moy, S.G. Bray, and C. Bloomfield, 2011. Controls on near-surface sinking particle fluxes in the Sub-Antarctic and Polar Frontal Zones in the Southern Ocean south of Australia in summer – perspectives from free-drifting sediment trap studies, *Deep-Sea Research II*, SAZ-Sense topical volume accepted.
- Elskens, M., F. Dehairs, B. Griffiths and T. Cattaldo, 2002. N Uptake conditions during summer in the Subantarctic and Polar Front Zones of the Australian sector of the Southern Ocean, *Journal of Geophysical Research - Oceans*, 107, 3182, 10.1029/2001JC000897.
- Elskens, M., W. Baeyens, N. Brion, S. De Galan, L. Goeyens, and A. de Brauwere, 2005. Reliability of N flux rates estimated from ¹⁵N enrichment and dilution experiments in aquatic systems. *Global Biogeochemical Cycles*, 19, GB4028.
- Fabry V.J., J.B. McClintock, J.T. Mathis and J.M. Grebmeier, 2009. Ocean acidification at high latitudes: The Bellwether. *Oceanography*, 22, 160-171.
- Fennel K., M.R. Abbott, Y.H. Spitz, J.G. Richman, 2003. Impacts of iron control on phytoplankton production in the modern and glacial Southern Ocean, *Deep-Sea Research II*, 50, 833-851.
- Fitch, D.T. and Moore, K.J., 2007. Wind speed influence on phytoplankton bloom dynamics in the Southern Ocean Marginal Ice Zone. *Journal of Geophysical Research*, 112, C08006, doi:10.1029/2006JC004061.
- Francois R., S. Honjo, R. Krishfield and S. Manganini, 2002. Factors controlling the flux of organic carbon to the bathypelagic zone of the ocean. *Global Biogeochemical Cycles*, 16, doi:10.1029/2001GB001722.
- Gallée H. and Schayes, G., 1994. Development of a three-dimensional meso-γ primitive equation model : Katabatic winds simulation in the area of terra nova bay, antarctica. *Monthly Weather Review*, 122, 671–685, 1994.
- Gladstone R.M. and Bigg G.R. and Nicholls K.W., 2001. Iceberg trajectory modeling and meltwater injection in the Southern Ocean. *Journal of Geophysical Research*, 106(C9): 19,903 – 19,915.

- Griffies S.M., Biastoch A., Boning C. , Bryan F., Danabasoglu G., Chassignet E.P., England M.H., Gerdes R., Haak H., Hallberg R.W., Hazeleger W., Jungclaus J., Large W.G., Madec G., Pirani A., Samuels B.LL, Scheinert M., Sen Gupta A., Severijns C.A., Simmons H.L., Treguier A.M., Winton M., Yeager S. and Yin J.J. 2009. Coordinated Ocean-ice Reference Experiments (COREs). *Ocean Modelling*, 26, (1-2), 1-46.
- Grotti, M., Soggia, F., Ianni, C. and Frache, R. 2005. Trace metals distributions in coastal sea ice of Terra Nova Bay, Ross Sea, Antarctica. *Antarctic Science*, 17, 289–300.
- Hansell D.A., 2002. DOC in the Global Ocean Carbon Cycle. In: Hansell, D. A. and Carlson, C. A. (Eds.), *Biogeochemistry of Marine Dissolved Organic Matter*. Academic Press, New-York, 685-716.
- Hecq, J.H., Guglielmo, L., Goffart, A., Catalano, G. and Goosse, H., 2000. A modeling approach to the Ross Sea plankton ecosystem. In: F.M. Faranda, Guglielmo, L., Ianora, A. (Editor), *Ross Sea Ecology*. Springer, pp. 395-411.
- Heinze C., 2004. Simulating oceanic CaCO₃ export production in the greenhouse. *Geophysical Research Letters*, 31, doi:10.1029/2004GL020613
- Hoffmann, L.J., I. Peeken, K; Lochte, P. Assmy and M. Veldhuis. 2006. Different reactions of Southern Ocean phytoplankton size classes to iron fertilization. *Limnology and Oceanography*, 51(3): 1217-1229.
- Holligan P.M., A. Charalampopoulou and R. Hutson, 2010. Seasonal distributions of the coccolithophore, *Emiliana huxleyi*, and of particulate inorganic carbon in surface waters of the Scotia Sea. *Journal of Marine Systems*, 82, 195–205.
- Holm-Hansen O. and C.D. Hewes, 2004. Deep chlorophyll-a maxima (DCMs) in Antarctic waters. *Polar Biology*, 27, 699-710.
- Hudson R.J.M and F.M.M. Morel, 1989. Distinguishing between extra- and intracellular iron in marine phytoplankton. *Limnology & Oceanography*, 34, 1113-1120.
- Hutchins D.A. and K.W. Bruland, 1998. Iron-limited diatom growth and Si:N uptake ratios in a coastal upwelling regime. *Nature*, 393, 561-564.
- Hutchins D.A., Witter A.E., Butler A. and Luther G.W. 1999. Competition among marine phytoplankton for different chelated iron species. *Nature*, 400: 858-861.
- Hutchins, D. A., P. N. Sedwick, G. R. DiTullio, P. W. Boyd, B. Quéguiner, F. B. Griffiths, and C. Crossley, 2001. Control of phytoplankton growth by iron and silicic acid availability in the subantarctic Southern Ocean: Experimental results from the SAZ project. *Journal of Geophysical Research*, 106, 31,559–31,572.
- Jeandel C., D. Ruiz-Pino, E. Gjata, A. Poisson, C. Brunet, E. Charriaud, F. Dehairs, D. Delille, M. Fiala, C. Fravallo, J.-C. Miquel, Y.-H. Park, P. Pondaven, B. Quéguiner, S. Razouls, B. Shauer and P.Tréguer, 1998. KERFIX, a time-series station in the Southern Ocean: a presentation. *Journal of Marine Research*, 17, 555-569.
- Kalnay E., M. Kanamitsu, R. Kistler, W. Collins, D. Deaven, L. Gandin, M. Iredell, S. Saha, G. White, J. Woollen, Y. Zhu, M. Chelliah, W. Ebisuzaki, W.Higgins, J. Janowiak, K. C. Mo, C. Ropelewski, J. Wang, A. Leetmaa, R. Reynolds, R. Jenne and D. Joseph, 1996. The NCEP/NCAR 40-year reanalysis project. *Bull. Am. Meteorol. Soc.*, 77, 437–470.
- Klaas C., Archer, D.E. 2002. Association of sinking organic matter with various types of mineral ballast in the deep sea: Implications for the rain ratio. *Global Biogeochemical Cycles*, 16(4): 1116.

- Lancelot C., Veth C. and Mathot S. 1991. Modelling ice edge phytoplankton bloom in the Scotia Weddell Sea sector of the Southern Ocean during spring 1988. *Journal of Marine Systems*, 2 : 333-346.
- Laws E.A., P.G. Falkowski, W.O. Smith Jr., H. Ducklow and J.J. McCarthy, 2000. Temperature effects on export production in the open ocean. *Global Biogeochemical Cycles*, 14, 1231-1246.
- Lee C., Wakeham S. and Arnosti C., 2004. Particulate organic matter in the sea: The composition conundrum. *Ambio*, 33 (8), 565-575.
- Lefebvre W., Goosse H., Timmermann R. and Fichefet T., 2004. Influence of the southern annular mode on the sea ice-ocean system. *Journal of Geophysical Research*, 109, C09005, doi:10.1029/2004JC002403.
- Leynaert A., E. Bucciarelli, P. Claquin, R.C. Dugdale, V. Martin-Jézéquel, P. Pondaven and O. Ragueneau, 2004. Effect of iron deficiency on diatom cell size and silicic acid uptake kinetics. *Limnology and Oceanography*, 49, 1134-1143.
- Lo Monaco C., N. Metzl, A. Poisson, C. Brunet and B. Schauer, 2005. Anthropogenic CO₂ in the Southern Ocean: Distribution and inventory at the Indian-Atlantic boundary (World Ocean Circulation Experiment line I6). *Journal of Geophysical Research - Oceans*, 110, C06010, doi:10.1029/2004JC002643.
- Mackie D.S., P.W. Boyd, G.H. McTainsh, N.W. Tindale, T.K. Westberry and K.A. Hunter, 2008. Biogeochemistry of iron in Australian dust: From eolian uplift to marine uptake, *Geochemistry, Geophysics, Geosystems*, G3, 9, Q03Q08, doi:10.1029/2007GC001813.
- Madec, G., P. Delecluse, M. Imbard and C. Lévy, 1998. OPA 8.1 Ocean General Circulation Model reference manual. Note du Pôle de modélisation, Institut Pierre-Simon Laplace, N°11, pp 91.
- Martin-Jézéquel V., M. Hildebrand and M.A. Brzezinski, 2000. Silicon metabolism in diatoms: implications for growth. *Journal of Phycology*, 36, 821-840.
- Mathiot P., 2009. Influence du forçage atmosphérique sur la représentation de la glace de mer et des eaux de plateau en Antarctique dans une étude de modélisation numérique. PhD Thesis, Joseph Fourier University, Grenoble 1, 196 pp.
- Matsumoto, K., J. L. Sarmiento and M. A. Brzezinski, 2002. Silicic acid 'leakage' from the Southern Ocean as a possible mechanism for explaining glacial atmospheric pCO₂. *Global Biogeochemical Cycles*, 16, doi: 10.1029/2001GB001442.
- Metzl, N., 2009. Decadal increase of oceanic carbon dioxide in the Southern Indian Ocean surface waters (1991-2007). *Deep-Sea Research*, II, doi:10.1016/j.dsr2.2008.12.007
- Metzl N., Tilbrook, B. and Poisson, A., 1999. The annual fCO₂ cycle and the sea-air CO₂ flux in the Sub-Antarctic Ocean. *Tellus B*, 51(4): 849-861.
- Milligan A.J., D.E. Varela, M.A. Brzezinski and F.M.M. Morel, 2004. Dynamics of silicon metabolism and silicon isotopic discrimination in a marine diatom as a function of pCO₂. *Limnology and Oceanography*, 49, 322-329.
- Ming L. and Garrett, C., 1997. Mixed Layer Deepening due to Langmuir circulation. *Journal of Physical Oceanography*, 27, 121-132.
- Moore K.J., Doney, S.C., Kleypas, J.A., Glover, D.M. and Fung, I.Y., 2002. An intermediate complexity marine ecosystem model for the global domain. *Deep-Sea Research II*, 49: 403-462.
- Moore J.K., Doney S.C. and Lindsay K., 2004. Upper ocean ecosystem dynamics and iron cycling in a global three-dimensional model. *Global Biogeochemical Cycles*, 18, GB4028, doi:10.1029/2004GB002220.

- Moore, J.K. and Braucher, O., 2008. Sedimentary and mineral dust sources of dissolved iron to the world ocean. *Biogeosciences*, 5, 631-656.
- Mosseri J., B. Quéguiner, L. Armand and V. Cornet-Barthaux, 2008. Impact of iron on silicon utilization by diatoms in the Southern Ocean: A case study of Si/N cycle decoupling in a naturally iron-enriched area. *Deep-Sea Research II*, 55, 801-819.
- Moy A.D., W.R. Howard, S.G. Bray and T.W. Trull, 2009. Reduced calcification in modern Southern Ocean planktonic foraminifera. *Nature Geoscience*, 2, 2009.
- Nelson, D.M., and J.J. Goering. 1977a. A stable isotope tracer method to measure silicic acid uptake by marine phytoplankton. *Anal. Biochem.* 78:139-147.
- Nelson, D.M., and J.J. Goering. 1977b. Near-surface silica dissolution in the upwelling region off northwest Africa. *Deep-Sea Research*, 24, 65-73.
- O'Leary, T., T.W. Trull, F.B. Griffiths, B. Tilbrook and A.T. Revill, 2001. Euphotic zone variations in bulk and compound-specific $\delta^{13}\text{C}$ of suspended organic matter in the subantarctic zone, south of Australia. *Journal of Geophysical Research*, 106, 31,669-31,684.
- Park Y.-H., J.-L. Fuda, I. Durand and A. C. Naveira Garabato, 2008. Internal tides and vertical mixing over the Kerguelen Plateau. *Deep-Sea Research II*, 55, 582-593.
- Parslow, J. S., P. W. Boyd, S. R. Rintoul, and F. B. Griffiths, 2001. A persistent subsurface chlorophyll maximum in the Interpolar Frontal Zone south of Australia: Seasonal progression and implications for phytoplankton-light-nutrient interactions, *Journal of Geophysical Research*, 106, 31,543–31,558.
- Pearce, I., Davidson, A.T., Thomson, P.G., Wright, S. and van den Enden, R., 2011. Marine microbial ecology in the Sub-Antarctic Zone: rates of bacterial and phytoplankton growth and grazing by heterotrophic protists. *Deep-Sea Research II*, SAZ-Sense topical volume, accepted.
- Pike, S.M., Buesseler, K.O., Andrews, J., Savoye, N., 2005. Quantification of Th-234 recovery in small volume seawater samples by inductively coupled plasma-mass spectrometry. *Journal of Radioanalytical and Nuclear Chemistry*, 263 (2), 355–360.
- Preunkert S., Legrand M., Jourdain B. Moulin C., Belviso S., Kasamatsu Nobue, Fukuchi M. and Hirawake T., 2007. Interannual variability of dimethylsulfide in air and seawater and its atmospheric oxidation by-products (methanesulfonate and sulfate) at Dumont d'Urville, coast Antarctica (1999-2003). *Journal of Geophysical Research*, 112, D06306, doi:10.1029/2006JD007585.
- Rayner N., Parker D., Horon E., Folland C., Alexander L., Rowel D., Kent E. and Kaplan A., 2003. Global analyses of sea surface temperature, sea ice and night marine air temperature since the late nineteenth century. *Journal of Geophysical Research*, 108(D14): 4407.
- Riebesell, U., A.T. Revill, D.G. Holdsworth and J.K. Volkman., 2000. The effect of varying CO₂ concentration on lipid composition and carbon isotope fractionation in *Emiliana huxleyi*. *Geochimica and Cosmochimica Acta*, 64, 4179-4192.
- Riebesell, U., Zondervan, I., Rost, B., Tortell, P.D., Zeebe, R.E. and Morel, F.M.M. 2000. reduced calcification of marine plankton in response to increased atmospheric CO₂. *Nature*, 407: 634-637.
- Rontani, J.F. and J.K. Volkman, 2003. Phytol degradation products as biogeochemical tracers in aquatic environments. *Organic Geochemistry*, 34, 1-35.
- Rontani, J.F., N. Zabeti and S.G. Wakeham, 2009. the fate of marine lipids: Biotic vs. abiotic degradation of particulate sterols and alkenones in the Northwestern Mediterranean Sea. *Marine Chemistry*, 113, 9-18.

- Rutgers van der Loeff, M.M. and Moore, W.S., 1999. Determination of natural radioactive tracers. In: Grasshoff, K., Ehrhardt, M., Kremling, K. (Eds.), *Methods of Seawater Analysis*. Verlag Chemie, Weinheim, pp. 365–397 (Chapter 13).
- Sabine, C.L., Feely, R.A., Gruber, N., Key, R.M., Lee, K., Bullister, J.L., Wanninkhof, R., Wong, C.S., Wallace, D.W.R., Tilbrook, B., Millero, F.J., Peng, T.-H., Kozyr, A., Ono, T. and Rios, A.F., 2004. The oceanic sink for anthropogenic CO₂. *Science*, 305, 367-371.
- Sarmiento J.L., N. Gruber, M.A. Brzezinski and J.P. Dunne, 2004. High-latitude controls of thermocline nutrients and low latitude biological productivity. *Nature*, 427, 56-60.
- Savoye N., F. Dehairs, M. Elskens, D. Cardinal, E. E. Kopczynska, T. W. Trull, W. Baeyens and F. B. Griffiths, 2004. N-uptake and new production in the Southern Ocean during spring conditions, *Geophysical Research Letters*, 31(3), L03301, 10.1029/2003GL018946.
- Sedwick P.N., S. Blain, B. Quéguiner, F.B. Griffiths, M. Fiala, E. Bucciarelli and M. Denis, 2002. Resource limitation of phytoplankton growth in the Crozet Basin, Subantarctic Southern Ocean. *Deep-Sea Research II*, 49, 3327-3349.
- Sedwick, P.N., DiTullio G.R., Hutchins D.A., Boyd P.W., Griffiths F.B., Crossley A.C., Trull T.W., and Queguiner B., 1999. Limitation of algal growth by iron deficiency in the Australian subantarctic region. *Geophysical Research Letters*, 26: 2865-2868.
- Shi D., Y. Xu, B.M. Hopkinson and F.M.M. Morel, 2010. Effect of Ocean Acidification on Iron Availability to Marine Phytoplankton, *Science*, 327, 676-679.
- Sigman D.M., M.A. Altabet, D.C. McCorkle, R. François and G. Fischer, 1999. The $\delta^{15}\text{N}$ of nitrate in the Southern Ocean: consumption of nitrate in surface waters. *Global Biogeochemical Cycles*, 13(4), 1149-1166.
- Sigman D.M., Casciotti K.L., Andreani M., Barford C., Galanter M. and Böhlke J.K., 2001. A bacterial method for the nitrogen isotopic analysis of nitrate in seawater and freshwater. *Analytical Chemistry*, 73: 4145-4153
- Sigman D.M., DiFiore P.J., Hain M.P., Deutsch C. and Karl D.M., 2009. Sinking organic matter spreads the nitrogen isotope signal of pelagic denitrification in the North Pacific. *Geophysical Research Letters*, 36, L08605, doi:10.1029/2008GL035784.
- Sigman, D. M., J. Granger, P. J. DiFiore, M. M. Lehmann, R. Ho, G. Cane, and A. van Geen, 2005. Coupled nitrogen and oxygen isotope measurements of nitrate along the eastern North Pacific margin, *Global Biogeochemical Cycles*, 19, GB4022.
- Smetacek, V., Assmy, P. and Henjes, J., 2004. The role of grazing in structuring Southern Ocean pelagic ecosystems and biogeochemical cycles. *Antarctic Science* 16, 541–558.
- Sohrin, Y., Iwamota S., Matsui M., Obata H., Nakayama E., Suzuki K., Handa N. and Ishii M., 2000. The distribution of Fe in the Australian sector of the Southern Ocean. *Deep-Sea Research I*, 47: 55-84.
- Tagliabue A. and K.R. Arrigo, 2005. Iron in the Ross Sea: 1. Impact on CO₂ fluxes via variation in phytoplankton functional group and non-Redfield stoichiometry, *Journal of Geophysical Research - Oceans*, 110, C03009, doi:10.1029/2004JC002531, 2005.
- Takahashi, T., Sutherland, S.C., Sweeney, C., Poisson, A., Metzl, N., Tilbrook, B., Bates, N., Wanninkhof, R., Feely, R.A. and Sabine, C., 2002. Global sea-air CO₂ flux based on climatological surface ocean pCO₂, and seasonal biological and temperature effects. *Deep-Sea Research II*, 49(9-10), 1601-1622.

- Takahashi, T., S. C. Sutherland, R. Wanninkhof, C. Sweeney, R.A. Feely, D. Chipman, B. Hales, G. Friederich, F. Chavez, A. Watson, D. Bakker, U. Schuster, N. Metzl, H.Y. Inoue, M. Ishii, T. Midorikawa, C. Sabine, M. Hoppema, J. Olafsson, T. Amarasson, B. Tilbrook, T. Johannessen, A. Olsen, R. Bellerby, Y. Nojiri, C.S. Wong, B. Delille, N. Bates and H. De Baar, 2009. Climatological Mean and Decadal Change in Surface Ocean pCO₂, and Net Sea-air CO₂ Flux over the Global Oceans. *Deep-Sea Research II*, doi:10.1016/j.dsr2.2008.12.009
- Takeda S., 1998. Influence of iron availability on nutrient consumption ratio of diatoms in oceanic waters. *Nature*, 393, 774-777.
- Timmermans, K.R., Gerringa, L.J.A, de Baar, H.J.W., van der Wagt, B., Veldhuis, M.J.W., de Jong, J.T.M., Croot, P.L., 2001. Growth rates of large and small Southern Ocean diatoms in relation to availability of iron in natural seawater. *Limnology and Oceanography*, 46(2): 260-266.
- Timmermann R., Beckmann A., Hellmer H.H., 2002. Simulations of ice-ocean dynamics in the Weddell Sea 1. Model configuration and validation. *Journal of Geophysical Research-Oceans*, 107, C3, 3024.
- Timmermann R., Goosse H., Madec G., Fichefet T., Etche C. and Dulière V., 2005. On the representation of high latitude processes in the ORCALIM global coupled sea ice-ocean model. *Ocean Modelling*, 8(1-2): 175-201.
- Timmermann R., Worby A., Goosse H., and Fichefet T., 2004, Utilizing the ASPeCt sea ice thickness data set to validate a global coupled sea ice –ocean model. *Journal of Geophysical Research*, 109, C07017, doi:10.1029/2003JC002242.
- Tison J., Worby A.P., Delille B., Brabant F., Papadimitriou S., Thomas D.N., de Jong J., Lannuzel D. and Haas C., 2008. Temporal evolution of decay summer first-year sea ice in the western Weddell Sea, Antarctica. *Deep-Sea Research II*, 55, 975-987.
- Tortell and F.M.M. Morel. 2002. Sources of inorganic carbon for phytoplankton in the eastern Subtropical and Equatorial Pacific Ocean. *Limnology and Oceanography*, 47: 1012–1022.
- Tortell P.D., C.D. Payne, Y. Li, S. Trimborn, B. Rost, W.O. Smith, C. Riesselman, R.B. Dunbar, P. Sedwick and G.R. DiTullio, 2008. CO₂ sensitivity of Southern Ocean phytoplankton. *Geophysical Research Letters*, 35, doi:10.1029/2007GL032583
- Tréguer P., Lindner L., Van Bennekom A.J., Leynaert A., Panouse M. and Jacques G., 1991. Production of biogenic silica in the Weddell-Scotia Seas measured with ³²Si. *Limnology and Oceanography*, 36:1217-1227.
- Trull T.W., S.G. Bray, S.J. Manganini, S. Honjo and R. François, 2001. Moored sediment trap measurements of carbon export in the Subantarctic and the Polar front Zones of the Southern Ocean, south of Australia. *Journal of Geophysical Research-Oceans*, 06, 31489-31509.
- Trull T.W., D. Davies and K. Casciotti, 2008. Insights into nutrient assimilation and export in naturally iron-fertilized waters of the Southern Ocean from nitrogen, carbon and oxygen isotopes. *Deep-Sea Research II*, 55, 820-840.
- Uitz J., H. Claustre, F. B. Griffiths, J. Ras, N. Garcia and V. Sandroni, 2009. A phytoplankton class-specific primary production model applied to the Kerguelen Islands region (Southern Ocean). *Deep Sea Research I*, 56, 541-560.

- Uppala, S.M., Kållberg, P.W., Simmons, A.J., Andrae, U., da Costa Bechtold, V., Fiorino, M., Gibson, J.K., Haseler, J., Hernandez, A., Kelly, G.A., Li, X., Onogi, K., Saarinen, S., Sokka, N., Allan, R.P., Andersson, E., Arpe, K., Balmaseda, M.A., Beljaars, A.C.M., van de Berg, L., Bidlot, J., Bormann, N., Caires, S., Chevallier, F., Dethof, A., Dragosavac, M., Fisher, M., Fuentes, M., Hagemann, S., Hólm, E., Hoskins, B.J., Isaksen, L., Janssen, P.A.E.M., Jenne, R., McNally, A.P., Mahfouf, J.-F., Morcrette, J.-J., Rayner, N.A., Saunders, R.W., Simon, P., Sterl, A., Trenberth, K.E., Untch, A., Vasiljevic, D., Viterbo, P., and Woollen, J., 2005. The ERA-40 re-analysis. *Quart. J. R. Meteorol. Soc.*, 131, 2961-3012. doi:10.1256/qj.04.176
- Varela D., C.J. Pride and M.A. Brzezinski, 2004. Biological fractionation of silicon isotopes in Southern Ocean surface waters. *Global Biogeochemical Cycles*, 18, GB01047.
- Vencharutti C., C. Jeandel and M. Roy-Barman, 2008. Particle dynamics study in the wake of Kerguelen Island using thorium isotopes. *Deep-Sea Research I*, 55, 1343-1363.
- Wagener T., Guieu C., Losno R., Bonnet S. and Mahowald N. 2008. Revisiting atmospheric dust export to the Southern Hemisphere ocean: Biogeochemical implications. *Global Biogeochemical Cycles*, 22, GB2006, doi:10.1029/2007GB002984.
- Wakeham, S.G., C; Lee, M.L. Peterson, Z. Liu, J. Szlosek, I.F. Putnam and J. Xue. 2009. Organic biomarkers in the twilight zone-Time series and settling velocity sediment traps during MedFlux. *Deep-Sea Research II*, 56, 1437-1453.
- Wassmann P., 1998. Retention versus export food chains: processes controlling sinking loss from marine pelagic systems. *Hydrobiologia*, 363, 29-57.
- Watson A.J. and Orr J.C., 2003. Carbon dioxide fluxes in the global ocean. In: M.J.R. Fasham (Editor), *Ocean biogeochemistry: The role of the ocean carbon cycle in global change*. Springer-Verlag, Berlin.
- Westwood, K.J., Griffiths, F.B., Webb, J. and Wright, S.W., 2011. Primary production in the Sub-Antarctic and Polar Frontal zones south of Tasmania, Australia; SAZ-Sense survey, 2007. *Deep Sea Research II*, SAZ-Sense Topical Volume, accepted.
- Wilkinson, K. J., and J. Buffle, 2004. Critical evaluation of physicochemical parameters and processes for modeling the biological uptake of trace metals in environmental (aquatic) systems. *IUPAC Ser. Anal. Phys. Chem. Environ. Sys.:* 445-533.
- Winter A., M. Elbrächter and G. Krause, 1999. Subtropical coccolithophores in the Weddell Sea. *Deep-Sea Research*, 46, 439-449.

Annex 1:

Copy of the publications (pdf's) are available on the following web site:

<http://anchsvr.vub.ac.be/dehairs>

Annex 2

Chronology of interactions with the end-user committee (names underlined are members of the end-user committee):

- February 20-24, 2006: Discussion with Thomas Trull about future collaboration and contribution of BELCANTO III to SAZ-Sense expedition, Ocean Sciences meeting, Hawaii.
- March 14-16, 2006: Discussions with Eugene Murphy & Hein de Baar concerning BELCANTO III contribution to EurOceans Southern Ocean Systems and ICED IPY; Barcelona.
- March 23-24, 2006: Discussions with Hein de Baar and Annick Wilmotte about outreach and BELCANTO III contribution to BE-POLES.
- May 23rd, 2006: Discussions with Nicolas Metz concerning application of Parametric Optimum Multi Parameter model developed at VUB to reconstruct barium and nutrient fields along transects in the Southern Ocean, Paris.
- July 7-9, 2006: Discussions with Nicolas Metz about synthesis of BELCANTO I & II results related to inorganic carbon dynamics, and a new joint CO₂ study on the Kerguelen plateau (Liège).
- October 2 – 5, 2006: Discussions with Tom Trull at WHOI, concerning BELCANTO III contribution to SAZ-Sense expedition, Jan-Feb 2007; Woods Hole, USA.
- November 15th 2006: Discussions with Eugene Murphy & Jean-Louis Tison concerning BELCANTO contribution to EurOceans Southern Ocean Systems and ICED IPY; Brussels,.
- December 5-8, 2006: Discussions with Nicolas Metz about the results of the joint CO₂ study south of Tasmania and the link of interannual variation of air-sea CO₂ fluxes and the Southern Annular Mode (Carbocean meeting, Las Palmas).
- Oct-Nov 2007: Hobart; discussions with Tom Trull during SAZ-Sense expedition: exchange of data; complementary analyses on same samples etc... organisation of the post-cruise workshop.
- June 27, 2007: organization of a Follow-Up Committee meeting at Vrije Universiteit Brussel; see Annex 3 for detailed minutes of the meeting (see details under A.2). Attending: H. de Baar (Royal NIOZ, Texel, The Netherlands); C. Jeandel (Laboratoire d'Etudes en Géophysique et Océanographie Spatiales; OMP, Toulouse, France); N. Metz (Institut Pierre Simon Laplace, Université Pierre et Marie Curie, Paris, France); E. Murphy (British Antarctic Survey); J.-L. Tison (Glaciologie, Université Libre de Bruxelles); M. Vancauwenberghe, Belspo.
- Jan. 2008: Concertation with Hein de Baar (NIOZ) in Cape Town concerning (i) the sampling strategy during the concurrent BONUS-GOODHOPE and ANTX23

- expeditions; (ii) the organisation of intercalibrations between scientists on board Polarstern and Marion Dufresne (Si-isotopes, Ba); (iii) the organisation of a joint IPY session during the upcoming ASLO meeting, Jan. 2009, Nice, France.
- May 27-28, 2008: EurOceans Workshop (Brussels) and e-mails: Discussions with Tom Trull (ACE-CRC, Hobart) concerning intercomparison and interpretation of SAZ Sense results, and joint publications of results in a special issue of Deep-Sea Research Part II.
 - September 2008: Discussions with Catherine Jeandel (LEGOS OMP, Toulouse) about contributions of Belcanto Si-isotopes and Ba-proxy to IPY-GEOTRACES. Discussions about intercalibration and data management policy (BGH results)
 - November 2008: Discussions with Eugene Murphy (BAS) about interactions between Belcanto and IPY-ICED during the IMBER-IMBIZO meeting, Miami, FL, and the final EurOceans meeting, Rome. Presentation of Belcanto results during both meetings.
 - December 2008. Paris. Discussions with Nicolas Metzl about integration of data-sets
 - Jan.-Febr. 2009: During a 2 month sabbatical leave of Frank Dehairs at ACE-CRC, Hobart, several discussions were held with Tom Trull, Andrew Bowie and Brian Griffiths (ACE-CRC Hobart) about: (i) contributions to and editorial management of the topical SAZ-Sense volume to appear in Deep-Sea Research Part II (Subantarctic Biogeochemistry, eds. B. Griffiths, A. Bowie & F. Dehairs); (ii) co-operation in the framework of the extended ACE-CRC program via the set-up of a formal agreement between VUB partner and ACE-CRC.
 - March 2009: Workshop Marseille, Endoûme: Discussions with Nicolas Metzl and Stéphane Blain about KEOPS results (effects of natural Fe fertilization) and the organization of a second KEOPS expedition to be organised eventually in 2010-2011.